Modelling regional sea-level changes in recent past and future

Aimée Slangen

ISBN 978-90-393-5868-9

Institute for Marine and Atmospheric research Utrecht (IMAU)
Faculty of Science, Department of Physics and Astronomy
Utrecht University, The Netherlands

An online version of this thesis is available via http://about.me/aimeeslangen

Cover: Relative sea-level anomaly from the global mean for the period 1985–2005 vs 2081–2100 (m) for the CMIP5 RCP4.5 model ensemble, adaptation of Figure 6.4a.

Modelling regional sea-level changes in recent past and future

Het modelleren van regionale zeespiegelveranderingen in het recente verleden en de toekomst

(met een samenvatting in het Nederlands)

PROEFSCHRIFT

ter verkrijging van de graad van doctor aan de Universiteit Utrecht
op gezag van de rector magnificus, prof. dr. G. J. van der Zwaan,
ingevolge het besluit van het college voor promoties
in het openbaar te verdedigen op

woensdag 12 december 2012 des middags te 12.45 uur

door

Aimée Berthe Agnès Slangen

geboren op 26 november 1984 te Rotterdam

Promotor:	Prof. dr. J. Oerlemans
Co-promotoren:	Dr. R. S. W. van de Wal
	Dr. L. L. A. Vermeersen

Dit proefschrift werd mede mogelijk gemaakt door financiële steun van de Nederlandse organisatie voor Wetenschappelijk Onderzoek (NWO), sectie Aard- en Levenswetenschappen (ALW) en het Netherlands Institute for Space Research (SRON) onder contract nr. ALW-GO-AO/07-14.

I was just guessing
At numbers and figures
Pulling the puzzles apart
Questions of science
Science and progress
Do not speak as loud as my heart

from 'The Scientist' by Coldplay, 2002

Though my hands are cold and my mouth is dry
Well this journey's told is a mountain high
Though the wind she burns like an angel's flame
she will give me strength so I can move again

from 'The Raft' by Fat Freddy's Drop, 2009

Contents

Samenvatting **ix**

1 Introduction **1**
1.1 Measuring sea-level change . . . 2
1.2 Processes contributing to sea-level change . . . 6
1.3 Recent developments in sea-level research . . . 12
1.4 This thesis . . . 14

2 Theoretical background **15**
2.1 Mass contribution . . . 16
2.2 Steric contribution . . . 27
2.3 Glacial Isostatic Adjustment . . . 29
2.4 Summation of patterns . . . 31

3 Regional sea-level variations in the recent past (1961-2003) **33**
3.1 Introduction . . . 34
3.2 Data and Methodology . . . 35
3.3 Comparing the observations to the models . . . 40
3.4 Discussion . . . 48
3.5 Conclusions . . . 51

4 Regional projections of sea-level change **53**
4.1 Introduction . . . 54
4.2 Data and Methodology . . . 56
4.3 Projections of local sea-level change . . . 62
4.4 Discussion of regional sea-level projections . . . 72
4.5 Summary and conclusions . . . 77

5 Uncertainties in the glacier contribution to sea-level change 81
5.1 Introduction . . . 82
5.2 Data and methods . . . 83
5.3 Reference experiment and past sea-level contribution . . . 87
5.4 Sensitivity experiments . . . 88
5.5 Conclusions . . . 101

6 Projecting twenty-first century regional sea-level changes 105
6.1 Introduction . . . 106
6.2 Methods . . . 106
6.3 Regional sea-level projections . . . 108
6.4 Discussion and conclusions . . . 111
6.5 Supplementary information . . . 113

7 Summary, conclusions and outlook 119
7.1 Summary and conclusions . . . 119
7.2 Outlook . . . 121

List of acronyms 125

Bibliography 127

Bedankt! / Thanks! 135

Publications 137

Curriculum Vitae 138

Samenvatting

Het klimaat op aarde verandert voortdurend. Als we kijken op de tijdschaal van ijstijden zien we dat veranderingen in het klimaat vooral worden veroorzaakt door variaties in de hoeveelheid inkomende straling van de zon. Op kortere tijdschalen kan het klimaat echter ook veranderen door bijvoorbeeld natuurlijke variaties in broeikasgassen of door vulkaanuitbarstingen. Verschillende waarnemingen laten zien dat sinds het begin van de industriële revolutie het klimaat ook verandert doordat de concentratie van broeikasgassen in de atmosfeer toeneemt door het gebruik van fossiele brandstoffen. Dit beïnvloedt de stralingsbalans van de aarde en veroorzaakt een versterkt broeikaseffect. Het gevolg hiervan is dat de wereldgemiddelde temperatuur in zowel de atmosfeer als de oceaan toeneemt, waardoor bijvoorbeeld gletsjers en poolkappen krimpen. Een belangrijk gevolg hiervan is dat de wereldgemiddelde zeespiegel stijgt, en dit heeft directe consequenties voor steden die aan de kust gebouwd zijn. Voor beleidsmakers is het daarom belangrijk te weten hoeveel de zeespiegel zal veranderen in de toekomst. Echter, de zeespiegel zal niet overal ter wereld op dezelfde manier veranderen. Het is daarom niet voldoende om de wereldgemiddelde stijging uit te zoeken, zoals in het recente verleden meestal werd gedaan. Nog veel belangrijker is het om de regionale veranderingen te bestuderen.

Voordat we verwachtingen van de toekomstige zeespiegelveranderingen kunnen maken, moeten we eerst begrijpen welke processen bijdragen aan deze veranderingen. Het is niet voldoende om simpelweg observaties uit het verleden te extrapoleren naar de toekomst, omdat processen als het terugtrekken van gletsjers, massaveranderingen op de poolkappen en de warmteopname in de oceaan niet lineair afhankelijk zijn van klimaatverandering. Elk van deze processen reageert op een andere manier op veranderingen in het klimaat, en zal ook een ander ruimtelijk patroon in de zeespiegelverandering veroorzaken. Het is daarom belangrijk om de fysica achter deze processen te begrijpen en deze kennis te gebruiken bij het maken van toekomstprojecties voor de

zeespiegelverandering. Het onderzoek in dit proefschrift is gericht op het modelleren van de verschillende processen die bijdragen aan zeespiegelverandering, en in het bijzonder bekijken we de regionale variaties die veroorzaakt worden door deze processen.

De zeespiegel kan ten eerste stijgen of dalen door het toevoegen of onttrekken van water aan de oceaan. Water toevoegen gebeurt bijvoorbeeld wanneer gletsjers krimpen of wanneer mensen grondwater oppompen voor irrigatie. De hoeveelheid water kan ook afnemen, bijvoorbeeld door het bouwen van dammen in rivieren of wanneer gletsjers groeien. Echter, op een regionale schaal is er nog iets anders aan de hand. We moeten dan namelijk ook rekening houden met veranderingen in het zwaartekrachtsveld. Volgens de gravitatiewet van Newton trekt alle massa op aarde elkaar aan. Als we de Groenlandse ijskap als voorbeeld nemen, en een deel van het ijs laten wegsmelten, vermindert hierdoor de aantrekkingskracht van het ijs op de oceaan. Het wellicht onverwachte gevolg hiervan is dat in de buurt van het ijs de zeespiegel daalt, terwijl juist verder weg de zeespiegel stijgt. Hierdoor veroorzaken wateruitwisselingen tussen land en oceaan een zeer specifiek regionaal patroon in de zeespiegel. Dit wordt het 'zelf-gravitatie effect' of 'zwaartekrachtseffect' genoemd.

Naast het zwaartekrachtseffect is er ook een reactie van het aardoppervlak op het herverdelen van massa. Immers, meer massa op een bepaalde plek betekent meer gewicht, waardoor de aardkorst omlaag gedrukt wordt. Het omgekeerde gebeurt als er minder massa komt te liggen op een bepaalde plek, waardoor de aardkorst kan terugveren. Dit gebeurt zowel direct, het 'elastische' effect, als vertraagd, het 'visceuze' effect. Deze vertraagde reactie speelt op tijdschalen van duizenden jaren, en wordt vaak 'post-glaciale opheffing' genoemd, of 'glacial isostatic adjustment (GIA)'. Dit proces zorgt ervoor dat bijvoorbeeld in Scandinavië de aardkorst nu nog steeds omhoog komt met 1 cm per jaar, omdat er in de laatste ijstijd, 20 duizend jaar geleden, een enorme ijsmassa lag. Deze aanpassingen van de aardkorst zorgen ook voor zeespiegelverandering, omdat de oceaanbodem stijgt of daalt.

Een andere belangrijke oorzaak van zeespiegelveranderingen zijn variaties in de dichtheid van het oceaanwater. Dit komt door variaties in de temperatuur of het zoutgehalte, waardoor het water kan uitzetten of krimpen. Wanneer water opwarmt zet het uit, en daardoor stijgt de zeespiegel. Het omgekeerde gebeurt wanneer het water zouter wordt: meer zout betekent een hogere dichtheid, waardoor het volume afneemt en de zeespiegel daalt. Deze dichtheidsveranderingen kunnen daarom zorgen voor lokale variaties in de zeespiegel, waarbij de temperatuurveranderingen doorgaans belangrijker zijn dan veranderingen in de zoutconcentratie.

Het eerste hoofdstuk in deze thesis bevat een algemene inleiding in de basisconcepten van zeespiegelverandering. Het legt uit welke methoden gebruikt kunnen worden om veranderingen te meten, beschrijft de belangrijkste processen en geeft een overzicht van recent onderzoek op dit gebied. In hoofdstuk 2 van dit proefschrift worden vervolgens de belangrijkste theorie en de gereedschappen om de verschillende processen te modelleren verder uitgewerkt.

De theorie die in hoofdstuk 2 is beschreven, wordt in hoofdstuk 3 getest voor de

periode 1961–2003. In dit hoofdstuk vergelijken we de gemodelleerde zeespiegelveranderingen met gemeten waarden op peilschaalstations langs de kust. De zeespiegelbijdragen die meegenomen worden in dit hoofdstuk zijn veranderingen in de hoeveelheid landijs (gletsjers en poolkappen), dichtheidsveranderingen in de oceaan, GIA, veranderingen in wateropslag op het land (grondwateronttrekking en het bouwen van dammen) en een correctie voor atmosferische drukveranderingen. De vergelijking van metingen met gemodelleerde bijdragen over deze periode van 43 jaar laat zien dat de modellen grotendeels in staat zijn om de lokale metingen te verklaren. Dit hoofdstuk toont hiermee aan dat het inzicht in de verschillende processen zodanig is dat de modellen ook gebruikt kunnen worden om toekomstige regionale veranderingen te modelleren.

In hoofdstuk 4 worden vervolgens de eerste stappen richting een regionale verwachting van toekomstige zeespiegelveranderingen beschreven. Tot nu toe werden vaak alleen wereldgemiddelde waarden voor zeespiegelverandering gepresenteerd, maar het doel in dit hoofdstuk is om de bijbehorende regionale verdeling te laten zien. De volgende processen worden meegenomen: variaties in ijsmassa in gletsjers en poolkappen, temperatuur- en zoutveranderingen in de oceaan, en GIA. Het gemodelleerde zeespiegelpatroon laat zien dat lokale waarden flink kunnen afwijken van het mondiaal gemiddelde, tot wel 70%. In het uiteindelijke regionale patroon zijn signalen van de afzonderlijke processen te herkennen, zoals een hoge ruimtelijke variabiliteit die veroorzaakt wordt door de dichtheidsveranderingen, maar ook een karakteristiek patroon dat veroorzaakt wordt door het smelten van landijs en het bijbehorende zwaartekrachtseffect. Verder zien we GIA-invloeden in regio's als Scandinavië en de Hudson baai. Verschillende klimaatscenario's worden besproken, en we constateren dat, hoewel de absolute zeespiegelstijging uiteraard varieert tussen de verschillende temperatuurscenario's, de ruimtelijke patronen sterk op elkaar lijken. De studie in dit hoofdstuk was de eerste die op deze manier gemodelleerde regionale patronen combineerde en deze gebruikte voor een toekomstverwachting van zeespiegelverandering.

Echter, ieder proces heeft zo zijn onzekerheden. Daarom wordt in hoofdstuk 5 gekeken naar de onzekerheden in de verwachte gletsjerbijdrage aan de zeespiegelverandering. In het bijzonder wordt gekeken naar de onzekerheden van het gletsjermodel, dat veranderingen in volume en oppervlak van gletsjers aan elkaar relateert om gletsjerveranderingen te modelleren. Een groot deel van de onzekerheid wordt bepaald door de gletsjer dataset, waarin de initiële oppervlaktes van de gletsjers geschat worden. Verder heeft de keus van het klimaatscenario grote invloed. Dit zijn de veranderingen in temperatuur en neerslag, die worden gebruikt om de veranderingen in gletsjervolume te berekenen. Ook de gevoeligheid van de gletsjers voor temperatuur- en neerslagveranderingen, de zogenoemde massabalansgevoeligheid, is een belangrijke factor in de onzekerheid. In totaal vinden we een gecombineerde onzekerheid in de gletsjerbijdrage aan de zeespiegelverandering van 35%.

Hoofdstuk 6 keert terug naar regionale zeespiegelprojecties. Echter, in dit hoofdstuk is het doel om de beste en meest recente data, modellen en kennis te benut-

ten om deze projecties te maken, in tegenstelling tot het onderzoek in hoofdstuk 4, waar de nadruk lag op het laten zien van regionale patronen bij de wereldgemiddelde zeespiegelwaarden van het IPCC klimaatrapport. Dezelfde processen als in hoofdstuk 4 worden meegenomen, maar ditmaal dus met recentere data. We gebruiken bijvoorbeeld een nieuwe set van klimaatmodelsimulaties, de zogenoemde CMIP5 model database, om de dichtheidsveranderingen te modelleren. Uit deze database gebruiken we ook temperatuur- en neerslagveranderingen om de gletsjerbijdrage te bepalen. Daarnaast gebruiken we nieuwe schattingen voor de massaveranderingen op de poolkappen: Groenland en Antarctica. We zien dat regionale verschillen tot 30% hoger kunnen zijn dan het wereldgemiddelde, en tot 50% lager. Op 10% van het totale oceaanoppervlak vinden we waarden die meer dan 25% afwijken van het gemiddelde. Ook laten we zien dat ieder proces dominant kan zijn, afhankelijk van de locatie en het gekozen klimaatscenario. Dit betekent daarom dat al deze processen meegenomen moeten worden om een zo goed mogelijke verwachting te maken van de zeespiegelverandering.

Het onderzoek in deze thesis laat vooral zien dat wereldgemiddelde zeespiegelverandering een te eenvoudig concept is. Regionale veranderingen zijn duidelijk zichtbaar in zowel de metingen als de modellen. Echter, regionale zeespiegelveranderingen worden door veel verschillende processen beïnvloedt, en er blijven nog voldoende vragen over voor toekomstig onderzoek. Niettemin laat het onderzoek in deze thesis zien hoe verschillende processen gemodelleerd kunnen worden en hoe deze bijdragen aan regionale variaties in de zeespiegel, hetgeen een belangrijke stap voorwaarts is in het zeespiegelonderzoek.

CHAPTER 1

Introduction

The Earth's climate is continuously changing. On ice age timescales, variations in climate are caused by variations in solar forcing due to small changes in the orbit of the Earth around the Sun, as described by the Milanković Theory (Milanković, 1930). On shorter timescales, natural variations in greenhouse gas concentrations or volcanic eruptions can influence the climate system. However, observations from various components of the Earth's climate system indicate that since the beginning of the industrial revolution the climate is changing due to anthropogenic activities as well (Solomon et al., 2007). Greenhouse gas concentrations have been increasing due to fossil fuel combustion, causing an enhanced greenhouse effect by increasing the radiative forcing of the Earth's atmosphere. As a result, the global mean air temperature and ocean temperature are rising, and glaciers and ice sheets are shrinking. An important consequence of this is that global mean sea level is rising.

This poses a challenge to mankind, because many cities are built near the coast. As sea level rises, coastal societies will need to face the problem that their coastal defenses against higher mean sea levels and extreme high stands may not be sufficient (Nicholls and Cazenave, 2010). To improve coastal management and planning of flood defenses, information on the future development of sea-level rise is necessary. However, sea-level rise is not uniform around the world, and therefore it is not sufficient to know how much the global mean sea level will rise in the future. Hence, there is a pressing need for information on a regional scale.

Making sea-level projections, both globally and locally, requires an understanding of the processes that contribute to sea-level change. It is not sufficient to simply extrapolate past observations into the future, since processes such as glacier retreat, ice sheet mass changes and ocean heat uptake are not linearly related to climate change.

Each of these processes respond to climate change in a different way and will produce a different regional signature. It is therefore very important to consider the physics of all these processes when making future projections.

This thesis focuses on regional variations in sea-level change, by using models that account for the different contributing processes. This first chapter provides a general introduction of the basic concepts of sea-level change research. It explains which methods can be used to measure changes in sea level, shows the main contributing processes to sea-level change, and provides an overview of the recent developments in sea-level change research. The chapter concludes with an outline of the research that is presented in this thesis.

1.1 Measuring sea-level change

Measurements of past sea level are crucial for increasing our understanding of the processes that cause sea-level change. To determine sea-level changes before 1700, which is when instrumental measurements started, there are several types of sea-level indicators that can be used. These indicators can be of geological, biological or archaeological nature, or a combination thereof (Lambeck et al., 2010). Geological indicators include for instance shorelines from the last interglacial that are found above the present sea level, or erosional notches in rocks above sea level. Fossil corals can be useful biological indicators, since most corals can only live within a certain distance of the ocean surface. Also fossil mollusks, oysters or mussels may be used as indicators. On a shorter timescale, human ports or settlements, for instance from Roman times, may provide archaeological information on sea level. A few examples of proxies are shown in Figure 1.1, where for instance A (Lidén, 1938) and B (Vorren and Moe, 1986) are based on geological evidence from sediments, C (Heyworth and Kidson, 1982) on submerged tree roots, and E (Fairbanks, 1989) and G (Chappell, 1983) on fossil corals. Most of the information obtained from proxies does not go back beyond the Last Glacial Maximum (LGM), about 20,000 years ago, since the onset of this glaciation and the subsequent deglaciation has erased many earlier marks. To determine sea-level change on timescales in the order of millions of years, isotope ratios in deep-sea sediment cores can be used as a proxy for the total ice volume on Earth, thus giving an indication of global mean sea level (Chappell and Shackleton, 1986; Bintanja and van de Wal, 2008; De Boer et al., 2011).

The first instrumental records of sea level start in the 1700's, when tide gauges were set up in Amsterdam, Stockholm, Kronstadt and Liverpool (Figure 1.2). The earliest tide gauges were simply rocks or wooden rods in the ocean (Figure 1.3a). Later, stilling wells with a float were used to eliminate wave effects. Nowadays, optical sensors are used to measure the sea level. Tide gauges measure the sea level relative to the Earth's surface, and thus do not detect vertical surface displacements. Tide gauge records are available through the website of the Permanent Service for Mean Sea Level (PSMSL, Woodworth and Player, 2003). This database contained 300 stations in 1950, increased

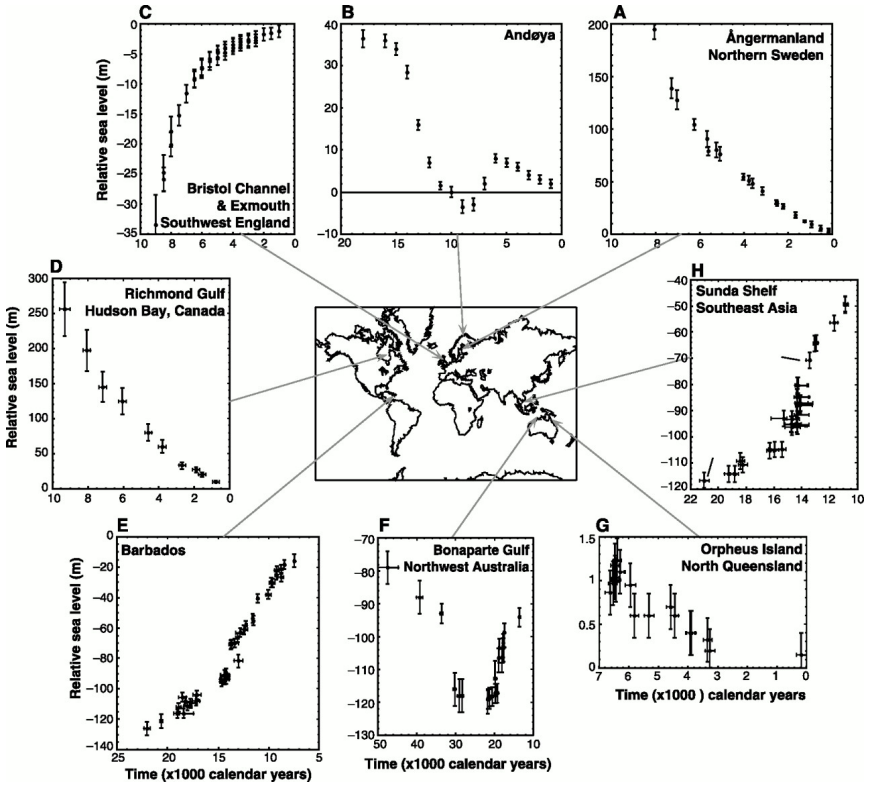

Figure 1.1: *Reconstructed past sea level using various paleo indicators. Figure from Lambeck and Chappell (2001).*

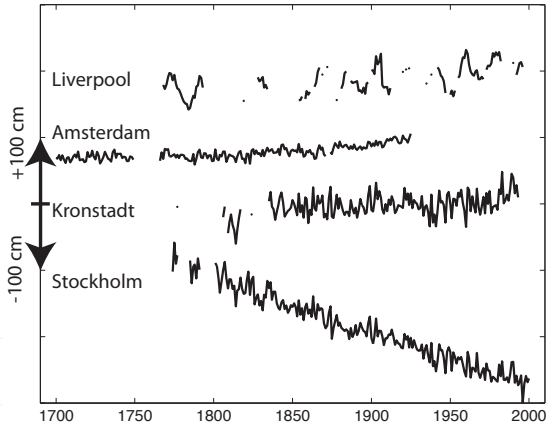

Figure 1.2: *Historical tide gauge observations (cm) from Liverpool (Woodworth, 1999), Amsterdam (Van Veen, 1945), Kronstadt (Bogdanov et al., 2000) and Stockholm (Ekman, 1988).*

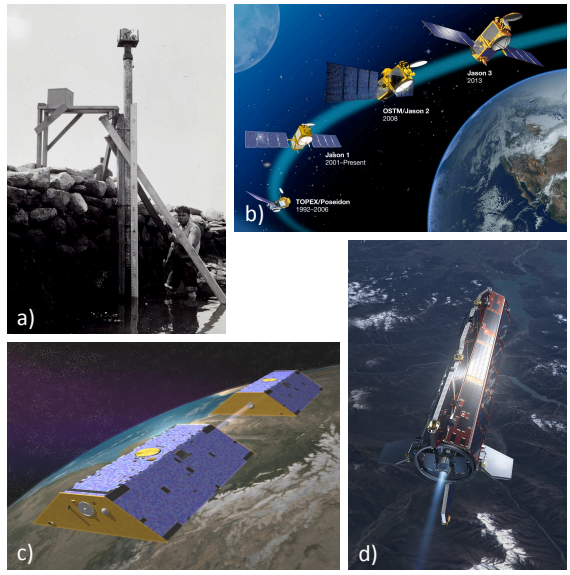

Figure 1.3: *Sea-level observation methods. a) Tide gauge (courtesy NOAA) b) Satellite altimetry (courtesy NASA) c) GRACE (courtesy JPL) d) GOCE (courtesy ESA).*

to over 900 records in the 1980's, and decreased to 500 records after that. Less than 100 of these stations are located in the Southern Hemisphere. This means that the number of records is not constant in space or time. Therefore, caution is required when these data are used to compute global mean sea-level changes. Uncertainties arise not only from the uneven distribution of the measurements, but also from vertical land movements at the measurement locations (e.g., Peltier, 2001; Wöppelmann et al., 2007), atmospheric pressure variations, and from non-climate related sea-level variability, such as tidal cycles.

The spatial resolution and coverage of sea-level measurements increased when satellite altimetry was introduced, starting in 1992 with the launch of the TOPEX/Poseidon radar altimeter satellite (Figure 1.3b). Together with the follow-up missions Jason-1 and Jason-2, the altimeter satellites have provided a continuous time series of sea-surface height with 10-day repeat cycles ever since. The satellites orbit at 1336 km altitude, and cover the ocean surface between 66°N and 66°S. In contrast to tide gauges, altimetry satellites measure sea surface height with respect to the Earth's center of mass, and thus provide an absolute measure of sea-level height. This means that the results need to be corrected for crustal motions to obtain the relative sea-level change as measured by tide gauges. The data must also be corrected for atmospheric pressure variations and tidal cycles, similar to the tide gauge measurements.

In 2002, the Gravity Recovery And Climate Experiment (GRACE) satellite was launched (Figure 1.3c). This satellite measures the time-varying gravity field of the Earth, which is a measure for mass changes. GRACE consists of two satellites, which

are 220 km apart at an altitude of 500 km in a polar orbit. When the first satellite passes over an area with a higher gravitational pull, it will accelerate and consequently the distance between the two will increase, and vice versa for a lower gravitational pull. In this way, GRACE measures the gravity of the total mass column below the satellite, but cannot distinguish between ice, water or mantle material. It is important to note that GRACE measures only mass changes and no volume changes resulting from density variations. The ground resolution of the data is around 300-400 km.

Complementary to GRACE, the Gravity field and steady-state Ocean Circulation Explorer (GOCE) satellite was launched in 2009 (Figure 1.3d). GOCE is in a polar orbit at 260 km altitude, which allows it to reach a ground resolution of around 100 km, an unprecedented spatial accuracy. GOCE measures the Earth's quasi-static gravity field, or the geoid, which is the ideal ocean surface as determined by gravity, without variations from tides and currents. Gravity is not the same everywhere, since Earth is not a perfect sphere, and densities vary from the ocean surface to the Earth's interior. The ocean surface at rest is shaped by gravity, where the gravitational force is always perpendicular to the ocean surface. Due to the large variations in density around the world, this implies that the ocean surface under the influence of gravity is also not a perfect sphere, but instead shows spatial variations. GOCE measurements of the spatially varying geoid can therefore be used to correct ocean height measurements for the static component. This allows for a better determination of ocean circulation and dynamics, which is very important for oceanic and sea-level research.

To determine present-day sea-level change, it is important to consider both *in situ* -tide gauge- as well as remote sensing measurements. The advantage of the tide gauge measurements is that they provide relatively long time series, while the satellite altimetry missions only have data starting in 1992. For climate change aspects, a 20-year time series as available from satellites might still include natural variability, which can only be filtered out using longer time series. On the other hand, the spatial coverage of the satellites is much higher, which eliminates the problem that tide gauges are biased towards coastal areas in the Northern Hemisphere. This is why for instance Church and White (2011) (updated from Church et al. (2004); Church and White (2006)) combine satellite altimetry and tide gauges by using the strengths of each method, namely high spatial resolution from satellites and long time series from tide gauges, to reconstruct sea-level fields back to 1880 using empirical orthogonal functions (EOFs). The reconstructed sea-level fields can be used to compute global mean time series, which are shown in Figure 1.4. Because less tide gauge records are available in 1880 than at present, the uncertainties increase going back in time. For the period 1993–2009, the yearly satellite altimetry global mean value is shown in black, indicating a good agreement between the reconstructed time series and the satellite observations. This is not a completely independent test, since the EOFs are based on satellite data in the first place. However, the time series can also be compared to other reconstructions, such as Holgate and Woodworth (2004), which are found to agree quite well (Church and White, 2011).

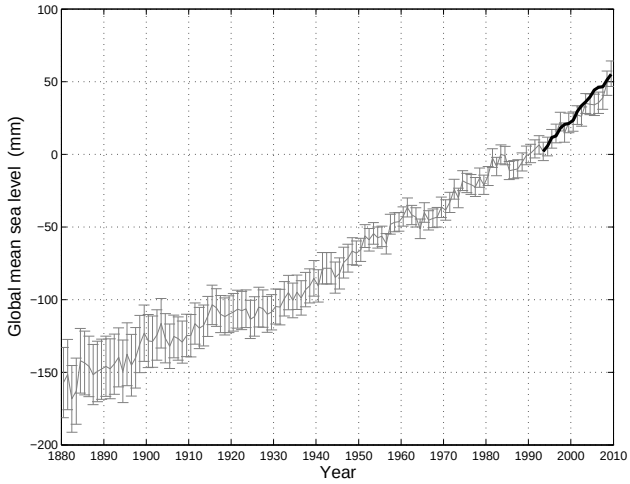

Figure 1.4: *Reconstructed annual mean global mean sea level (mm) with respect to 1990 in grey, with error bars representing one standard deviation. Satellite altimetry global mean sea level (mm) from 1993 to 2009 in black. All data from Church and White (2011).*

1.2 Processes contributing to sea-level change

In this thesis, several causes of sea-level change will be treated, as schematically shown in Figure 1.5a. The first is the addition or withdrawal of ocean mass, which can either be caused by land ice mass changes or by terrestrial exchange processes such as groundwater pumping. A second possibility is the vertical displacement of the Earth's crust due to redistribution of mass, indicated in Figure 1.5a as GIA, or Glacial Isostatic Adjustment. The third process considered here is the increase or decrease in ocean volume through density variations due to temperature and salinity changes. This section briefly describes each of these processes, and explains how these processes influence sea-level change globally and regionally. More in-depth information on the models used to compute the regional sea-level change patterns resulting from these processes will be provided in Chapter 2.

First, it is important to define what we mean by the term sea-level change. Figure 1.5b shows the two reference frames that are often used in sea-level research. On the left is the *absolute* sea-level change, which measures the sea-surface height change with respect to the Earth's centre of mass. This is the sea-level change that is measured by altimetry satellites, as satellites move around the Earth's centre of mass. In this reference frame, it is difficult to determine whether sea-level changes are caused by an increase in the water column or by a vertical displacement of the Earth's crust. The right arrow in Figure 1.5b shows the meaning of the term *relative* sea-level change, which is the difference between the ocean surface and the ocean floor. This is the type of sea level that is measured by tide gauges, as these devices are attached to the solid-earth surface. To obtain *relative* sea-level change from satellite altimetry,

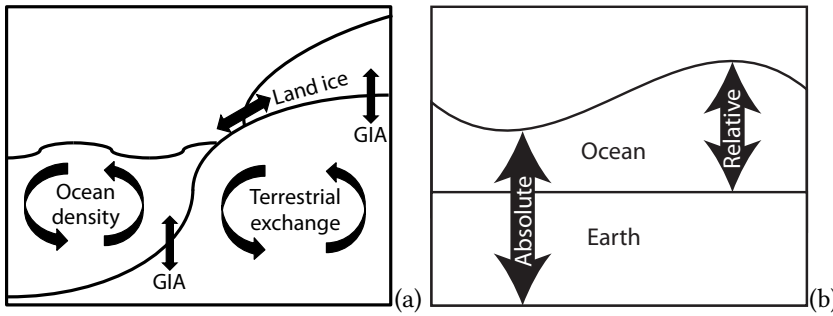

Figure 1.5: *(a) Sea-level change processes considered in this thesis. Land ice = glaciers, ice caps and ice sheets; Ocean density = temperature and salinity; Terrestrial exchange = groundwater and dam impoundment; GIA = glacial isostatic adjustment. (b) Different reference frames: absolute sea-level change vs. relative sea-level change.*

the measurements must be corrected for vertical surface displacement. The advantage of this reference frame is that it indicates changes in the water column only. Unless mentioned otherwise, all sea-level change values presented in this thesis are *relative* sea-level changes.

The most important source of fresh water on Earth is land ice, which currently holds around 65 m of potential global mean sea-level rise. From this, the majority is stored in the Antarctic Ice Sheet (AIS), which holds around 56.6 m. Another 7.3 m is stored in the Greenland Ice Sheet (GIS) and the remainder of 0.6 m is stored in the Glaciers and Ice Caps (GIC) around the world (Lemke et al., 2007). Although GIC only store a small percentage of the total land ice, their present contribution to sea-level rise is relatively large; most have been retreating rapidly over the past century (e.g. Figure 1.6). GIC respond much faster to climate changes than the two large ice sheets, because they have a much larger mass turnover due to their location in often warmer and wetter areas (Oerlemans and Fortuin, 1992). As a result, GIC currently account for over half of the total land ice contribution to sea-level change. The Intergovernmental Panel for Climate Change Fourth Assessment Report (IPCC AR4) estimated a glacier contribution of 0.77 ± 0.22 mm/yr between 1993 and 2003 (Figure 1.7, Bindoff et al., 2007). However, the mass loss of the ice sheets is currently accelerating (Velicogna, 2009), and this is expected to contribute more and more to sea-level change in the coming century. The mass balance of the ice sheets is the sum of the surface mass balance (SMB) and the ice dynamical discharge. The SMB describes the climate on the ice sheet, such as snow fall and surface melting. Model studies using regional atmospheric climate models show no significant changes over the past three decades for the Antarctic SMB (Lenaerts et al., 2012), while the SMB for Greenland is found to be decreasing, which means that mass loss is increasing (Ettema et al., 2009). Recent observations of the ice dynamics show that the dynamical contribution is increasing, but these changes cannot be explained by climate change alone. However, the mechanisms behind variations in the ice sheet dynamical discharge are not very well understood

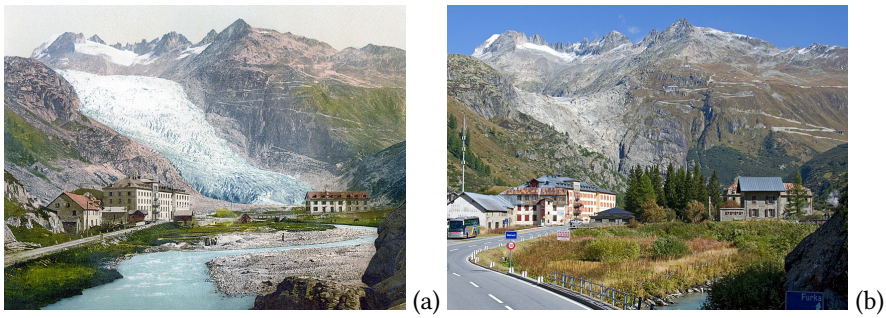

Figure 1.6: *Repeat imagery showing the retreat of the Rhonegletscher, Switzerland (from swisseduc.ch/glaciers, by J. Alean and M. Hambrey).* **(a)** *Hand coloured postcard from 1900* **(b)** *Photograph taken in 2008.*

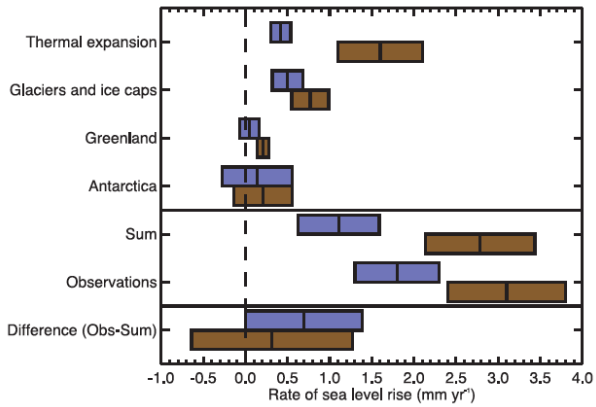

Figure 1.7: *IPCC AR4 estimates of the rates of sea-level change (mm/yr) for the separate contributions compared to the observations, for the period 1961-2003 in blue and 1993-2003 in brown (Figure 5.21 from Bindoff et al., 2007).*

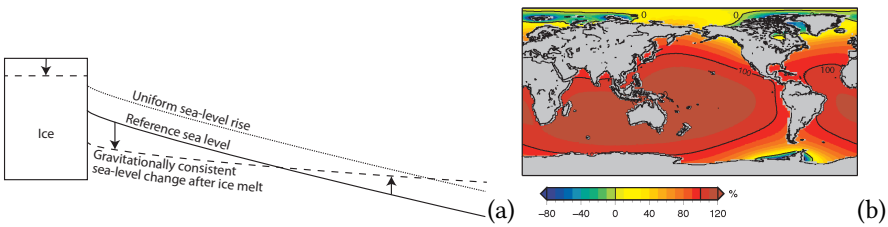

Figure 1.8: *The gravitational effect explained* **(a)** *Conceptual figure of the gravitational effect* **(b)** *Gravitationally induced relative sea-level change pattern due to glacier melt, including rotational and deformational effects, relative to the global mean change (%).*

yet and thus the estimates of the dynamical contribution to sea-level change carry large uncertainties (e.g., Pritchard et al., 2009; Rignot et al., 2011).

A second source of fresh water is the water stored on the continents in for instance snow, lakes, permafrost, groundwater or dams, together referred to as the terrestrial contribution. Changes in terrestrial storage can be caused by climate change, such as permafrost melt or snow melt, but also by human influences, such as the building of dams, or a combination of both, such as groundwater storage change. In IPCC AR4, the net contribution of the terrestrial exchange is estimated at zero for the past century (Bindoff et al., 2007), and thus not included in Figure 1.7. However, more recent studies point towards an increasing terrestrial contribution to sea-level change in the near future. Recent estimates of water impoundment behind dams (Chao et al., 2008) indicate that this has been a negative contribution to sea-level change over the past century, causing a sea-level fall. However, the number of newly built dams is decreasing, which means that this negative contribution will become smaller in the future. In contrast, groundwater extraction is a large positive contributor to global mean sea-level rise (Konikow, 2011; Wada et al., 2012), and is currently estimated to be larger than the water storage behind dams, with increasing values in the future.

All mass changes, either from land ice or from terrestrial exchange, have a distinct influence on the regional sea-level change pattern. When water is added to the ocean due to for instance glacier melt, one would intuitively expect that the water is divided equally over the ocean surface, thus causing a uniform sea-level rise. However, there are gravitational effects that need to be considered when redistributing the water, which cause a non-uniform sea-level change (Woodward, 1886; Farrell and Clark, 1976; Mitrovica et al., 2001). According to Newton's law of universal gravitation, mass attracts mass. This means that the land ice and the ocean water attract each other, resulting in an ocean that is pulled up against the ice. This is indicated in Figure 1.8a by the line labeled 'Reference sea level'. This figure shows the concept of the gravitational effect in the absence of solid-earth deformation. In reality, the sea level is not higher around the ice sheets, because the weight of the ice sheet will cause a deformation of the solid earth over time. When in this conceptual figure a part of the land ice melts and the water is divided uniformly over the ocean, sea level will rise according to the line labeled 'Uniform sea-level rise'. However, due to the gravitation on Earth, the gravitational pull of the ice decreases when the ice melts. As a result the ice melt instead leads to a lowering of the sea level close to the ice. Since there is mass added to the ocean, this implies that further away the sea level will need to rise to conserve the mass. This results in the line that is labeled 'Gravitationally consistent sea level after ice melt' in Figure 1.8a.

When the gravitational principle is applied to the melt of glaciers around the world, this results in a sea-level change pattern as shown in Figure 1.8b. The figure shows the sea-level change relative to the global mean sea-level change in percentage as computed with a sea-level model. This sea-level model uses the gravitational effect which was described in the previous paragraph, and will be explained more thoroughly in

Section 2.1.3. In Figure 1.8b, the 100% lines show where the regional sea-level change is equal to the global mean sea-level change, which corresponds to the location in Figure 1.8a where the dashed and the dotted lines cross. The 0% lines in Figure 1.8b indicate locations with no sea-level change, which corresponds to the crossing of the dashed and the solid line in Figure 1.8a. Figure 1.8b demonstrates that even when water is added to the ocean by land ice melt, sea level will fall close to the main melt sources, for instance near Svalbard, the Canadian Arctic and the Antarctic Peninsula. It also shows that in the equatorial regions the sea level will rise more than the global mean value, which implies that regions further away from the source of the change will experience the largest sea-level rise. In the case of the Netherlands this means that melt in Antarctica will have a much larger impact than melt in Greenland, since Greenland is much closer. For the same amount of melt on both ice sheets, the Dutch coast will experience three times more sea-level rise from Antarctic melt than from Greenland melt.

The gravitational effect needs to be considered for all contributions to sea-level change that involve an addition or removal of ocean load, so it applies not only to the land ice contributions but also to the terrestrial exchange contribution. Therefore, even when the global mean contribution of for instance the terrestrial exchange is zero as estimated in IPCC AR4 (Bindoff et al., 2007), this does not result in zero sea-level change at a regional scale, since the sea-level pattern is determined by the location of the mass change.

Apart from the change in the gravitational field as described above, the redistribution of mass due to ice melt or terrestrial exchange will also affect the Earth's rotation rate and the location of the rotation axis with respect to the Earth's surface. The rotation rate of the Earth can be compared to that of a spinning ice skater: rotation is slower when the skater stretches his arms, comparable to more mass on the Earth's equator, and rotation is faster when the arms are pulled in, comparable to more mass near the poles. In addition to the rotation rate, the location of the rotation axis with respect to the Earth's surface can change due to mass variations at the surface and inside the Earth. Because the Earth is deformable, it can adapt to these mass changes by shifting the rotation axis over the surface. This phenomenon is called polar wander. Polar wander occurs on timescales of days, due to atmospheric pressure change or ocean tides, to timescales larger than centuries, due to Glacial Isostatic Adjustment. These variations in rotation axis and rate are caused by redistributions of mass, but in turn also cause mass redistribution, and thus have a distinct influence on the regional sea-level pattern.

In addition to the rotational and gravitational effects, there is a response of the solid earth to changes in the mass loading at the Earth's surface, which causes regional variations in sea-level change. The relaxation of the solid earth is a viscoelastic process, which is a combination of instantaneous -elastic- and delayed -viscous- behaviour. The initial response to loading or unloading mass is instantaneous or elastic, which results in a direct uplift or depression of the crust. Additionally, there is a more gradual or

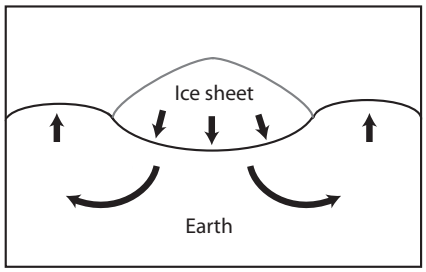

(a)

(b)

Figure 1.9: (a) *Principles of Glacial Isostatic Adjustment* **(b)** *Boat house above sea level, near Gävle, Sweden (photo: A. Slangen).*

viscous effect on timescales in the order of thousands of years, which is called Glacial Isostatic Adjustment (GIA) (e.g., Vermeersen and Schotman, 2009). During an ice age, large ice sheets are formed, thus locally increasing the load, which depresses the crust (see Figure 1.9a). Consequently, mantle material flows away from this location, and causes a downward movement below the ice sheet, and an upward movement around the ice mass which forms the so-called peripheral bulges. When the ice sheet melts again, the process takes place in reverse order, causing an uplift at the former location of the ice sheet and a downward movement of the bulges. At present, the melt of the large ice sheets after the Last Glacial Maximum (LGM) and the redistribution of their meltwater still influences sea level everywhere. In regions like Scandinavia and the Hudson Bay, GIA is even the dominant process in sea-level change, with an uplift of up to 1 cm/year. In Scandinavia we find for instance boat houses that were built 100 years ago which are now located 1 meter above sea level (Figure 1.9b). This implies that GIA is a very important process to consider for regional sea-level changes. GIA is implicitly included in Figure 1.7, because the tide gauge measurements have been corrected for GIA. GIA also explains most of the regional differences in the long sea-level records that are shown in Figure 1.1. The figure shows that for locations in former ice covered regions (A and D) GIA results in sea-level fall, where former ice free regions (E and H) show a sea-level rise.

In addition to the previous processes, volume changes caused by density variations are an important contribution to global and regional sea-level change. Density variations can be caused by variations in temperature or salinity in the ocean water. When ocean water heats up in a warming climate, the density decreases, which leads to an increase in volume and thus to sea-level rise. In this way, warming the water with 0.1°C can cause a sea-level rise of 1 to 2 cm over a water column of 1000 m (Church et al., 2010). For the period 1993-2003, the global mean contribution from temperature changes is estimated to be approximately half of the observed total global mean sea-level rise (Figure 1.7). Salinity changes have the opposite effect: a higher salinity leads to increasing density and thus decreasing volume and sea-level fall. Salinity variations can for instance occur locally through the addition of fresh water to the ocean. Averaged over the entire ocean however, the salinity component is very close to zero, since

the total salt content in the ocean barely changes. This means that for global mean sea-level change, salinity can be neglected. However, when looking at regional sea-level variations through density changes, both temperature and salinity need to be considered, although temperature is the dominant contribution (Church et al., 2010). The combined temperature -thermosteric- and salinity -halosteric- contribution is referred to as the steric contribution.

1.3 Recent developments in sea-level research

The introduction of satellite altimetry by the end of the twentieth century was an important step forward for sea-level research. Global maps of sea-level change became available, which was a major contribution to the understanding of sea-level change processes. In addition to satellite altimetry, the Argo-network was launched in 1999 and expanded to over 3000 floats since 2000 (Gould et al., 2004). The Argo network monitors temperature and salinity in the upper 1–2 km of the ocean, thus providing valuable information on the spatial distribution of steric variations. Also for the other contributions new measurement methods were set up, such as ESA's CryoSat or NASA's ICESat to monitor the land ice mass changes. Combining all these types of measurements has led to a better understanding of the processes causing sea-level change.

Despite the advances in understanding the contributing processes, in 2007 the global mean sea-level budget for the period 1961-2003 could still not be closed in the IPCC AR4 (Bindoff et al., 2007, Figure 1.7). Measurements over the period 1961–2003, primarily done by tide gauges, indicated a global mean rate of change of around 1.8 mm/yr (Douglas, 2001; Miller and Douglas, 2004; Church et al., 2004; Holgate and Woodworth, 2004; Church and White, 2006). The contribution of land ice for this period was estimated at approximately 50%, while about a quarter was attributed to steric variations (Figure 1.7, blue bars). This resulted in a gap between measured and explained sea-level change, since the estimated contributions only added up to 1.1 mm/yr, albeit with large uncertainties. For the more recent period of 1993–2003, the difference between measured and explained sea-level change was found to be zero within the uncertainty ranges (Figure 1.7, brown bars), likely due to the satellite-based global observational data that are available for that period.

A major part of the sea-level research after IPCC AR4 focused on closing the global mean sea-level budget for the 1961–2003 period. Several studies found that the contribution of the steric component was underestimated in IPCC AR4 (Domingues et al., 2008; Ishii and Kimoto, 2009; Levitus et al., 2012). This was caused by instrumental biases in measurements from bathythermographs, instruments that measure temperature versus depth (Gouretski and Koltermann, 2007; Wijffels et al., 2008; Levitus et al., 2009). Also, new estimates for the deep ocean component below 700 m depth have been published recently (Purkey and Johnson, 2010; Levitus et al., 2012), which was before assumed constant over the entire ocean basin. Other studies (e.g., Moore et al., 2011;

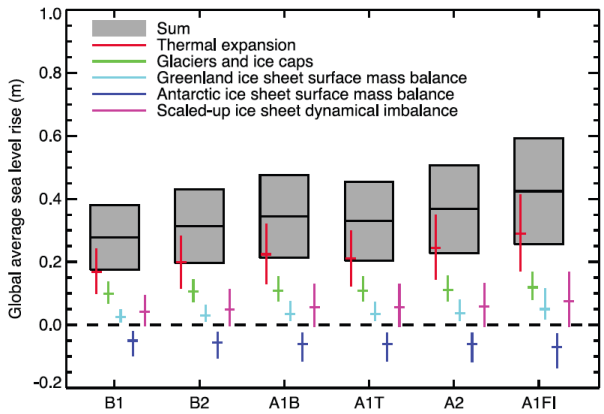

Figure 1.10: *Global mean sea-level change projections (m) between 1980–1999 and 2090–2099 based on six SRES scenarios. Sum does not include scaled-up ice sheet dynamical imbalance (Figure 10.33 from Meehl et al., 2007b).*

Church et al., 2011) use higher land ice estimates to decrease the discrepancy between measurements and models. For the glacier contribution this is based on results from Cogley (2009b) and Radić and Hock (2010), and for the ice sheet estimates it is based on Rignot et al. (2008b), Rignot et al. (2011) and Van den Broeke et al. (2009). Also the addition of groundwater depletion estimates (Konikow, 2011; Wada et al., 2012) and dam retention estimates (Chao et al., 2008) helped closing the budget. Another possible explanation for the discrepancy between observed and explained sea-level rise over this period could be related to regional effects.

Apart from a sea-level budget over the past half century, IPCC AR4 also presented global mean sea-level projections for the end of the twenty-first century (Figure 1.10, Meehl et al., 2007b). Figure 1.10 shows the IPCC AR4 projections for 6 different emission scenarios, ranging from a conservative and environmental friendly scenario -B1- to a strongly warming and fossil-fuel intensive scenario -A1F1-. These ranges are based on an ensemble of Atmosphere-Ocean coupled General Circulation Models (AOGCM's). For all scenarios, the expected average rate of sea-level rise is higher than the rate that was observed in the twentieth century (Figure 1.7), but the uncertainties are large, which leads to a wide range of projections.

In addition to the global mean projections, IPCC AR4 showed a regionally varying sea-level projection for the steric component (Meehl et al., 2007b, their Figure 10.32), but not for any of the other sea-level contributions. However, regional sea-level change is more relevant for coastal management than global mean values, and therefore regional sea-level variability became a focal topic in sea-level change research since IPCC AR4. For instance, the steric sea-level pattern as presented in IPCC AR4 was further studied, focusing on the common features and the large differences in regional steric patterns between the climate models (e.g., Pardaens et al., 2010, 2011; Yin et al., 2010).

Other studies have considered the influence of mass changes on the sea-level pattern due to gravitational effects, either from land ice changes or from terrestrial exchange processes (Mitrovica et al., 2009; Bamber et al., 2009; Bamber and Riva, 2010; Riva et al., 2010). Regional patterns of the projected twenty-first century contribution from land ice melt to sea-level rise were first presented in Slangen et al. (2012, Chapter 4 of this thesis). Also, the influence on the ocean circulation of the addition of fresh water due to the melt of the ice sheets has been studied intensively. It was found that the response of the ocean to fresh water forcing ranges from a fast response in the order of days (Gower, 2010; Lorbacher et al., 2012), to a response in the order of decades (e.g. Stammer, 2008; Stammer et al., 2011), depending on the type of flow that is studied. However, none of these studies present projections beyond 50 years into the future. The influence of water impoundment behind dams on the spatial pattern of sea-level change was presented in Fiedler and Conrad (2010), but only for the past half century.

So far, there are only a few studies which have combined regional patterns from the steric and the mass contributions to sea-level change (Kopp et al., 2010; Slangen et al., 2012), and only Slangen et al. (2012) included GIA and provided projections for twenty-first century sea-level change. The next step is now to add more processes and to reduce the uncertainties that are associated with regional projections. For this, a better understanding of all contributions to sea-level rise and their influence on regional variability is needed.

1.4 This thesis

The research that is described in this thesis focuses specifically on modelling the regional patterns in sea-level change. Although all the above-mentioned processes will be considered, emphasis lies on the glacier contributions and the resulting influence of ice mass changes on the gravitational pattern in the ocean. Chapter 2 describes the models and theory that were used in this thesis to obtain regional fields of sea-level change for each of the contributions. The subsequent chapter will focus on past sea-level variations, between 1961 and 2003, and show whether the measured regional variations by tide gauges can be reproduced by the models and data that are currently available. This will be an indication of our level of understanding of the processes causing sea-level change at a regional scale. Chapter 4 will then focus on the future, and show how the output from atmosphere-ocean coupled climate models can be used to project future regional sea-level variations. The main goal of this chapter is to show the regional patterns that belong to the global mean values as presented in the IPCC AR4 report (Meehl et al., 2007b). An important contributor to sea-level change is the change in mass of glaciers and ice caps. Chapter 5 describes an uncertainty analysis of the glacier model used to project future glacier changes, and gives an indication which factors need to be improved to reduce these uncertainties. Finally, Chapter 6 presents the most recent regional sea-level projections for the twenty-first century. The thesis is concluded with a brief summary of the main results.

CHAPTER 2

Theoretical background

This chapter will focus on the methodology used to model the sea-level change processes that were introduced in Chapter 1. The mass change contributions to sea-level change are presented in Section 2.1. This section describes the principles of the volume-area based glacier model used to project the glacier contribution to sea-level rise, and the ice sheet and terrestrial contributions. The section ends with a derivation of the equation used in the sea-level model to compute gravitationally consistent sea-level patterns. Section 2.2 presents the methodology for the steric contribution. Section 2.3 will focus on the Glacial Isostatic Adjustment contribution to regional sea-level change. The final section of this chapter explains how the contributions are combined into a total sea-level change pattern.

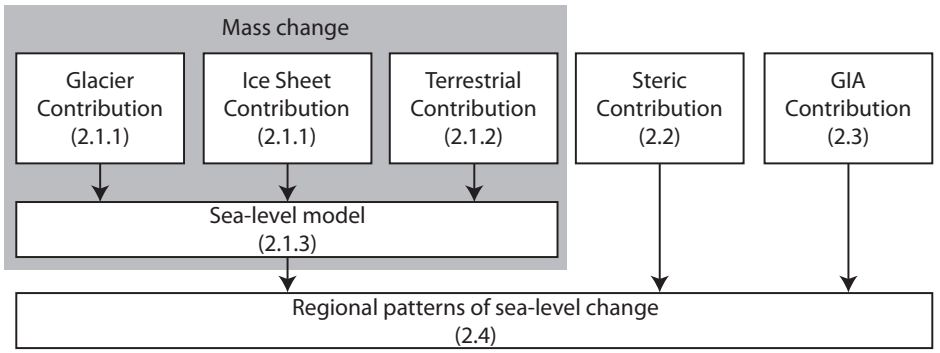

Figure 2.1: *Diagram depicting the methodology used to compute regional patterns of sea-level change. Numbers in brackets refer to the section in which each contribution is described.*

2.1 Mass contribution

2.1.1 Land ice contribution

The majority of land ice is stored in the two large ice sheets on Greenland and Antarctica. Only 1% of the land ice is stored in the Glaciers and Ice Caps (GIC) outside the ice sheets. However, they are of major interest for sea-level change research on century timescales, since most have been rapidly retreating the past century, thereby accounting for over 50% of the land ice contribution to current sea-level rise (Figure 1.7, Bindoff et al., 2007; Steffen et al., 2010). A significant contribution is to be expected for the near future, as the response time of GIC to climate changes is typically in the order of several decades, depending on the GIC's geometry and mass turnover (Leclercq and Oerlemans, 2012, and references therein).

Glaciers and ice caps (GIC)

GIC are slowly moving masses of ice, located there where the annual snow fall exceeds the annual melt. Over time, the snow will turn into ice under the influence of its own weight and temperature variations. The ice flows from the accumulation area, where annual snowfall exceeds annual melt, towards the ablation area, where there is more ice melt than snow fall. The net mass gain or loss over these areas determines the total mass balance of the GIC. If the mass balance is zero, GIC are in balance with climate. The total mass balance is the sum of the surface mass balance - mainly snowfall and melt - and other processes, such as calving at the glacier terminus or subglacial melt. The altitude that separates the accumulation area from the ablation area is called the equilibrium line altitude (ELA). This altitude is largely determined by temperature, since temperature generally decreases with altitude, allowing snowfall above a certain altitude and melt below a different altitude. However, also precipitation is very important, and large amounts of snowfall may lower the ELA, since more energy is needed to melt the thicker snowpack. If precipitation remains constant, the ELA shifts to higher altitudes in a warming climate. This decreases the accumulation area and increases the ablation area, and thus will cause the mass balance of the GIC to decrease, which means that they will shrink.

GIC are generally situated in warmer and wetter climates than the two large ice sheets, which causes them to have a relatively large mass turnover, a short response time and a large climate sensitivity. Therefore, they adapt to changes in climate much faster than the ice sheets. Nevertheless, GIC still need time to adjust to changing conditions, and thus in a changing climate they are constantly in imbalance with climate.

Over time, several methods have been developed which are used to estimate the evolution of GIC and their response to climatic changes. A physically based approach would be to use flow line models forced by appropriate mass balance schemes. However, these require detailed input, such as bed topography, ice thickness and knowledge of the microclimate. These data are not available for the more than 200,000 GIC

on Earth, and therefore it is not possible to use this approach on a global scale yet. As an alternative, scaling methods can be used, which are based on relatively simple geometric features of glaciers, such as the length or the area, and their relation to the volume of the GIC. Examples are volume-length scaling (Oerlemans et al., 2007; Leclercq et al., 2011), volume-area scaling (e.g. Bahr et al., 1997; Van de Wal and Wild, 2001), or volume-area-length scaling (Radić and Hock, 2011). These methods use empirical relations derived for a small set of GIC, which are extended to a global scale. Additionally, the required mass balance changes may be obtained by using seasonal sensitivity characteristics (Oerlemans and Reichert, 2000), by modelling the changes in mass balance profiles (Raper and Braithwaite, 2006), by applying a simplified mass balance model (Radić and Hock, 2011), or by using a relation between mass balance sensitivity and precipitation (e.g. Gregory and Oerlemans, 1998; Van de Wal and Wild, 2001). An even more schematic way to obtain a global estimate of GIC changes is to use a scaling relation between global temperature change and total ice volume without area size classes or latitudinal dependence, as applied in the Intergovernmental Panel on Climate Change (IPCC) Fourth Assessment Report (AR4) (see Appendix 10.A.3 in Meehl et al., 2007b).

For Chapters 4 to 6 of this thesis, we use a glacier model that is based on the volume-area scaling method (e.g. Bahr et al., 1997; Van de Wal and Wild, 2001) to project GIC volume changes. This methodology was developed by Bahr et al. (1997), who derived a theoretical relation between volume and surface area of glaciers, and confirmed the theory using observations from 100 glaciers. The volume-area method assumes that the area of a GIC is proportional to its volume using a power law:

$$V = cA^{\gamma}, \tag{2.1}$$

where c and γ are scaling parameters. These parameters can be derived using observations. Unless mentioned otherwise, we use for glaciers a value of 1.375 for γ (Bahr et al., 1997; Chen and Ohmura, 1990), and 1.25 for ice caps (Bahr et al., 1997). For c we adopt the value of 0.2055 $\mathrm{m}^{3-2\gamma}$ for glaciers and 1.7026 $\mathrm{m}^{3-2\gamma}$ for ice caps, as derived by Radić and Hock (2010). The sensitivity of the volume-area model to small variations in these parameters will be described in Chapter 5 of this thesis.

The specific glacier model used in this thesis is developed by Van de Wal and Wild (2001), and it calculates the evolution of GIC in time given a certain initial glacier inventory. The volume change of all GIC is calculated while accounting for the change of glacier area (A) in time (t), mass balance (B), temperature changes (ΔT) and precipitation changes (ΔP), by applying the following expression:

$$\frac{dV}{dt} = \sum_{j=1}^{n}\sum_{k=1}^{m} A(j,k,t) \cdot \left\{ \Delta T_{\mathrm{s}}(j,t)\frac{dB_{P(j,t)}}{dT_{\mathrm{s}}} + \Delta T_{\mathrm{ns}}(j,t)\frac{dB_{P(j,t)}}{dT_{\mathrm{ns}}} + \Delta P(j,t) \right\} \tag{2.2}$$

In Equation 2.2, glacier area A is summed over n regions and m size bins. dT_{s} are local summer temperature variations (summer is June/July/August in the Northern Hemisphere, December/January/February in the Southern Hemisphere), and dT_{ns} are non-summer temperature variations. The mass balance sensitivity is a function of the local annual precipitation P according to the relations from Zuo and Oerlemans (1997):

$$\frac{dB}{dT_{\mathrm{s}}} = -0.259P^{0.427} \tag{2.3}$$

$$\frac{dB}{dT_{\mathrm{ns}}} = -0.387P^{0.683} + 0.259P^{0.427} \tag{2.4}$$

Temperature (T) and precipitation (P) are taken from Atmosphere-Ocean General Circulation Models (AOGCM's) using the nearest neighbour approach (Van de Wal and Wild, 2001). Both T and P are time dependent, which implies that the mass balance sensitivity itself changes over time as well. Furthermore, the model requires a prescribed present-day area and volume of all GIC, which are taken from a glacier inventory.

To illustrate how the GIC in the volume-area model respond to changes in temperature and precipitation, we show results from a few simple experiments. As input for the model we use a glacier inventory that is an extended version of the WGI-XF (Cogley, 2009a), which has a World Glacier Inventory core (WGI, National Snow and Ice Data Center, 1999), and is combined with Icelandic and Alaskan data (Radić and Hock, 2010). The GIC are sorted into 19 larger regions in the world according to Figure 2.2. More information on this inventory can be found in Chapter 5 of this thesis. To account for the present imbalance of the GIC with climate, the model applies a global temperature increase of 0.7 °C 100 yr^{-1} over the period 1865 to 2009 (Trenberth et al., 2007). The initial precipitation rate is taken from climate model data, using 12 AOGCM's from the CMIP5 data base, as presented in Chapter 4 of this thesis. This is needed to determine the mass balance sensitivity as given in Equations 2.3 and 2.4.

Figure 2.3 shows the results of experiments with no temperature and precipitation change compared to global temperature changes of 1, 2 or 4 °C 100 yr^{-1} in combination with precipitation changes of 0, 5 or 10% per K. All volume is normalized with respect to the total volume in 2010. It is striking that even when no temperature or precipitation changes are applied, by 2100 the GIC will have lost 12% of their original volume in 2010. This is because the GIC are not yet in balance with the present climate, there is a time lag. This shows that the volume loss would be underestimated if this present imbalance is not accounted for, as will also be discussed in Section 5.4.1.

When comparing the solid lines in Figure 2.3, which represent temperature change only, we see that a larger temperature increase causes more volume loss. For an increase of 1 °C 100 yr^{-1}, the volume is reduced to only 83% of its original volume in 90 years, while a temperature increase of 4 °C 100 yr^{-1} leaves only 72%. This shows that the amount of volume loss is not linearly related to temperature increase. For a 1 degree warming, an additional 5% of the initial volume is lost, while for a 4 degrees

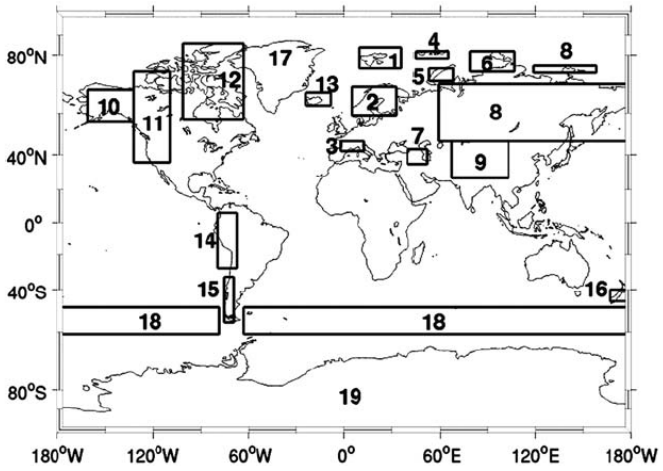

Figure 2.2: *Glacier region distribution, from Radić and Hock (2010).*

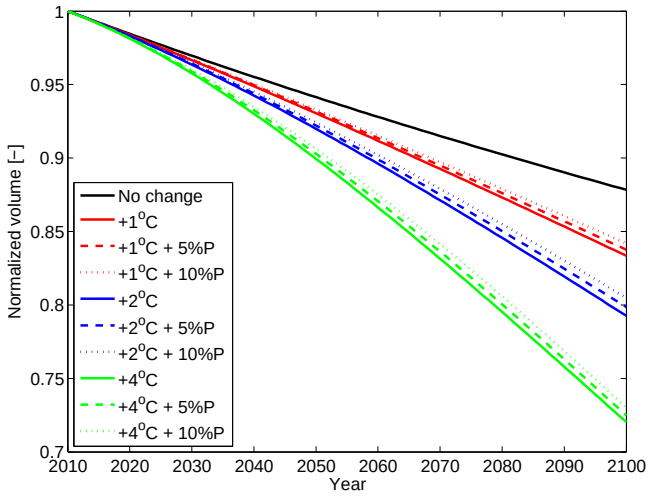

Figure 2.3: *Normalized GIC volume ($\frac{V_t}{V_{2010}}$), using simplified future scenarios for the volume-area glacier model. Colours indicate different temperature variations in degrees per century. Dashed and dotted lines indicate a precipitation increase of 5% and 10% per degree warming, respectively.*

warming, the additional loss is 14%, or 3.5% per degree. This is because the small GIC disappear quickly in any of these scenarios, while the response time of the larger GIC is longer than the period of 90 years shown here, and thus these will be maintained over the next 90 years (see also Figure 5.4).

In contrast to temperature change, a precipitation increase has a small but positive effect on the glacier volume, as shown by the dashed lines in Figure 2.3. This is because

more precipitation means that more mass will be added to the glacier, thus giving it a more positive, or less negative, mass balance. However, the volume-area model uses the precipitation to compute the mass balance sensitivity (Equations 2.3 and 2.4), which means that if the precipitation is increased, so is the sensitivity of the glaciers' mass balance to temperature variations. If the mass balance sensitivity would be set to be constant, more precipitation would have a larger positive effect than is now displayed in Figure 2.3. However, since the mass balance sensitivity is not constant, the increase in sensitivity largely compensates for the positive effect of the increased precipitation amount resulting in the dashed lines in Figure 2.3. As a result, the positive influence of a precipitation increase is not nearly as large as the negative influence of an increasing temperature.

In Chapters 4 to 6 of this thesis, the temperature and precipitation forcing used for the glacier model are based on climate model output. This spatially varying climate forcing, combined with the evolution of glacier volume change in predefined regions, will be used to compute a regional sea-level pattern of the GIC contribution to sea-level change.

Greenland and Antarctic ice sheet

Although GIC currently account for a large contribution to sea-level rise, the two largest ice masses on Earth, the Greenland Ice Sheet (GIS) and the Antarctic Ice Sheet (AIS) cannot be ignored. They can potentially contribute around 65 meters to global mean sea-level rise (Lemke et al., 2007). It is therefore crucial to understand the processes that regulate the mass transport from the ice sheets to the ocean. Because the ice sheets are in a cold and dry climate, their mass turnover is relatively small and thus the response time is very large. Due to their different size, geometry and dominant physical processes, the volume-area approach cannot be used to model the evolution of the ice sheets. Instead, different methods to estimate the ice sheet contribution to sea-level change are used throughout this thesis, which will be described in each chapter separately. This section will only briefly describe the main processes that determine ice sheet mass loss.

The ice sheets are very large masses of ice, formed by snow compaction. Under the influence of its own mass, the ice flows towards the margins of the ice sheet, where it enters the ocean, through either meltwater runoff or calving of ice-bergs. The surface mass balance (SMB) of an ice sheet is, similar to that of a glacier, defined as the net mass gain or loss at the surface. The mass gain is mainly snowfall, but can also be from water vapour deposition or rainfall. Mass loss at the surface occurs through meltwater runoff and snow sublimation. The SMB is largely determined by the climate on the ice sheet, and can therefore be modelled using regional atmospheric climate models such as RACMO2 (Ettema et al., 2009; Lenaerts et al., 2012).

However, the total mass balance of the ice sheets has another important component, being the discharge of ice at the margins of the ice sheet. In the past decade, accelerations in the dynamical discharge have been observed (e.g., Velicogna, 2009;

Rignot et al., 2011; Howat et al., 2011), which cannot be explained by warm air temperatures. These dynamical processes include for instance an increased velocity of Antarctic and Greenland outlet glaciers caused by thinning of the glaciers and ice shelves (e.g., Pritchard et al., 2009), or grounding line migration on an inland slope (e.g., Vaughan, 2008). The processes governing these changes are still only marginally understood, although there is increasing evidence that basal melting of ice shelves plays an important role (Pritchard et al., 2012). Therefore, in this thesis we will use several estimates for the dynamical discharge, which are based on extrapolation of observations, and are very uncertain since it is unknown whether the current changes will continue, decrease or accelerate.

2.1.2 Terrestrial water storage contribution

Apart from the land ice, there are also many other sources of water on the continent which may contribute to sea-level change. These are together referred to as the terrestrial water storage contribution. We can distinguish three types of terrestrial storage: surface storage - e.g., lakes, rivers, wetlands, reservoirs -, subsurface storage - groundwater, soil water -, or snowpack storage (Meehl et al., 2007b). Because the sources and sinks of terrestrial water storage are very diverse in location and size, detecting and modelling these changes is very difficult (Milly et al., 2010).

The amount of water storage on land may change either due to climatic change (natural or anthropogenic), or due to direct human influence. Climate-driven changes can for instance occur in the snowpack, permafrost, shallow groundwater or surface water such as lakes. The latter may also change due to direct human influences, for instance by using the lake water for irrigation purposes. However, the two largest contributions to sea-level change from terrestrial water storage exchange are human-induced. The building of dams and artificial reservoirs is a large sink and groundwater mining a large source (Milly et al., 2010).

The building of dams and artificial reservoirs causes a sea-level fall, with an amount of water stored in reservoirs that has been increasing in de 20^{th} century to a total of around 10,800 km^3 (Chao et al., 2008). The rate of sea-level change resulting from water impoundment behind dams was around -0.5 mm yr^{-1} in the 1980's and has now decreased to around -0.25 mm yr^{-1}, because less dams are being constructed.

Groundwater mining is a terrestrial component which causes sea level to rise. In dry regions, groundwater is often the only source of freshwater. However, groundwater is not easily refilled and therefore the excess groundwater ends up in the ocean. Estimates of the current contribution differ depending on the method used. For instance, Wada et al. (2010, 2012) use a flux-based method, which computes the difference between groundwater abstraction and recharge. They find that the groundwater contribution to sea-level rise increased from 0.035 ± 0.0009 mm yr^{-1} in 1900 to 0.57 ± 0.09 mm yr^{-1} in 2000, with an expected increase to 0.82 ± 0.13 mm yr^{-1} in 2050. In the study by Konikow (2011) on the other hand, a volumetric approach is used, which considers confined areas where groundwater depletion is taking place.

Konikow (2011) finds a contribution of 0.014 mm yr $^{-1}$ between 1900 and 1950, and 0.403 mm yr $^{-1}$ for the period 2001–2008, which is substantially lower than the estimates by Wada et al. (2012). Whereas the dam impoundment contribution is decelerating, the groundwater contribution is increasing and expected to keep on increasing in the coming century (Milly et al., 2010; Wada et al., 2012). Hence, the net terrestrial storage is foreseen to increase in the future.

To obtain the regional pattern of sea-level change that results from the terrestrial component, it is not only important to know how large the global contribution to sea-level change is, but also to know where these mass variations take place. The estimates of Wada et al. (2012) and Chao et al. (2008) provide such regional information and can therefore be used to compute regional sea-level patterns, as will be shown in Chapter 3.

2.1.3 The sea-level model

All the changes of mass discussed in the previous two sections have a distinct effect on the regional pattern in sea-level change. This section will explain the cause of these regional variations using a melting ice sheet as an example. Note however that this effect must be considered for all mass changes and therefore also for terrestrial water storage exchange contributions.

When land ice melts, water is added to the ocean. If the water is distributed uniformly over the ocean area, the eustatic or global average sea-level rise (ϵ_e) can be computed according to

$$\epsilon_e = \frac{M_i}{A_w \rho_w} \tag{2.5}$$

with M_i the ice mass, A_w the ocean surface area and ρ_w the ocean density (~ 1028 kg/m^3). However, this equation does not account for the fact that melt water from land ice does not distribute uniformly over the ocean due to gravitational effects and induced changes in the shape and rotation of the Earth (e.g. Woodward, 1886; Farrell and Clark, 1976; Vermeersen and Sabadini, 1999). Instead, we need to use the sea-level equation to compute sea-level changes as a result from mass redistribution from the ice sheets to the ocean. In this section we will therefore show the derivation of the standard sea-level equation following Farrell and Clark (1976) and Vermeersen and Schotman (2009).

Let us assume that the Earth is completely covered by water, then the gravitational potential (ϕ) on the Earth's surface can be described by

$$\phi(r) = \frac{GM_e}{r} \qquad (r \geq R) \tag{2.6}$$

with G the gravitational constant ($\sim 6.673 \cdot 10^{-11}$ $m^3 kg^{-1} s^{-2}$), M_e the Earth's mass including the water at the surface, r the radial distance and R the radius of the Earth (~ 6371 km).

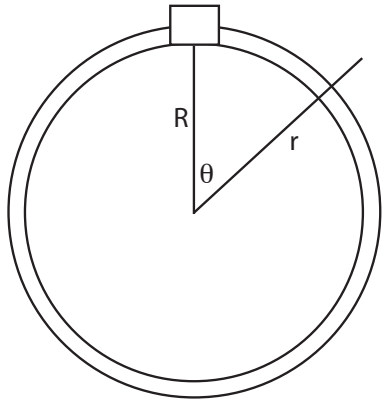

Figure 2.4: *Simplified Earth with uniform ocean and ice sheet.*

If an ice mass is formed in a point mass at the Earth's surface (see Figure 2.4), the gravitational potential will change and depend on the radius r and the angular distance θ from the ice mass M_i according to

$$\phi_1(r,\theta) = \frac{G(M_e - M_i)}{r} + \frac{GM_i}{\sqrt{r^2 + R^2 - 2Rr\cos\theta}}. \tag{2.7}$$

For $r = R$, this equation can be written as

$$\phi_1(R,\theta) = \frac{G(M_e - M_i)}{R} + \frac{GM_i}{2R\sin(\theta/2)}, \tag{2.8}$$

which results in a potential field that is not radially symmetric anymore, and thus a uniform sea-level change cannot be a solution any longer. The sea level is instead at small distance

$$\phi_1(R+\epsilon,\theta) = \phi(R). \tag{2.9}$$

Since $M_i \ll M_e$ and $\epsilon \ll R$, the new potential to first order can be written as

$$\phi_1(R+\epsilon,\theta) = \phi_1(R,\theta) + \epsilon\frac{\partial\phi_1(R,\theta)}{\partial r}. \tag{2.10}$$

Using $\partial\phi_1/\partial r = \partial\phi/\partial r = -g$ and $g = \frac{GM_e}{R^2}$, with g the gravitational acceleration ($= 9.81\ m/s$), ϵ can be expressed as

$$\epsilon(\theta) = \frac{M_i R}{M_e}\left(\frac{1}{2\sin(\theta/2)} - 1\right). \tag{2.11}$$

Since every $R+\epsilon+c$ is an equipotential surface for $c \ll R$, we need the conservation

of mass to find the equipotential surface that represents the sea level. The amount of water extracted from the ocean must be equal to the water added to the ice (conservation of mass), following

$$\int_0^{2\pi}\int_0^{\pi}\int_R^{R+\epsilon+c} dV = -M_i/\rho_w, \tag{2.12}$$

where $dV = r^2\sin(\theta)drd\theta d\phi$, which gives

$$2\pi\int_0^{\pi}\rho_w c R^2\sin\theta d\theta + M_i = 0. \tag{2.13}$$

In combination with the mass of the Earth $M_e = \frac{4}{3}\pi R^3\rho_e$ (ρ_e the Earth's density $= 5500\ kg/m^3$), for c this yields

$$c = -\frac{M_i R\rho_e}{M_e 3\rho_w}. \tag{2.14}$$

Combining Equations (2.11) and (2.14) gives the actual sea-level change as a difference in radial distance between the initial and the final sea surface:

$$\epsilon(\theta) + c = \epsilon_1(\theta) = \frac{M_i R}{M_e}\left(\frac{1}{2\sin(\theta/2)} - 1 - \frac{\rho_e}{3\rho_w}\right). \tag{2.15}$$

This equation represents the sea-level change as a consequence of the loss of ocean mass and the addition of ice mass, with the gravitational effect included, in contrast to the eustatic sea-level change in Equation (2.5). The eustatic change for a melting ice sheet on an Earth with a completely water-covered surface is represented in the last term on the right of Equation (2.15):

$$\epsilon_e = \frac{M_i R}{M_e}\frac{\rho_e}{3\rho_w} = \frac{M_i R\rho_e}{\frac{4}{3}\pi R^3\rho_e 3\rho_w} = \frac{M_i}{4\pi R^2\rho_w} = \frac{M_i}{A_w\rho_w}. \tag{2.16}$$

The other two terms represent the distortion of the ocean surface due to the gravitational effect. The ratio (H) between eustatic (ϵ_e) and gravitational sea-level change (ϵ_1) can be computed following

$$H = \frac{\epsilon_1}{\epsilon_e} = \frac{\frac{1}{2\sin(\theta/2)} - 1 - \frac{\rho_e}{3\rho_w}}{\frac{\rho_e}{3\rho_w}}. \tag{2.17}$$

This ratio, as shown in Figure 2.5, indicates that irrespective of the amount of ice melt, the sea level falls for radial distance θ between 0 and $\sim$ 20 degrees ($\sim$ 2200 km), sea level rises less than the eustatic value for θ between $\sim$ 20 and 60 degrees ($\sim$ 6700 km), and rises more at a larger radial distance. This gravitational effect was first described by Woodward (1886).

However, this is not the only effect that needs to be considered. Changes in surface

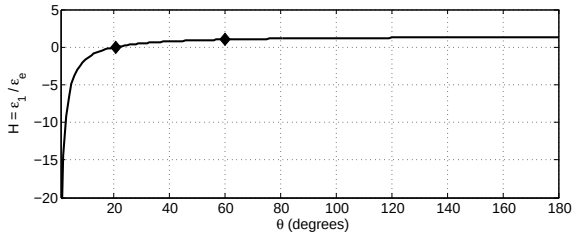

Figure 2.5: *Ratio of sea-level change with (ϵ_1) and without (ϵ_e) the gravitational effect taken into account, with respect to the radial distance from the melt source. Diamonds indicate where the ratio is 0 (no sea-level change) and 1 (eustatic sea-level change), respectively.*

load also cause deformations of the Earth's surface, which in turn affect the Earth's gravity field and cause an additional redistribution of ocean water. This was recognized by Farrell and Clark (1976), who derived the sea-level equation, which allows for computing the gravitational sea-level change pattern and solid-earth deformation due to ice mass variations. The sea-level equation contains the so-called Green function ϕ^G, which expresses the change in gravitational potential as a result of adding a point mass on the Earth's surface, and the response of the solid earth to this point mass. By convolving the Green function with the spatial distributions of ice mass changes (I) and sea-level changes (S), the net change in gravitational potential on the Earth's surface is

$$\phi_1(\theta, \lambda) = \rho_i \phi^G *_I I(\theta, \lambda) + \rho_w \phi^G *_O S(\theta, \lambda), \tag{2.18}$$

with ρ_i the ice density and $*_{I,O}$ the convolutions over the ice and ocean area. This change in gravitational potential causes a change in sea level, which is at a different potential surface

$$S(\theta, \lambda) = \frac{\phi_1(\theta, \lambda)}{g} + c, \tag{2.19}$$

where c includes the conservation of ice and ocean mass $M_I - M_O = 0$. Combining 2.18 and 2.19 yields the sea-level equation

$$S(\theta, \lambda) = \frac{\rho_i}{g} \phi^G *_I I(\theta, \lambda) + \frac{\rho_w}{g} \phi^G *_O S(\theta, \lambda) + c \tag{2.20}$$

where we see that sea-level change is a function of itself. The first term on the right describes the change in gravitational potential through ice mass change, the second term the change through the redistribution of ocean water.

In addition to solid-earth deformation, the influence of these mass variations on the Earth's rotation rate and the position of the rotation axis needs to be considered (e.g. Mound and Mitrovica, 1998; Milne and Mitrovica, 1998; Vermeersen and Sabadini,

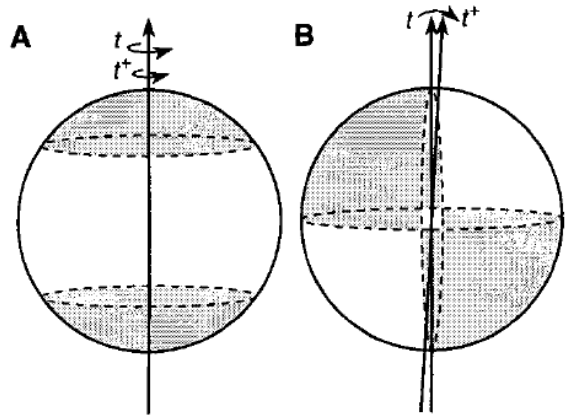

Figure 2.6: *Schematic illustration of regional sea-level changes due to variations in* **(a)** *the rate and* **(b)** *the orientation of the Earth's rotation vector from time t to t^+. The dashed lines indicate the line of no sea-level change, grey areas a sea-level rise and white areas a sea-level fall. Figure from Mound and Mitrovica (1998).*

1999). As explained in the introduction, the rotation rate and position of the rotation axis may change due to redistribution of mass. Figure 2.6a shows how changes in the rotation rate affect regional sea-level change. When the rotation rate decelerates, due to for instance tidal deceleration, sea level will rise in the grey-shaded areas and fall in the unshaded regions, making the Earth thinner at the equator and wider near the poles. The influence of changes in the position of the rotation axis results in a different pattern, as shown in Figure 2.6b. It divides the ocean surface into four parts, with the maximum local sea-level change at 45° from the poles.

All these effects -gravitation, solid-earth deformation and rotation- are incorporated in the sea-level model that is applied in this thesis. This model (Schotman, 2008) solves the sea-level equation using a pseudo-spectral approach (Mitrovica and Peltier, 1991). The Earth model is based on PREM (Dziewonski and Anderson, 1981), and is elastic, compressible and radially stratified. We may use this elastic approach, because we look at timescales in the order of a century when we consider the response of the Earth and oceans to present-day changes in ice masses and terrestrial storage. For long-term responses, a visco-elastic Earth model is needed to account for Glacial Isostatic Adjustment as a result from Late Pleistocene ice mass variations. This component is added as a separate contribution to sea-level change, as will be described in Section 2.3. Because the time scale for which we use the sea-level model is relatively short, we use a model that does not account for moving coastlines, since the increase or decrease of the ocean surface is negligible on these short timescales compared to the other effects that are considered. The ice density (ρ_i) is fixed at 918 kg/m^3 and the ocean density (ρ_w) at 1028 kg/m^3 (Millard et al., 1987).

Because all the terms in the sea-level equation depend on each other, sea-level

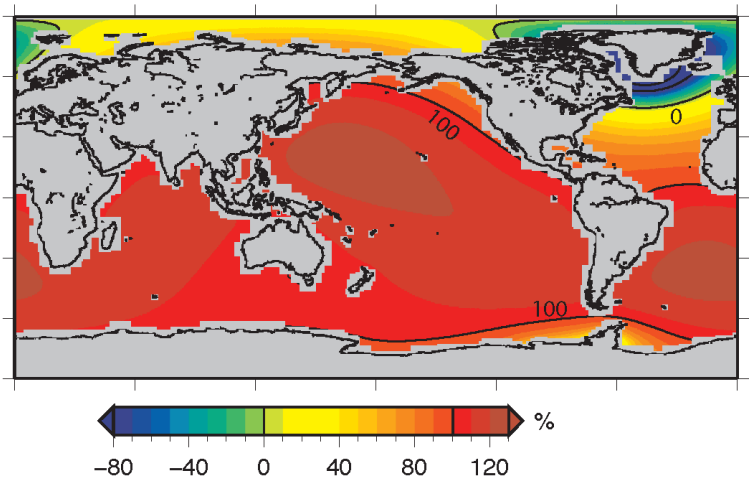

Figure 2.7: *Relative sea-level change pattern due to ice sheet melt based on IPCC AR4 ice sheet estimates (See Chapter 4), including gravitational, deformational and rotational effects, local change relative to the global mean change (%). Global mean is indicated by the 100%-line, no change by the 0%-line.*

changes as a result from mass changes cannot be computed at once. Instead, the model uses an iterative process to compute the new sea-level pattern. When mass is put in the ocean, it depresses the Earth's crust, and simultaneously changes the gravity field and rotation of the Earth. Gravitational changes then cause a redistribution of the water, and hence the load on the Earth's crust changes too, as well as the rotation. Usually three iterations are needed to converge to a new sea-level pattern. An example of a regional sea-level pattern resulting from ice sheet melt is shown in Figure 2.7. This figure shows that sea level falls close to the melt sources, and rises more when the distance to the melt source increases. Similar results from the sea-level model will be more thoroughly described in Chapters 3 to 6.

2.2 Steric contribution

An other important contribution to regional sea-level change is caused by density variations in the ocean water, which cause the volume to change. For the same input of heat, warmer water will expand more than colder water; more saline water will expand more than less saline water; and water at a larger depth and thus higher water pressure will expand more (Church et al., 2010). This means that the density will vary greatly depending on the circumstances, and thus local variations in density are therefore very important for local sea-level variations. Variations in sea level due to density variations from temperature and salinity changes are referred to as the steric contribution to sea-level change.

Over the past few decades, the global mean steric contribution is estimated to be around 25% of the total observed change for the period 1961-2003, increasing to 50% for the period 1993-2003 (See Figure 1.7, Bindoff et al., 2007). However, the exact value is still subject to debate. The observations presented in IPCC AR4 (Bindoff et al., 2007) were found to be influenced by an instrumental bias in the bathythermograph measurements (Gouretski and Koltermann, 2007), for which the more recent estimates have been corrected (Wijffels et al., 2008; Levitus et al., 2009). The past steric contribution is estimated by spatially interpolating the available temperature and salinity measurements since the 1950's. This leads to global mean values over the second half of the twentieth century ranging from 0.29 ± 0.06 mm yr^{-1} (Ishii and Kimoto, 2009) to 0.52 ± 0.8 mm yr^{-1} (Domingues et al., 2008) for the upper 700 meters of the ocean, and 0.54 ± 0.05 mm yr^{-1} for the upper 2000 meters (Levitus et al., 2012). These values are all based on the same data, but differ due to the use of different interpolation techniques to obtain ocean-covering fields from point measurements. In Chapter 3 we will use the Levitus et al. (2012) data set for the period between 1961 and 2003, since this is the only dataset providing an estimate for the upper 2000 meters, and is thus the most complete steric contribution estimate presently available.

For the future steric contribution to sea-level change, which will be presented in Chapters 4 and 6, we use output from an ensemble of AOGCM's. These models provide output for both past and future, such that, for the past decades, the output can be compared to measurements. Comparisons show that the CMIP3 AOGCM's can approximately reproduce the 1961-2000 temperature changes (Church et al., 2010), although there are differences between AOGCM's that include or exclude the volcanic forcing (Domingues et al., 2008; Gregory et al., 2012). For future projections, these climate models are driven by scenarios that describe either the emissions of greenhouse gas concentrations (Chapter 4) or the changes in radiative forcing (Chapter 6). When a range of climate models is forced by the same scenario, this provides an envelope of possible responses of the climate system to a certain forcing, the so-called model ensemble. The output of these climate models comprises a large range of variables, from which we use the global mean steric change and the regional sea surface height above geoid to compute the steric component by adding them together.

Additionally, the model results need to be corrected for the so-called model drift (Katsman et al., 2008). Many of the pre-industrial control runs of the AOGCM's show an increasing steric sea level, while they should be in steady-state because the temperature forcing is constant. This suggests that the spin-up period of the models is not long enough to obtain a steady-state in the deep ocean, and this will also be the case for the future model runs. Therefore, the future steric contribution was corrected for the linear trend in the pre-industrial control run.

Another correction done on the model output data is the so-called inverse barometer (IB) correction. This accounts for low-frequency atmospheric pressure variations due to changes in atmospheric circulation, which changes the atmospheric loading on top of the ocean surface. A pressure increase of 1 mbar yields a lowering of the ocean

surface of 1 cm (Ross, 1854; Wunsch and Stammer, 1997; Stammer et al., 2011). In Chapter 3, this results in a small change in the sea-level trend, with a strong meridional signature.

The steric contribution is a regionally highly varying sea-level pattern, as shown in Figure 2.8. This high variability occurs because changes in density and changes in ocean dynamics are closely linked, since the ocean circulation governs the redistribution of heat and salt. Therefore, the steric component is not only a field of density variations; instead it also shows some of the changes in ocean dynamical processes that cause changes in the sea surface height. This is why the modelled future steric contribution is constructed using the global mean steric change plus the local dynamic topography. However, there is a difference in the dynamical processes that are captured by the models and the observed steric changes. The main difference is that the AOGCM's do not account for changes in the ocean dynamics that are caused by the addition of freshwater to the ocean through land ice melt, while this is implicitly included in the observations. Although this effect is probably of second order importance (Kopp et al., 2010; Stammer et al., 2011), it would be better to include it in future projections, but this requires a very high resolution of the ocean model and is therefore currently not feasible.

2.3 Glacial Isostatic Adjustment

When mass is redistributed at the Earth's surface this causes not only a change in the equipotential surface of gravity as explained in Section 2.1.3, but also a deformation of the solid earth, as shown in Figure 1.9. The difference between these two surfaces is the relative sea-level change. The rheological behaviour of the solid earth can be approximated by a linear Maxwell viscoelastic model, which consists of two parts that are connected in series. The elastic part of vertical deformation after a mass change can be imagined as a spring: it deforms instantaneously and completely when pressure is applied, and returns back to its original shape once the pressure is removed again. The second component of the deformation is the time-dependent, viscous part, which can be imagined as a dashpot, moving slowly but gradually. The speed of this process depends on the viscosity of the mantle ($\sim 10^{21}$ Pa·s, Haskell, 1935) and the thickness of the lithosphere (~ 100 km).

During the Last Glacial Maximum (LGM), the Greenland and Antarctic ice sheet were larger than they are now. Additionally, there were two other large ice sheet complexes in the Northern Hemisphere: the Laurentide ice sheet over North America and the Fennoscandian ice sheet over Scandinavia. After the LGM, these ice sheets lost an amount of mass equal to about 130 m of global mean sea-level rise, as shown in Figure 1.1e. During the LGM, the formation of the ice sheets forced the Earth's crust below them to subside due to their enormous weight. This caused the mantle material below to flow away to the sides of the ice sheet, which caused upward movement next to the ice sheets: the peripheral bulges. After the LGM, the Laurentide and Fennoscandian

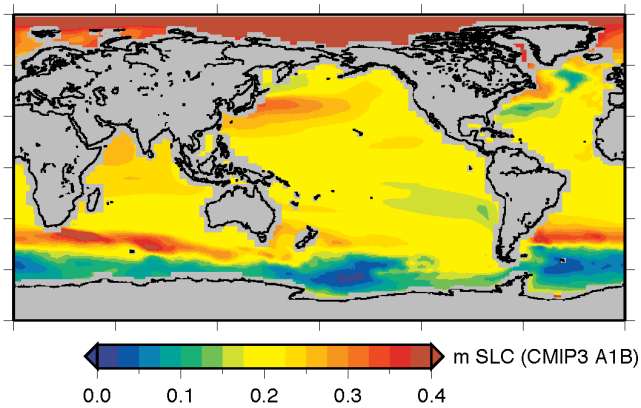

Figure 2.8: *Ensemble mean steric sea-level contribution (m) for CMIP3 scenario A1B between 1980-1999 and 2090-2099 (See also Chapter 4).*

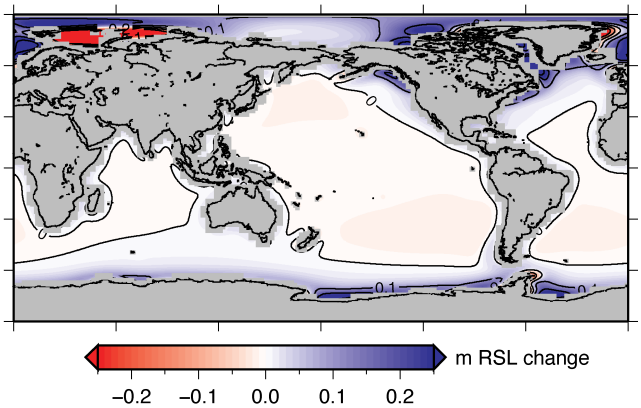

Figure 2.9: *GIA sea-level contribution (m) (Peltier, 2004) between 1980-1999 and 2090-2099.*

ice sheets melted and the water was added to the ocean. However, the Earth did not immediately return to its original shape, due to the viscous behaviour of the mantle, but it only recovered very slowly. Even nowadays, the melt of the LGM ice sheets still influences sea level everywhere, with maximum uplift rates of up to a centimeter per year in Scandinavia and the Hudson Bay, causing sea level to fall (e.g., Vermeersen and Schotman, 2009). This process is called Glacial Isostatic Adjustment (GIA).

Studies of GIA are heavily dependent on estimates on the viscosity of the mantle, the thickness of the lithosphere and the ice history. The problem in GIA modelling is that Earth rheology and ice history are mutually dependent. There are two possible approaches to find a GIA solution: either a certain Earth rheology is assumed based on geodynamics, or a certain ice loading history is assumed. When one of the two is set, the other can be deduced. In both cases, relative sea-level curves are used to obtain a

GIA estimate, similar to the ones presented in Figure 1.1. In this thesis, two different GIA estimates will be used, which are both based on the ice-history approach: in most chapters, the GIA contribution to sea-level change is based on the ICE5G deglaciation history with VM2 viscosity profile (Figure 2.9; Peltier, 2004). In addition, in Chapters 3 and 4 the ANU model (Nakada and Lambeck, 1988, updated in 2004-2005) is used in a comparison. Both models are in principle constrained by the same historical relative sea-level information, and therefore provide a rather similar sea-level pattern for most of the ocean. However, there are some differences between these models close to the locations of the Pleistocene ice sheets due to differences in the Earth rheology, as will be discussed in Chapters 3 and 4.

2.4 Summation of patterns

The previous sections described how each of the contributions to sea-level change may be modelled. To obtain a total field of regional sea-level change, all the patterns obtained from land ice, terrestrial storage, steric and GIA are added together. For the past regional patterns as presented in Chapter 3 this gives a field of regional variations that can be compared to tide gauge measurements. The uncertainty in the total pattern is based on the uncertainties in each of the contributing data sets. For the future projections as described in Chapters 4 and 6, summing the contributions results in an ensemble of the different climate models that were used to compute the land ice and steric contributions. The uncertainties provided in these chapters are based on the spread of the models in the ensemble, and are thus an indication of the agreement among the various climate models.

A drawback of this method of computing the total regional sea-level pattern is that there is no feedback between the freshwater that is being added to the ocean due to land ice melt and changes in the ocean circulation and density. After all, when freshwater is added near for instance Greenland, this locally decreases the salt content and temperature. Although it is subject of debate how large the influence of this freshwater forcing on the ocean circulation exactly is, it is expected to be a second order effect (Kopp et al., 2010; Stammer et al., 2011). It is therefore not crucial when focusing on the regional pattern, but it would be better to include it. Ideally, the approach should be similar to the approach from Kopp et al. (2010), who combine the gravitational, elastic and rotational effects of GIS melt -termed static equilibrium sea level- with the effects of GIS melt on temperature, salinity and circulation changes - termed dynamic sea level. However, Kopp et al. (2010) do not include land ice melt other than GIS, nor the effects of warming climate, but instead only impose an artificial GIS melt rate. Including all ice masses and a changing climate would be a very time consuming computational process since the models used to compute ocean dynamical and density changes from freshwater input need to have a very high resolution to represent all the ocean dynamical processes correctly. Therefore they cannot be coupled to large scale climate models yet.

CHAPTER 3

Regional sea-level variations in the recent past (1961-2003)

In the Intergovernmental Panel on Climate Change Fourth Assessment Report (IPCC AR4), the global mean sea-level budget for the period 1961–2003 could not yet be closed satisfactorily. Since then, many studies have attempted to close the global budget. In this study, we focus on the regional sea-level patterns instead of the global mean sea-level change. We compare local measurements from tide gauges to modelled regional patterns to see how much we understand of the physical processes underlying regional sea-level patterns. Processes that are included are land ice mass changes, terrestrial storage changes, steric changes, atmospheric pressure changes and Glacial Isostatic Adjustment (GIA). The study focuses on the mean linear trend between 1961 and 2003.

We find that for the period 1961–2003 in 14 of the 17 regions the observed values can be explained with the available models, by comparing the regional means of observations and models. We show that it is statistically possible that the measurements and models are drawn from the same normal distribution. Because of the high local variability in the measurements, we expect that the explained variability could be increased by improving the steric contribution rather than the land ice or terrestrial contributions, which would only result in smooth changes on a larger spatial scale. We show that replacing the modelled contributions by different estimates can improve the explained variability in some regions, but does not result in an overall improvement. Experiments in which the different components are varied within their uncertainty limits, show that local improvements are possible at the expense of the global explained variability.

This chapter is based on: Regional sea-level variations in the recent past (1961-2003), by A. B. A. Slangen, R. S. W. van de Wal, L. L. A. Vermeersen and Y. Wada, *In preparation.*

3.1 Introduction

Rising sea levels can have serious implications for coastal communities in the future (Nicholls and Cazenave, 2010), and thus sea-level change is a central issue in the field of climate change. In order to predict future changes, it is important to understand past sea-level changes. However, in the IPCC AR4 (Bindoff et al., 2007), a discrepancy was found in the global mean sea-level trend for the period 1961–2003, between the tide-gauge observations (1.8 ± 0.5 mm yr $^{-1}$) and the estimated contributions to sea-level change (1.1 ± 0.5 mm yr $^{-1}$). This showed that the understanding of past changes was not complete. Since then, much work has been done on the subject, and several studies have managed to close the global sea-level budget for different periods (e.g., Church and White (2011) for 1972–2008 and Gregory et al. (2012) for the 20^{th} century). Here, we focus on the same period as presented in IPCC AR4, which is 1961–2003.

Studying regional sea-level patterns might increase our understanding of the changes that were observed over the past half century. Therefore, this study will examine various processes underlying regional variations in sea-level change. In general, sea level can change due to variations in mass, variations in volume, or vertical land motions. These processes cause differences in the rate of sea-level change, both in time and in space. Processes that are included in this study are land ice mass changes (Dyurgerov and Meier, 2005; Bindoff et al., 2007), thermosteric variations (Levitus et al., 2012), GIA (e.g., Nakada and Lambeck, 1988; Peltier, 2004), and human-induced changes in terrestrial storage such as groundwater extraction (Konikow, 2011; Wada et al., 2012) and water impoundment behind dams (Chao et al., 2008; Fiedler and Conrad, 2010). In addition, the sea level is corrected for long-term changes in atmospheric pressure (Ross, 1854; Wunsch and Stammer, 1997). All changes discussed are relative sea-level changes, and thus defined as the difference between the ocean floor and the ocean surface (see Section 1.2 in this thesis).

The regional sea-level patterns from these processes are partly available from measurements, while others require a gravitationally consistent sea-level model to compute the spatial pattern (e.g., Woodward, 1887; Farrell and Clark, 1976; Mitrovica et al., 2001). This results in a set of sea-level contribution maps, which will then be compared to measurements made by tide gauges, as provided by the Permanent Service for Mean Sea Level (PSMSL) (Woodworth and Player, 2003). Tide gauges are devices attached to the Earth's surface which measure local variations in sea level. They are sparse in spatial and temporal coverage, and therefore the measurements will be grouped into 17 regions to increase the representability of the measurements. This study will focus on the sea-level trends in these regions for the period 1961–2003.

The comparison of observed sea level to the different components is not straightforward. Closing the global mean budget has proven to be difficult, and when going to a regional level, even more difficulties emerge. To model regional patterns, detailed information is needed on for instance the locations of land ice melt, or locations of groundwater extraction. This information can be obtained from satellite imagery,

but only for recent time periods. Going back in time, reliable measurements become sparse, which leads to more uncertain estimates for all contributions. Also the measurements done by tide gauges have larger uncertainties further back in time.

The central question is: how well do we understand measured sea-level changes on a regional scale? To find this out, this study examines whether the tide gauge measurements can be explained with the currently available models and data. In Section 3.2, the selection method of the tide gauge data will be described, as well as the data and models used to calculate the various contributing sea-level patterns. Section 3.3 covers the comparison of the tide gauges to the modelled contribution. Section 3.4 discusses the use of different data sets for the modelled contributions to improve the explained variability. Finally the conclusions are summarized in Section 3.5.

3.2 Data and Methodology

This section introduces the various datasets and models that were used in this study. We first describe the selection of the tide gauges (Section 3.2.1), and then the modelling of the various processes (Section 3.2.2).

3.2.1 Tide gauge selection

The observations that are used to compare the models to are tide gauge records, which were extracted from the Permanent Service for Mean Sea Level (PSMSL) data base (Woodworth and Player, 2003). First, all the Revised Local Reference (RLR) tide gauge records which contain at least 20 yearly values in the period 1961–2003 were chosen. Then, a linear regression was performed to calculate the average trend over this period using Equation 3.1. This equation calculates the linear sea-level trend, while accounting for the 18.6 year lunar nodal cycle (Baart et al., 2012). The 18.6 year nodal cycle is one of the components driving the tides on Earth, and it influences the tidal amplitude on longer time scales.

$$h(t) = \underbrace{\beta_0}_{mean\ level} + \underbrace{\beta_1 t}_{trend} + \underbrace{a \sin\left(\frac{2\pi t}{18.6}\right) + b \cos\left(\frac{2\pi t}{18.6}\right)}_{nodal\ cycle} \tag{3.1}$$

In Equation 3.1, h is the sea level measured at time t in years, β_0 is the initial sea level at $t = 0$, β_1 the average rise per year, and a and b are constants which are calculated separately for each tide gauge record. Solving Equation 3.1 gives a set of sea-level trends (β_1) measured at 494 tide gauge stations. The records are not corrected for GIA, which will be added as a separate sea-level contribution.

Uncertainties in the tide gauge time series may not only arise from vertical land movements due to tectonics or GIA, as discussed in Section 1.1 of this thesis, but also from changes in the surroundings of the tide gauges, which are often located in or near harbour areas. To smoothen errors in the local information obtained at the tide

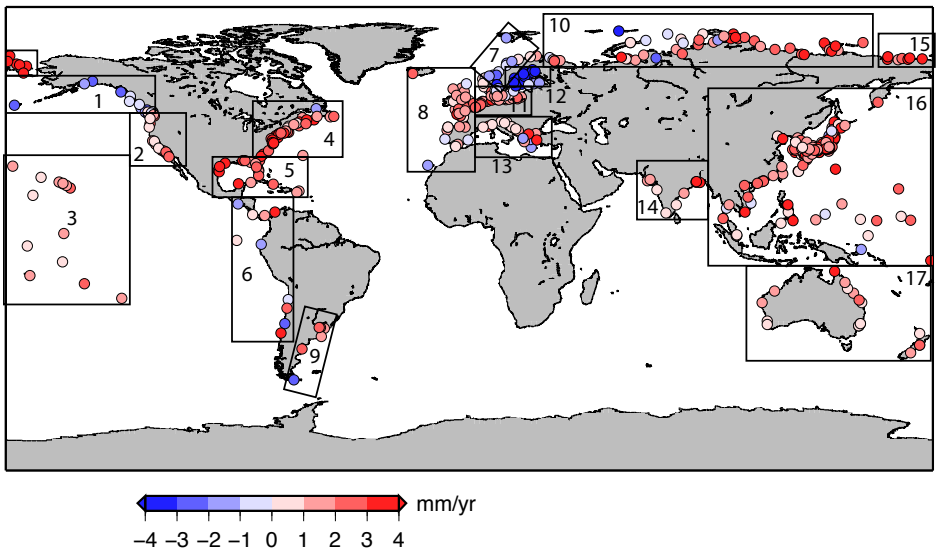

Figure 3.1: *Tide gauge trends (mm yr^{-1}) for the period 1961–2003; 494 records with each at least 20 years of data are sorted into 17 regions. Data from the PSMSL data base (Woodworth and Player, 2003). Region 9 contains the least records (7 records), region 16 contains the most records (138 records).*

gauge, the measurements are sorted into 17 regions, as shown in Figure 3.1. Where possible, the regions are taken such that the measurements show a reasonable consistency within the region. However, it is important to note that it is not assumed that the measurements in a region are representative for the entire ocean surface in the region. In Section 3.3, the comparison between observations and models will focus on the measurement locations in these 17 regions, and compare local measurements to local model values. Therefore, it is not important that the 17 regions do not to cover the entire ocean surface.

3.2.2 Modelling the contributing processes

This study considers the following contributions to sea-level change: land ice mass variations, steric variations, GIA and terrestrial exchange. In addition, the sea level is corrected for large-scale atmospheric pressure variations. In order to compare the modelled contributions to the tide gauge measurements, regional fields of all these contributions are needed. All fields that are described in this section are shown in Figure 3.2, and the global mean values and accompanying uncertainty ranges are provided in Table 3.1. All regional fields are presented on a 1×1 degree grid.

In order to calculate the sea-level pattern resulting from land ice mass variations, we need estimates of the location and amount of the land ice changes in the period 1961-2003. For the two largest ice masses on Earth, the Greenland Ice Sheet (GIS)

Table 3.1: *Global sea-level trends (mm yr $^{-1}$) of the various contributions for 1961-2003.*

Contribution	Reference	mm yr $^{-1}$
AIS	Lenaerts et al. (2012); Rignot et al. (2011)	0.19 $\pm$ 0.44
GIS	Ettema et al. (2009); Rignot et al. (2011)	0.14 $\pm$ 0.16
Glaciers	Dyurgerov and Meier (2005)	0.53 $\pm$ 0.18
Thermosteric (0–2000m)	Levitus et al. (2012)	0.57 $\pm$ 0.05
Thermosteric (> 2000m)	Purkey and Johnson (2010)	0.12 $\pm$ 0.10
Inverse Barometer	CMIP5 model ensemble	-0.01 $\pm$ 0.05
Dams	Chao et al. (2008)	-0.55 $\pm$ 0.17
Groundwater	Wada et al. (2012)	0.35 $\pm$ 0.09
GIA	ICE5G (Peltier, 2004)	0.03 $\pm$ 0.02
Sum		1.37 $\pm$ 0.55
Observations	Bindoff et al. (2007)	1.80 $\pm$ 0.50

and the Antarctic Ice Sheet (AIS), estimates from the regional climate model RACMO2 (Ettema et al., 2009; Lenaerts et al., 2012) are used for the Surface Mass Balance (SMB) component. The dynamical component for both ice sheets is based on data from Rignot et al. (2011). For the Glaciers and Ice Caps (GIC), Dyurgerov and Meier (2005) provide mass balance estimates of 13 large GIC regions across the world. This is not the most recent estimate of the past GIC contribution, but it is the only one that provides the locations of mass change, unlike Cogley (2009a), who provides a global mean time series only. The difference in global mean values between the two data sets is less than 10%, and the value of Cogley (2009a) is within the uncertainty range of the global mean GIC contribution to sea-level change ($\pm$ 0.18 mm yr $^{-1}$) as given by Dyurgerov and Meier (2005).

To model the variations in sea level caused by differences in the ice mass contribution, we use the sea-level model as described in Section 2.1.3 of this thesis. The resulting modelled sea-level patterns of the land ice contributions are shown in Figure 3.2a and 3.2b, for the ice sheets and GIC, respectively. All values are mean trends in mm yr $^{-1}$ for the period 1961–2003. The response of the sea-level pattern to the gravitational variations is clearly visible in Figure 3.2a, which shows the sea-level change due to mass changes on the AIS and the GIS. Due to the loss of gravitational attraction, close to the ice sheet the sea level falls, while locations at a distance of at least 2200 km experience a sea-level rise. This process is more thoroughly described in Section 2.1.3 of this thesis. Although GIC melt occurs in multiple locations, Figure 3.2b still shows a clear gravitational effect, with the main sea-level rise occurring around the equator.

Another large contribution to sea-level change is caused by volume changes due

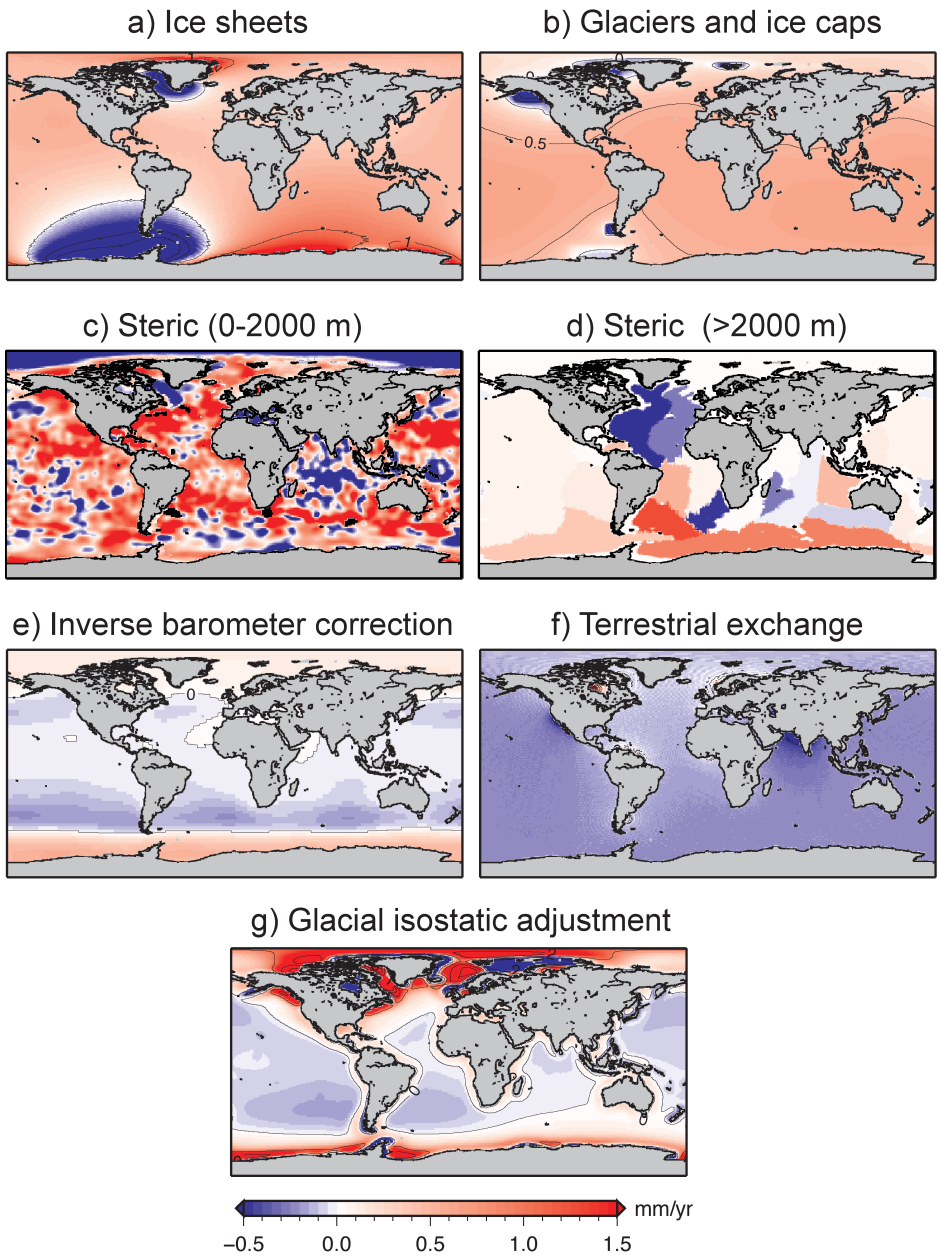

Figure 3.2: *Regional sea-level trends (mm yr^{-1}) over the period 1961–2003 for the following contributions;* **(a)** *Ice sheets (AIS and GIS),* **(b)** *Glaciers and ice caps (GIC),* **(c)** *Upper steric (0–2000 m),* **(d)** *Lower steric (>2000 m),* **(e)** *Inverse barometer correction,* **(f)** *Terrestrial exchange from groundwater extraction and reservoir impoundment,* **(g)** *Glacial isostatic adjustment. Accompanying global mean trends are shown in Table 3.1. Missing data in* **(c)** *in black.*

to local variations in temperature and salinity of the ocean water, together referred to as the steric contribution. Historical measurements of temperature and salinity are available at various locations, times and depths, and they need to be interpolated to obtain a data set that covers the entire ocean. In this study we use the most recent data set of Levitus et al. (2012) for the upper 2000 m of the ocean (Figure 3.2c). The linear least squares trend is calculated using the monthly thermosteric data from 1961 to 2003.

Not only the upper layer of the ocean, but also the deep part of the ocean is warming, although less than the upper layer. There is very little data available for this part of the water column, especially for the earlier part of our time period. In IPCC AR4, the deep ocean contribution was therefore estimated to be constant at 0.1 mm yr^{-1}. More recently, Purkey and Johnson (2010) presented estimates per basin for the ocean below 1000 m for the period 1990–2000. We use their estimated regional field below 2000 m (Figure 3.2d), and assume that their rate of change is also valid for the period 1961–2003, which is probably a valid assumption since the deep ocean responds much slower to changes in the atmosphere than the upper ocean and the warming is therefore more constant.

Sea level may also vary as a result of large-scale atmospheric pressure variations and must therefore be corrected for these changes. An increase of 1 mbar in pressure at the ocean surface will cause a sea-level fall of 1 cm (Ross, 1854; Wunsch and Stammer, 1997). For the past change in sea-level pressure, we use historical runs from the total CMIP5 climate model ensemble (37-member mean, from http://climexp.knmi.nl), and compute the mean trend in sea-level pressure between 1961 and 2003. The resulting trend in sea-level change (Figure 3.2e) shows that although the global mean change is very small, variations in pressure can cause local sea-level changes with a strong meridional pattern.

Two other contributions considered in this study are the human-induced changes in the terrestrial storage of water by groundwater depletion and water impoundment behind dams (see also Section 2.1.2 of this thesis). Our estimate for past groundwater depletion is based on data from Wada et al. (2012), while for the water impoundment behind dams we use the data from Chao et al. (2008). Similar to the land ice contributions, changes in terrestrial water storage cause a redistribution of mass and thus have an impact on the gravitational field, the rotation and the deformation of the Earth. Therefore, the same sea-level model was used as was done for the land ice change (see Section 2.1.3), where the ice density is replaced by the water density. The two data sets are combined into the total terrestrial storage contribution, and the resulting regional pattern is shown in Figure 3.2f. The water impoundment behind dams and the groundwater depletion partly compensate each other over the period 1961–2003, but nevertheless lead to a negative contribution for the terrestrial storage because water storage behind dams is larger (Table 3.1). Regional sea level falls near regions of mass loss on land, which are in this case the regions where groundwater depletion takes place, for instance near the Indian coast (Figure 3.2f). On the other hand, sea level

rises near areas of mass gain on land, which are regions where dam construction takes place. In Figure 3.2f this is the case around South America, for instance.

As was discussed in Section 2.3 of this thesis, GIA is the response of the solid earth to loading and unloading of large ice masses in the past. A few models are available to represent the sea-level variations as a result of GIA. Here we use mainly the present-day GIA from the ICE-5G(VM2) model (Figure 3.2f, Peltier, 2004). In Section 3.4, we will use the ANU model (Nakada and Lambeck, 1988, updated in 2004-2005) for comparison. As GIA patterns change only slowly over time, we apply the present-day pattern over the entire period 1961–2003. We assign a local uncertainty of 20% to the sea-level field from GIA, which is based on the difference between the ICE5G and the ANU model.

When the global mean values in Table 3.1 are summed and compared to the observations, there is a difference in the mean, but within the uncertainty ranges. A comparison to the study of Church et al. (2011), who closed the sea-level budget for the period 1972–2008, and an explanation of the differences between their study and this work is presented in Section 3.4.

3.3 Comparing the observations to the models

Table 3.1 shows that the sum of all the modelled contributions as presented in Section 3.2.2 is 1.37 ± 0.55 mm yr $^{-1}$. The modelled regional pattern of the sea-level trend over the period 1961-2003 is shown in Figure 3.3. As a first comparison between measurements and models, this figure also shows the measured tide gauge trends. At first glance, the figure shows influences from different contributions, for instance from the steric component with its small scale variability, but also GIA around for instance Svalbard and sea-level fall due to land ice melt near Greenland and Antarctica. Also, according to the models, sea level has been rising in the majority of the ocean surface.

For a better analysis of the agreement between the modelled contributions and the observations, we zoom in on Figure 3.3. This is done in Figures 3.4a to 3.4d, which show close-ups from the 17 regions as defined in Figure 3.1, where regions are grouped by number. In all figures, the observations are plotted in circles on top of the model grid.

Figure 3.4a shows regions 1 to 5, which are all regions around the North American continent. In all of these regions, the agreement between modelled contributions and data is quite good. The negative trends in the Gulf of Alaska (region 1) are captured by the models, and from Figure 3.2 we can see that these negative values are caused by the melt of Alaskan glaciers and the resulting change in gravitation and elastic deformation. The higher values just offshore are a combination of the upper steric (Figure 3.2c) and the long-term GIA (Figure 3.2g) contributions. Both regions 2 (west coast USA) and 3 (North Pacific Ocean) show positive trends in observations and models, mainly caused by the steric contribution (Figure 3.2c), and amplified by positive values in the land ice contributions (Figure 3.2a and 3.2b). In region 2, both observations and

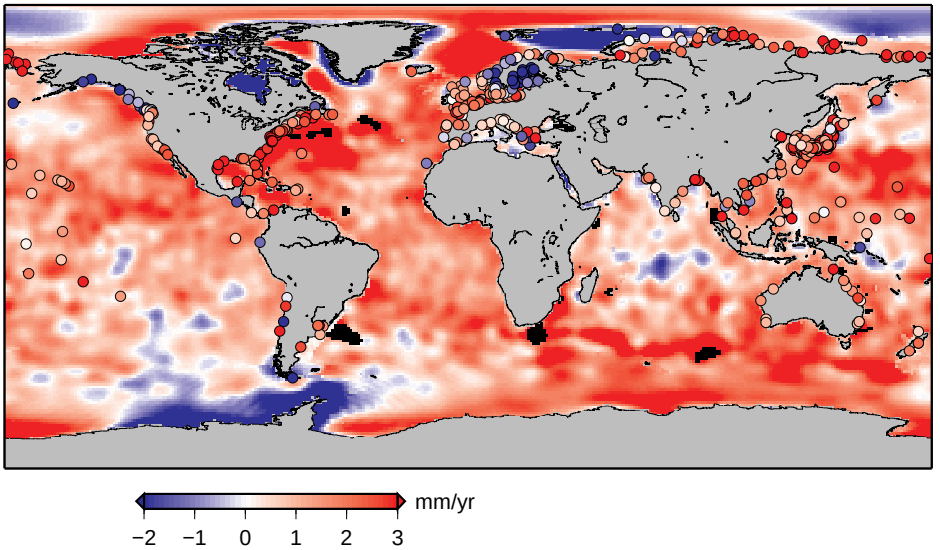

Figure 3.3: *Sum of the modelled sea-level trend (mm yr^{-1}) over the period 1961–2003, containing all the contributions as shown in Figure 3.2 (missing data in black). Tide gauge trends in circles. NB. colour scale is different from Figure 3.1.*

models are smaller in the centre and increase towards the north and south. Along the east coast of the USA (region 4), we observe high trends, which are also present in the modelled contributions of GIA (Figure 3.2g) and the upper steric (Figure 3.2c). Remarkably, there is one negative observation in the north of region 4, which is also captured by the models and is caused by GIA (Figure 3.2g). Region 5, the Caribbean, shows only positive observations, and also the models yields positive trends in the majority of the region. Unfortunately, there were no observational time series long enough to confirm the negative trend in the upper steric contribution in the southwestern part of the Gulf of Mexico.

Figure 3.4b shows regions 6 to 9, located around South America and Europe. For region 6, the west coast of South America, observations and models are not in agreement. The observations show very different signals, varying from very positive to very negative, while the models give a rather uniform trend. This might indicate that there are local coastal processes here that are not included in the models which influence the observations. At the east coast of South America (region 9), there seems to be a better agreement in the sign, with positive values towards the North, although the observations are much higher than the models, which indicate a very small trend. Moving towards Europe, region 7 shows the Norwegian coast. The negative trends in the observations are caused by land uplift as a result from GIA. These are present in the GIA model, with a very sharp shift to large positive values just offshore. Region 8, the European coast, shows that models and observations agree rather well along the Dutch, French and Spanish coast, but not very good in the north of the UK.

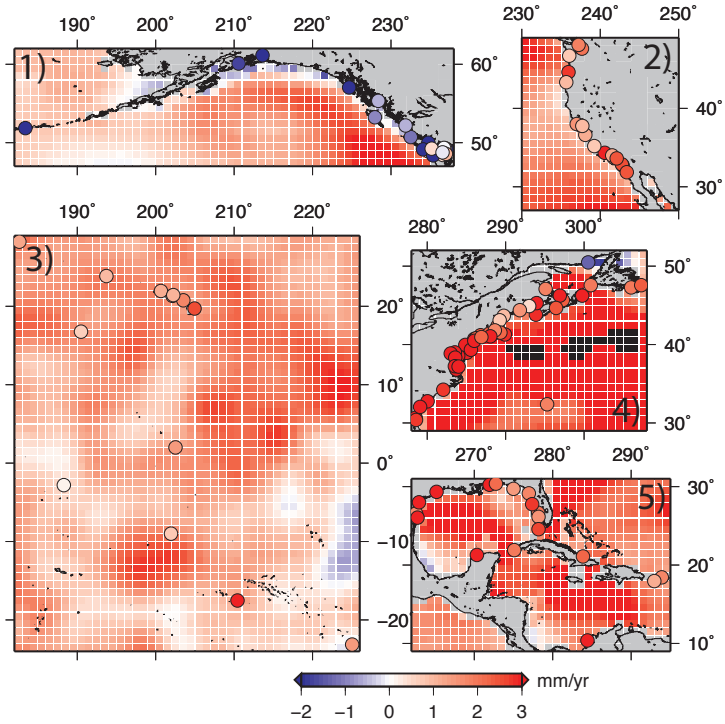

Figure 3.4a: *Regions (1) Gulf of Alaska (2) West coast USA (3) North Pacific Ocean (4) East coast USA (5) Caribbean. Zoom of Figure 3.3. Region numbers as in Figure 3.1. Land in grey, missing data in black.*

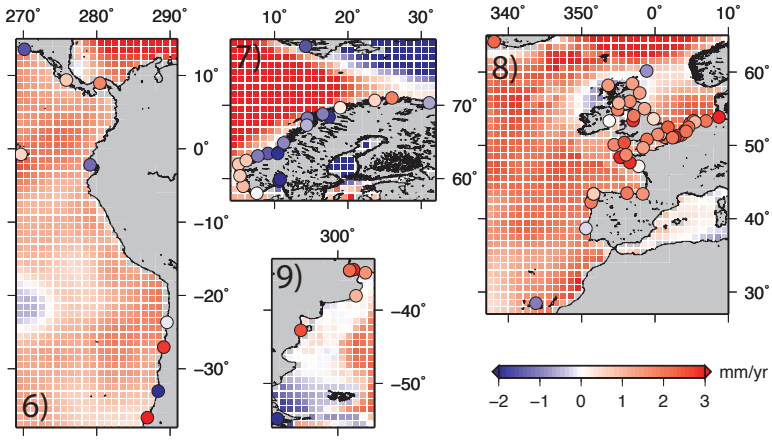

Figure 3.4b: *Regions (6) South American west coast (7) Norway (8) West European coast (9) South American east coast. Zoom of Figure 3.3. Region numbers as in Figure 3.1. Land in grey, missing data in black.*

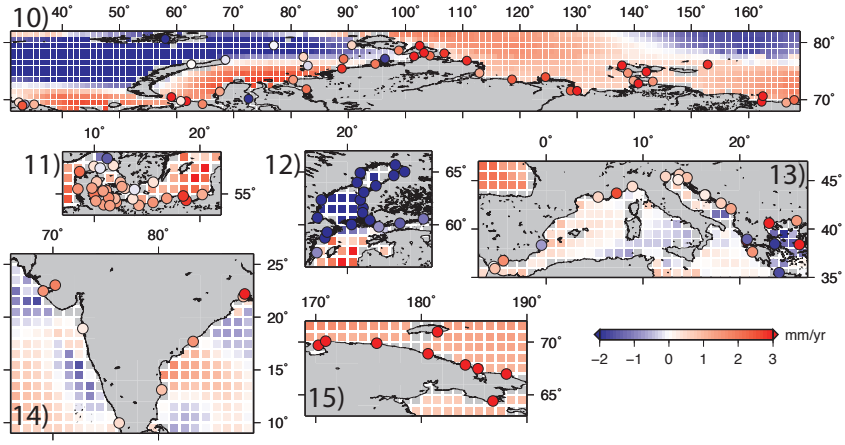

Figure 3.4c: *Regions (10) Arctic Ocean (11) Baltic South (12) Baltic North (13) Mediterranean (14) India (15) Arctic East. Zoom of Figure 3.3. Region numbers as in Figure 3.1. Land in grey, missing data in black.*

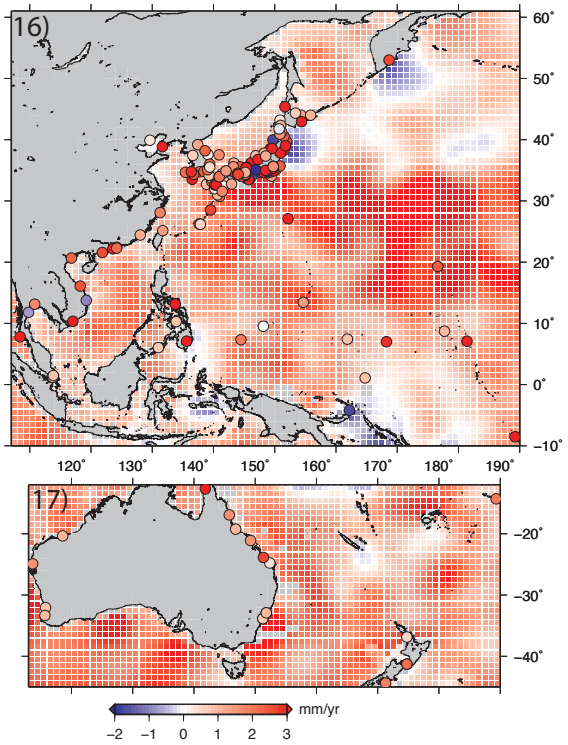

Figure 3.4d: *Regions (16) North Pacific West (17) South Pacific West. Zoom of Figure 3.3. Region numbers as in Figure 3.1. Land in grey, missing data in black.*

Regions 10 to 15 are shown in 3.4c, with regions in Europe, around the Arctic Ocean and India. In region 10, which covers most of the Arctic Ocean, the observations show variable trends. Some are captured quite good by the models, for instance near Svalbard, while other observations are not. The sign of the trend is right most of the time, but not the precise value. Region 11 shows the southern part of the Baltic Sea and the Danish coast. This part of the Baltic is just outside the GIA uplift region from the Fennoscandian ice sheet, unlike the tide gauge stations in region 12, in the Northern part of the Baltic, which are heavily influenced by GIA uplift. In both regions, the agreement between the observations and models is quite good, with positive values in region 11 and negative values in region 12. Region 13, the Mediterranean, shows large variations in the observations, which are not captured by the models. The reason for this is that these models are probably too coarse to represent a region as complex as the Mediterranean, where for instance also tectonics play a role (e.g., Pirazzoli, 2005). The Mediterranean basin is therefore often studied separately, using smaller grid resolutions (e.g., Gomis et al., 2008; Tsimplis et al., 2011). The tide gauge measurements around India, region 14, all show a positive trend, but the pattern is not completely captured by the models. A sea-level fall is modelled due to groundwater extraction (Figure 3.2f) and the steric contribution (Figure 3.2c), but the measurements show a positive trend in for instance the two north-westerns tide gauges. Region 15, the Eastern Arctic Ocean, is located east of region 10. In this region, the observations all show very high positive trends, ranging from 3.7 to 5.0 mm yr^{-1}. The models also show positive trends, but their values are much lower. None of the components show exceptionally high values in this region. However, based on Figure 3.2 the only contribution that would potentially be capable of such high local trends is the steric component.

The last two regions are shown in Figure 3.4d. Region 16 contains the largest set of measurements (138 records), of which most are located along the Japanese coast. The overall signal is positive, though a few observations indicate negative trends. In the south, the tide gauge trend in Papua New Guinea is well-captured by the models, while up in the north of Japan, the observations are mostly positive but the models indicate a negative trend, mainly due to the steric component (Figure 3.2c). The tide gauge stations around Australia and New Zealand, in region 17, all indicate positive trends. This is also shown in the models, where trends are high because this region is in the far-field of the land ice melt signal, and also experiences a positive steric contribution.

For a more quantitative analysis of the differences between observations and models, we compute regional averages for the 17 regions as defined in Section 3.2.1. From the models, the data are extracted at the locations within a 1 degree radius from the tide gauge stations to create artificial station data. A larger radius would lead to the inclusion of more modelled values further away from the coast, which would in for instance region 1 (Figure 3.4a) lead to an overestimation by the model data. A smaller radius is not possible, because the model data are all on a 1×1 degree grid. This is a relatively large grid size, and therefore coastal processes at smaller scales, for instance related to sediment transport, may be an explanation for some of the differences be-

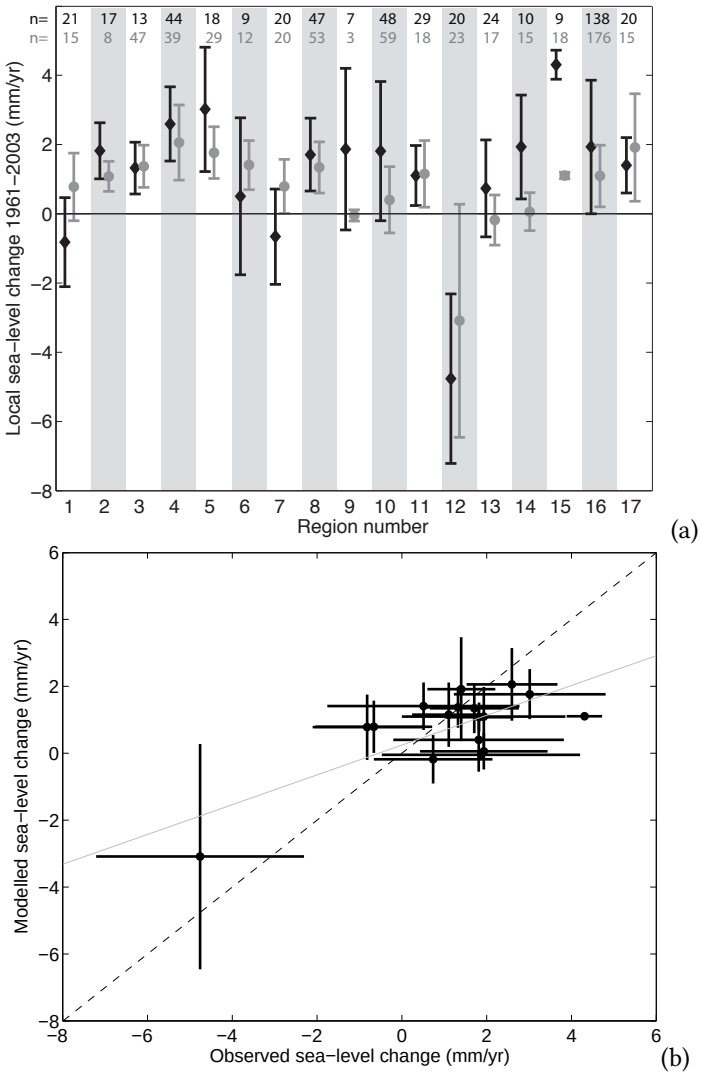

Figure 3.5: (a) *Regionwise comparison of observations (black) and models (grey) (mm yr^{-1}), error bars indicate 1 σ standard deviation within the regions. n indicates the number of tide gauges (black) and model grid points (grey) that is included in each region. Region numbers as in Figure 3.1.* **(b)** *Observations (x-axis) vs. models (y-axis) (mm yr^{-1}), error bars indicate 1 σ standard deviation within the regions. R^2=0.54 based on mean values, grey line is least squares line, dotted line is 1:1-line.*

tween observations and models. The artificial station data are sorted in 17 regions, similar to the tide gauges. In this way, we compare the regionalised observations to the regionalised artificial stations.

Within each region, we compute the mean and standard deviation for the modelled

values and the observations, for which the results are shown in Figure 3.5. Figure 3.5a shows that in some regions the model means and the observational means agree very well -regions 3 (North Pacific Ocean) and 11 (Baltic South)-, while in one region there is no overlap at all -region 15 (Arctic East)-. This was already clear from Figure 3.4c, where the high observations in region 15 could not be explained by the modelled contributions. In a large number of regions, the modelled mean $\pm$ 1σ largely overlaps with the observed mean $\pm$ 1σ, and the sign of the observed and modelled mean trends is the same. However, in some regions the observations and models have opposite signs; regions 1 (Gulf of Alaska), 7 (Norway), 9 (South American east coast) and 13 (Mediterranean). In regions 1 and 7, this can be explained by the fact that at the coast the models have a very large gradient towards the open sea due to GIA. Because the artificial stations are taken within 1 degree from the measurements, these higher values just offshore are included in the modelled average. In region 9, the modelled values are almost zero, while the observations are mainly positive, as shown in Figure 3.4b. In region 13 there is quite some overlap within the 1σ range, but the highly variable pattern in this region leads to a positive mean for the observations and a negative mean for the models. In this region, more sophisticated models are needed to represent the small scale variability. Overall, in only 5 regions there is a large disagreement between observations and models, and in 2 of these regions this can be attributed to the averaging method. This means that in 14 of the 17 regions the models do a reasonably good job in explaining the observations. Figure 3.5b shows how the observation-model pairs from Figure 3.5a relate to the 1:1-line. Following

$$R^2 = 1 - \frac{residual\ sum\ of\ squares}{total\ sum\ of\ squares} \tag{3.2}$$

(Wonnacott and Wonnacott, 1990), we find for this set of models an R^2-value of 0.54 for the mean points. This indicates that in general the mean observation-model pairs are not close to the 1:1-line, as is clear from the figure. However, since the variability inside the regions is quite large, the quality of the models should not only be based on the mean points. Instead, when including the σ in the regions, we see that in most regions the mean$\pm\sigma$ does cross the 1:1-line.

To examine whether it is statistically possible that both the regional observational means and the regional modelled means are drawn from the same population with a common mean and standard deviation, we will perform an analysis of variance. This can only be done under the assumption that both sets are normally distributed. If we look in Figure 3.6 at the bar histograms of the entire set of observed (blue bars, 494 observations) and modelled contributions (red bars, all 23,715 grid points of Figure 3.3), we conclude that a normal distribution of the data is a reasonable assumption. These bar histograms also show that the observations have a larger variability than the models: the spread of the blue bars is larger than the spread of the red bars. The lines in this figure show the probability density functions that were derived from the regional mean values, as presented in Figure 3.5. Again, the observations in blue indi-

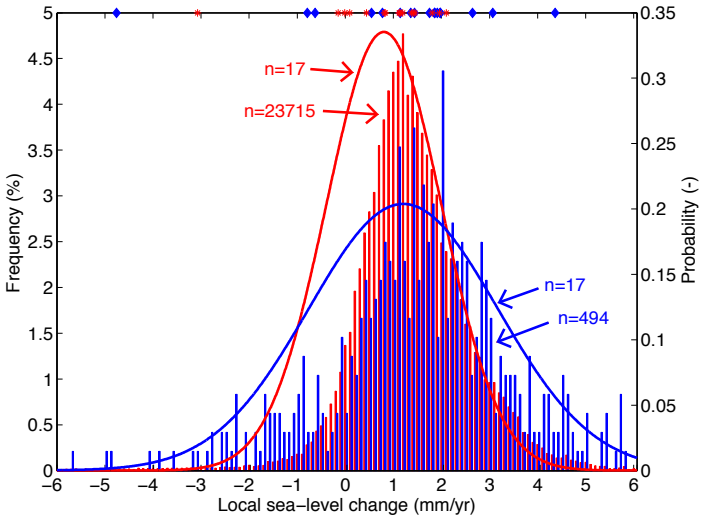

Figure 3.6: Left axis *Bar histograms (%, binwidth 0.1 mm yr^{-1}) of the total set of observed (blue bars) and modelled (red bars) local sea-level change trend (mm yr^{-1}).* **Right axis** *Linear probability density functions (-) derived from the 17 regional means of observations (blue line) and models (red line), with the 17 regional means of observations (blue diamonds) and models (red asterisks) in mm yr^{-1} at the top of the figure.*

cate a larger spread than the model data in red. This indicates that this combination of modelled contributions is not sufficient to explain the high variability within the tide gauge set. This might be due to a scaling problem, since the model data are on a 1×1 degree grid, but it may also indicate that there is a missing process. For both the models and the observations, the figure shows that the regional normal distribution -the line- slightly differs from the total normal distribution -the bar histogram-. This is because the 17 regions in which the tide gauges are sorted do not cover the entire ocean and are biased towards the Northern Hemisphere. Especially for the modelled sea-level change, we see that the regions are biased low with respect to the entire modelled ocean surface.

Under the assumption that the datasets are normally distributed, we compute the F-statistic to see whether the 17 regional values from the observations and models could be drawn from the same normal distribution. For this we use the following equation (Wonnacott and Wonnacott, 1990):

$$F = \frac{n s_{\bar{X}}^2}{s_p^2}, \tag{3.3}$$

in which n is the number of regions (17), $s_{\bar{X}}^2$ is the variance between the sample means (0.08), and s_p^2 the variance within the two samples (2.62). This yields an F-test value of 0.52. F would need to be larger than 2.869 (at a 10% significance level, degrees of free-

dom between the two sets = 1; degrees of freedom within the two sets of 17 regions = 32) to reject the null hypothesis that these two sets are drawn from the same distribution (Wonnacott and Wonnacott, 1990). This means that the differences between the two distributions are not significant, indicating that there is a large probability that the observations and the models are based on the same distribution. This confirms that the models can explain most of the variability found in the observations, with the exception of the more extreme observations.

3.4 Discussion

This discussion consists of two parts. In the first part we will show the influence of using different data sets for the various modelled contributing processes on the explained variability in the regions. In the second part we will explain why the global mean observed and modelled contributions as presented in Table 3.1 do not completely match, while recently Church et al. (2011) managed to close the sea-level budget.

3.4.1 Varying the modelled contributions

In this first part, we replace the data used in the previous sections by different data sets or estimates. We will do this for one contribution at a time, and compare the results to the results presented in Figures 3.5a.

For the ice sheets, we examine the effect of using the lower values that were presented in IPCC AR4 (Bindoff et al., 2007). For the period 1961–2003, their estimates are 0.05 mm yr^{-1} for GIS and 0.14 mm yr^{-1} for AIS. If we compare this to the results in Figure 3.5a, we find that this slightly improves the estimates in regions 1 (Gulf of Alaska), 7 (Norway), 9 (South American east coast), 12 (Baltic North) and 17 (South Pacific West). In all these regions, except region 9, the observations are lower than the modelled values. Decreasing the ice sheet contribution causes a sea-level fall in all far-field regions, and thus only improves the values in regions where observations are smaller than the models. Region 9 is a near-field region for Antarctica and thus experiences less sea-level fall due to less ice sheet melt, en thus an increase in value. However, overall it seems that decreasing the ice sheet contribution does not lead to a higher amount of explained variability. Because there are so little near-field observations, the modelled ice sheet contribution is barely constrained, and as a result, small differences in the ice sheet contribution do not lead to a significant change in the explained variability.

For the GIC, we study the effect of an addition of 0.18 mm yr^{-1}, divided proportionally over the 13 regions of Dyurgerov and Meier (2005). This increases the explained variability in all the regions in Figure 3.5a where the observations are larger than the models, but decreases the agreement for regions where the models are larger than the observations. This is because increasing the GIC contribution causes an increase in sea level in most parts of the ocean and in most of the 17 regions, except

those close to the GIC regions: regions 1 (Alaska) and 10 (Arctic Ocean).

Instead of the Levitus et al. (2012) data, we used the Ishii and Kimoto (2009) data with 0.33 mm yr $^{-1}$ for the steric contribution rather than 0.57 mm yr $^{-1}$. The data sets are not completely independent, since they are derived from the same measurements. The main difference is that the Ishii and Kimoto (2009) data cover the upper 700 m, while the Levitus et al. (2012) data represent the upper 2000 m of the ocean. However, most of the tide gauges are located at the coast, where the ocean is relatively shallow, and the depth range is thus probably less than 700 m. Nevertheless, the Ishii and Kimoto (2009) contribution is almost half the Levitus et al. (2012) contribution, which of course causes differences. In 6 of the 17 regions, the Ishii and Kimoto (2009) data marginally improves the explained variability, while larger improvements are found in regions 12 (Baltic North) and 13 (Mediterranean). In region 12, the Ishii and Kimoto (2009) steric contribution is much smaller, which brings the models closer to the observations. In region 13 on the other hand, the Ishii and Kimoto (2009) contribution is larger, which increases the explained variability. Apart from these two regions, the Levitus et al. (2012) data lead to an overall better explanation of the observations.

The groundwater estimate from Wada et al. (2012) is replaced by data from Konikow (2011), which contributes 0.20 mm yr $^{-1}$. This compensates less for the negative contribution from the water impoundment behind dams, leading to a more negative terrestrial contribution. Therefore, using this contribution generally lowers the modelled regional means, except in regions 2 (West coast USA) and 14 (India). This is because these two regions are the regions with the most groundwater extraction, and because they are close to the sources, sea level will fall less when less groundwater is extracted. Overall, using this contribution does not significantly improve the explained variability in the regions.

Although very small on average, GIA can locally be a quite large or even dominant contribution. We therefore compare the ANU model (Nakada and Lambeck, 1988, updated in 2004-2005) to the ICE5G contribution (Peltier, 2004). The main difference between the two data sets is the extent of the influence of the Laurentide and Fennoscandian ice sheets and the accompanying forebulges. As a result, using the ANU data improves the model estimate in regions 7 (Norway), 12 (Baltic North) and 15 (Artic East), but gives a worse model estimate in region 11 (Baltic North). The differences are very small in the other regions. The large differences in regions 7, 12 and 15 indicate that the ANU model provides a better Fennoscandian ice sheet extent towards the east, but less good towards the south, which is probably due to the use of a different Earth rheological model.

Overall, improvements from using different data sets are rather small. The best improvement would be to use ANU instead of ICE5G for the GIA contribution, which is the only change in contribution that caused a significant improvement in the R^2-value. However, this is mainly caused by improvements in a few regions while not all regions improve when this model is used. For the other contributions, the use of a different dataset only caused small variations in the R^2-value, and thus this does not

point in the direction of a preference for either one of the other data sets. We have also attempted to change multiple contributions at a time to increase the R^2-value, but this too did not result in significantly better solutions.

3.4.2 Closing the sea-level budget

In this second part of the discussion, we focus on the closure of the global mean sea-level budget. In Church et al. (2011) (henceforth C11), the different contributions and the measured global mean sea-level change were found to agree within 0.05 mm yr $^{-1}$, while Table 3.1 shows that for the contributions used in this study there is a difference of 0.43 mm yr $^{-1}$. We will now compare our Table 3.1 to their Table 1 per contribution and explain the differences.

The contribution for AIS in this study is 0.11 mm yr $^{-1}$ less than in C11. However, C11 states that the AIS contribution may be anywhere between 0 and 0.4 mm yr $^{-1}$, so both estimates are equally likely and within each others uncertainty ranges. For GIS, there is only a difference of 0.02 mm yr $^{-1}$, which is very small compared to the total of 1.80 mm yr $^{-1}$. At first sight, a much more striking difference is caused by the GIC. In C11, the estimated GIC contribution for the period 1971–2008 is 0.67$\pm$0.03, based on results from Cogley (2009b), while we base our GIC contribution for the 1961–2003 period on the older data from Dyurgerov and Meier (2005). This is done because the Cogley (2009b) data do not provide a regional distribution of the change, but only a global mean contribution. However, when examining the Cogley (2009b) data for the period 1961–2003, we find a trend of 0.57 mm yr $^{-1}$, which means that the Dyurgerov and Meier (2005) estimate differs only 0.04 mm yr $^{-1}$. The higher value of 0.67$\pm$0.03 is therefore mainly caused by high values in the last pentad of the C11 period.

For the steric contribution, C11 splits the ocean in three layers. For the 0–700 m, they use updated Domingues et al. (2008) data, for 700–3000 they use a linear trend of 0.07$\pm$0.10 mm yr $^{-1}$ based on Levitus et al. (2005); Antonov et al. (2005), and for the abyssal ocean they use trends from Purkey and Johnson (2010). In this study, we use a more recent dataset (Levitus et al., 2012) for the upper 2000 m, and also the Purkey and Johnson (2010) data for the deep ocean, but this time below 2000 m instead of 3000 m in C11. Summed up this results in a difference of 0.12 mm yr $^{-1}$ for the steric component. However, the data from Domingues et al. (2008) give an 0.15 mm yr $^{-1}$ lower estimate for the period 1961–2003 than for the C11 period, which explains the difference, since the deep ocean trends are taken to be constant.

For the terrestrial exchange component, we have used data from Chao et al. (2008) for the water impoundment behind dams and from Wada et al. (2012) for the groundwater extraction. C11 use the same data for the water impoundment behind dams, but due to the difference in period their contribution is less negative than the value used in this study, a difference of 0.11 mm yr $^{-1}$. This is because this contribution has been decreasing over the past 50 years. On the other hand, the difference is exactly opposite for the groundwater extraction. In C11, data from Konikow (2011) are used, which are smaller than the Wada et al. (2012) estimates, leading to a difference of 0.09 mm yr $^{-1}$.

C11 also adds a third component to the terrestrial exchange, termed natural terrestrial storage, but it is unclear where these sources are located and thus we can not use them in this study.

Overall it appears that the difference between the budget closure in C11 and this study is in fact not that large. The differences can be explained mostly by the difference in time period, and also by the use of data sets that are only available as global mean values, whereas this study requires local information. This shows that budget closure depends heavily on the period chosen and the data used.

3.5 Conclusions

In this study we compared the modelled regional sea-level trend patterns for the 1961–2003 patterns to observed sea-level trends. For this we combined models from the following contributions to regional sea-level change: land ice, steric, GIA, terrestrial storage and the inverse barometer correction.

In Section 3.3, we showed that the explained variability of the observations by the models differs per region. In some regions, the models can explain the observations rather well, while in others, the observations are much larger or smaller than can be explained by the models. The high spatial variability in the observations indicates that this probably cannot be solved by using different estimates for the land ice contributions, which cause a rather smooth pattern. Instead, it hints towards the solution being in the steric component which also has a high variability and is not well known for the earlier part of the 1961–2003 period, with sparse data in the polar oceans. Another cause might be that sub-grid scale coastal processes, such as sediment processes, would need to be included to fully explain the observations. Part of the discrepancy may also be inherent to the tide gauge measurements themselves, which measure very local changes and might thus include non-climate related changes such as harbour works or local tectonics.

Nevertheless, we find that in 14 of the 17 regions the measurements can for a large part be explained by the models. Comparing the regional means of observations and models yields an R^2 value of 0.54. We have also shown that it is statistically possible that the observations and models are based on the same normal distribution, but also that the extremes in the observations are not present in the models.

In Section 3.4.1, we discussed the use of different models and data, and how this might improve the explained variability in some regions, by using a different ice sheet estimate for instance. However, in most regions these improvements are very small. The only exception was the GIA contribution, which notably improved the models in regions 7 and 12, but heavily decreased the agreement in region 11.

From Section 3.4.2, it appeared that the closure of the sea-level budget heavily depends on the period that is taken. It would probably be best to study yearly time series, but this requires a much higher temporal accuracy and lower uncertainties for especially the earlier time periods. For a shorter period, it would be a very good pos-

sibility to add satellite altimetry data to the observations, and compare these to the models. A large advantage of altimetry satellites over tide gauges is that they are not bound to the coast, but instead cover almost the entire ocean surface. Therefore, the use of satellites enables a much better comparison to the spatial patterns in the modelled components. In addition, comparing tide gauges, which measure *relative* sea level, to altimetry satellites, which measure *absolute* sea level, might provide valuable additional information on sea-level change. Satellite altimetry data are only available starting from 1992, which currently gives a timeseries of 20 years. It is therefore difficult to derive long-term trends in sea level and hence short-term temporal variability may complicate the interpretation of local sea-level patterns. However, the altimetry timeseries is still expanding and will thus become an even more valuable data source in the future.

Acknowledgements
We would like to thank the NODC and M. Ishii for the thermosteric data, J. Lenaerts for the RACMO SMB fields, P. Stocchi and R. Riva for the GIA contribution and the sea-level model, PSMSL for the tide gauge records, G.J. van Oldenborgh for making the climate data available via the Climate Explorer, and B. Chao for the dam impoundment data. Thanks to Y. Wada for preparing the terrestrial data for use in the sea-level model.

CHAPTER 4

Regional projections of sea-level change

Sea-level change is often considered to be globally uniform in sea-level projections. However, local relative sea-level change can deviate substantially from the global mean. Here, we present maps of twenty-first century local relative sea-level change estimates based on an ensemble of coupled climate model simulations for three emission scenarios. In the Intergovernmental Panel on Climate Change Fourth Assessment Report (IPCC AR4), the same model simulations were used for their projections of global mean sea-level rise. The contribution of the glaciers and ice caps (GIC) to local relative sea-level change is calculated with a glacier model, based on a volume-area approach. The contributions of the Greenland (GIS) and Antarctic ice sheets (AIS) are obtained from IPCC AR4 estimates. The relative sea-level distribution resulting from the land ice mass changes is then calculated by solving the sea-level equation for a rotating, elastic Earth model. Next, we add the pattern of steric sea-level changes obtained from the coupled climate models and a model estimate for the effect of Glacial Isostatic Adjustment (GIA). The resulting ensemble mean relative sea-level pattern reveals that many regions will experience relative sea-level changes that differ substantially from the global mean. For the A1B ensemble, local relative sea-level change values range from -3.91 to 0.79 m, with a global mean of 0.47 m. Although the amplitude differs, the spatial patterns are similar for all three emission scenarios. The spread in the projections is dominated by the distribution of the steric contribution, at least for the processes included in this study. Extreme ice loss scenarios may alter this picture. For individual sites, we find a standard deviation for the combined contributions of approximately 10 cm, regardless of emission scenario.

This chapter is based on: Towards regional projections of twenty-first century sea-level change based on IPCC SRES scenarios, by A. B. A. Slangen, C. A. Katsman, R. S. W. van de Wal, L. L. A. Vermeersen and R. E. M. Riva, *Climate Dynamics*, 38 (5-6), 1191–1209, 2012, doi: 10.1007/s00382-011-1057-6.

4.1 Introduction

In a warming climate, the global mean sea level is expected to rise, which will have serious implications for coastal communities (Nicholls and Cazenave, 2010). Therefore, sea-level change is a central research topic in climate change studies. The IPCC AR4 (Meehl et al., 2007b) presents projections for global sea-level change of 0.21 to 0.48 m under the Special Report on Emission Scenarios (SRES) A1B scenario for the period 1980-1999 to 2090-2099, excluding carbon cycle feedbacks and excluding the recently observed dynamical changes in ice sheets. Adding their estimate for the dynamical effect of ice sheet mass loss yields a global mean sea-level estimate of 0.20 to 0.61 m (Meehl et al., 2007b, Table 10.7).

However, the IPCC projections are limited to a global mean value and do not consider the large regional variations induced by several processes. Possible causes of regional variations include the gravitational effects resulting from land ice mass changes (e.g., Woodward, 1887; Farrell and Clark, 1976; Mitrovica et al., 2001), thermal expansion (e.g., Landerer et al., 2007a; Wijffels et al., 2008), ocean dynamics (e.g., Landerer et al., 2007a; Yin et al., 2010) and GIA (e.g., Peltier, 2004). In this study we incorporate all these effects in a local scenario using the IPCC SRES scenarios A1B, A2 and B1, to illustrate the importance of regional sea-level variations in a warming climate. Some processes are better understood and modelled in these simulations than others. In particular the ice sheet contributions used in IPCC AR4 were acknowledged to have limitations and possibly underestimate their future contributions (e.g. Rignot et al., 2008a,b, 2011; Velicogna, 2009). However, we do apply them here to allow for a comparison of the regional patterns with the well-known global mean IPCC AR4 estimates.

Throughout this paper, all sea-level changes discussed are *relative* sea-level changes. These are the changes relative to the Earth's surface, as measured by devices attached to the surface, for instance tide gauges. Relative sea-level change is different from absolute sea-level change, which is the change with respect to the center of mass of the Earth, as measured by air-borne devices such as satellite altimeters.

Land ice mass changes represent a large contribution to sea-level change. Melt water from land ice does not distribute uniformly over the ocean, due to gravitational effects and induced changes in the shape and rotation of the Earth (e.g. Vermeersen and Sabadini, 1999). The gravitational effect is the direct manifestation of Newton's law of universal gravitation (mass attracts mass), which implies that land ice attracts ocean water. When ice melts, the gravitational attraction of the ice sheet weakens, so the sea level falls near the ice (up to a radius of $\sim$2200 km), rises less than the global mean from $\sim$2200 km to $\sim$6700 km, and rises more than the global mean at a larger radial distance (see also Section 2.1.3 of this thesis). In addition, changes in surface load (in this case represented by land ice masses and the global ocean) cause a deformation of the Earth's surface, which in turn affects the Earth's gravity field and causes an additional redistribution of ocean water. This coupling between surface

mass changes and solid-earth deformation, also known as self-gravitation, was already described by Woodward (1887), but only implemented in a numerical model by Farrell and Clark (1976), who introduced the 'Sea-Level Equation'. This equation computes both the sea-level change and the solid-earth deformation due to ice mass variations. In addition, ice melt and solid-earth deformation cause a redistribution of mass that affects the Earth's rotation rate and the position of its rotation axis (e.g. Vermeersen and Sabadini, 1999) and hence the sea-level change pattern (Milne and Mitrovica, 1998).

Another large contribution to sea-level change arises from local changes in temperature and salinity of the seawater; the thermosteric and halosteric contributions. Warming of the ocean in response to rising atmospheric temperatures results in an increase of volume and hence sea-level rise. A higher salinity has the opposite effect, as it increases the density of the ocean water. Like the sea-level change resulting from land ice mass changes, steric sea-level changes (variations in ocean temperature and salinity) are far from spatially uniform (Cazenave and Nerem, 2004). Although in many places local thermosteric changes are dominant (see for example Bindoff et al., 2007, Figure 5.15b), changes in ocean salinity can also lead to substantial local sea-level variations (Antonov et al., 2002). These local steric changes are closely linked to ocean circulation changes, as the latter are driven by local density gradients (Meehl et al., 2007b, Section 10.6.2).

In order to obtain regional patterns of sea-level change, the processes mentioned above need to be modelled. The first component considered is the land ice contribution to sea-level change. For this contribution, the changes in the ice mass of glaciers and ice caps (GIC) have been modelled by a volume-area model (Bahr et al., 1997; Van de Wal and Wild, 2001, Section 2.1.1 of this thesis), to obtain, in contrast to the IPCC AR4, a regional pattern of the glacier mass loss. Additionally, the mass changes of the Greenland (GIS) and Antarctic ice sheets (AIS) have been computed with model-derived relations between temperature and ice sheet mass change as outlined in IPCC AR4 (Meehl et al., 2007b). The magnitude and location of all land ice mass changes serve as input for a sea-level model (Section 2.1.3 of this thesis), which calculates a gravitationally consistent field of sea-level change while accounting for rotational processes. The second component considered is the steric component (i.e. changes in ocean density and circulation, Section 2.2 of this thesis), for which we use the results of Atmosphere-Ocean coupled General Circulation Models (AOGCM's) provided in the Coupled Model Intercomparison Project phase 3 (CMIP3) database (Meehl et al., 2007a). The AOGCM's provide a global mean and local sea-level change relative to the mean due to circulation changes resulting from temperature and salinity variations. The third component added is the sea-level change resulting from GIA (Section 2.3 of this thesis), which is the present-day viscoelastic response of the Earth's crust to changes in ice masses throughout the last glacial cycle. To model the influence of GIA on regional sea-level change the result of the ICE-5G(VM2) glaciation-deglaciation model (Peltier, 2004) is used.

To allow for a comparison of the IPCC AR4 global mean estimates (Meehl et al.,

2007b) to the regional patterns, all results presented in this study are, on purpose, based on the same data as used in IPCC AR4. The only exception is the use of a new data set for the contribution of the GIC. The reason for this is that the present study requires a data set that provides locations and initial volume of the individual GIC to calculate regional scenarios for this contribution, while the IPCC data only provide a global value for all GIC combined. The outcome of this study to be considered as a first step towards the development of regional projections for sea-level change, complementary to the global mean projections in IPCC AR4. Although in IPCC AR4 the self-gravitation effect is recognized as a cause of regional sea-level variations (Bindoff et al., 2007, Section 5.5.4.4), it is not considered for the projections of future sea-level change (Meehl et al., 2007b). Here we will quantify this effect in detail. The local variations in steric sea-level change were discussed in Meehl et al. (2007b). Additionally to the contributions presented in IPCC AR4, the influence of GIA on sea-level change is considered, which can have very large effects locally.

This study is the first attempt to combine the three most important components affecting sea-level change on a regional scale, which has not been done before to our knowledge. Scientifically all ingredients are available for these three components to make the step from global projections to local projections and to provide specialized information regarding sea-level change, for which there is an increasing demand from governments and policy makers.

There are some potential contributions to local sea-level variations that are not included in this study because of a lack of appropriate data or model results. Examples are surface movements due to tectonic effects or subsidence, changes in storm surge height (although climatic changes of wind direction and wind speed are included in the steric contribution), water impoundment behind dams, groundwater storage change and the influence of freshening due to land ice melt on the ocean circulation. Hence, the results of this study should be considered as a first attempt to construct a regional projection for sea-level change with room for improvement as science progresses.

The paper is structured as follows. Section 4.2 describes all models and the data used to construct the spatially varying fields of sea-level change. In Section 4.3 the results are shown, for the separate contributions and for the total projected sea-level change. A discussion of the results is presented in Section 4.4 and finally in Section 4.5 the conclusions are described.

4.2 Data and Methodology

In this section, all models and data used in this study are discussed. A schematic of the methodology applied to construct the scenarios for local sea-level change is presented in Figure 4.1. The land ice contribution (Section 4.2.1) is split up in two components: the glaciers and ice caps (GIC); and the large ice sheets, Greenland (GIS) and Antarctica (AIS). Both respond differently to climatic changes and thus the ice mass changes need to be modelled in a different way. Once the magnitude and locations of all land ice mass

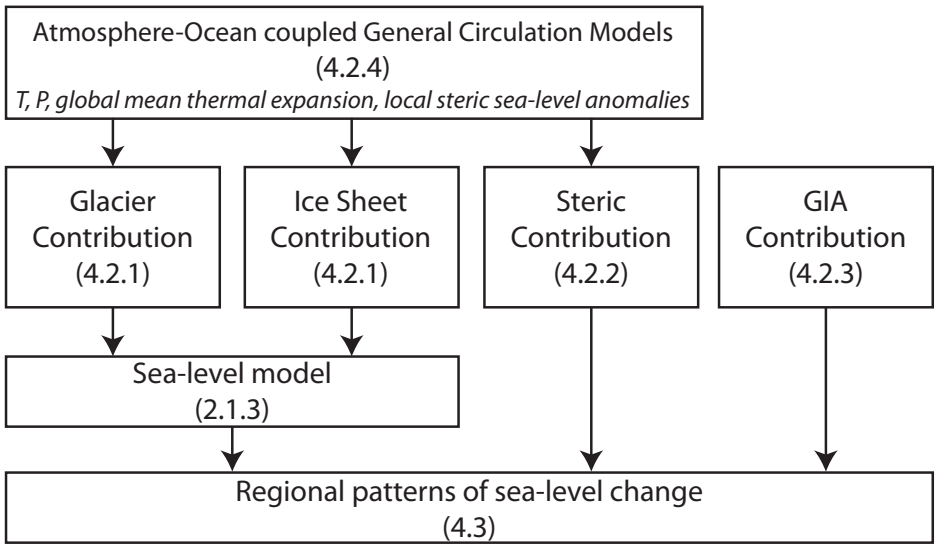

Figure 4.1: *Schematic depicting the methodology applied in this study. Global climate models provide temperature (T) and precipitation (P) required to calculate the land ice contributions, and global mean thermal expansion and local sea-level anomalies due to temperature and salinity variations for the steric contribution. Numbers in brackets refer to the sub-sections in which the different components are discussed.*

changes are known, a sea-level model (See Section 2.1.3 of this thesis) is used to compute the local sea-level pattern resulting from the melting land ice. The spatial pattern of the steric contribution is computed using global mean thermal expansion data and local sea-level anomalies due to temperature and salinity variations (Section 4.2.2). To account for the present-day response to ice mass changes after the Last Glacial Maximum (LGM), a spatially varying field of GIA is taken from the ICE-5G(VM2) model (Section 4.2.3), and added to the other contributions. This results in spatial patterns of future sea-level change, which will be discussed in Section 4.3. This section ends with a description of the coupled climate models that provide most of the data used to calculate both the land ice and the steric contributions (Section 4.2.4).

4.2.1 Land ice contribution

Glaciers and ice caps (GIC)

We use a glacier model to estimate the sea-level change contribution from mass changes of GIC, which is defined as all land ice apart from AIS and GIS. This model is based on volume-area scaling (e.g., Bahr et al., 1997; Van de Wal and Wild, 2001; Radić et al., 2007, 2008), and described in detail in Section 2.1.1 of this thesis. T and P are taken from the AOGCM's (Section 4.2.4) using the nearest neighbour approach (Van de Wal and Wild, 2001). The imbalance of GIC at present is accounted for by starting

the calculations in 1865, and applying a temperature increase of 0.6 °C 100 yr^{-1} over the period 1865–1990.

The glacier volume-area model requires a prescribed present-day area and volume of all GIC. As no complete inventory of all GIC exists, several estimations of total GIC volume and area have been made based on incomplete glacier inventories, for instance by Ohmura (2004), Dyurgerov and Meier (2005), Raper and Braithwaite (2005) and Radić and Hock (2010). Estimates of global GIC volume of the first three studies were used in IPCC AR4 and vary from 0.15 to 0.37 m sea-level equivalent (SLE), excluding small glaciers around the ice sheets (Lemke et al., 2007). However, computing a spatially varying pattern of sea-level change not only requires a volume-estimate, but also the locations of the GIC, so the global estimates as used in IPCC AR4 cannot be used here. The data base of Radić and Hock (2010) does contain location data, so those data are used to prescribe the initial area and volume for the glacier model. They find a present-day GIC volume of 0.41±0.03 m SLE excluding the glaciers around the ice sheets, and 0.60±0.07 m including those glaciers. This is larger than the IPCC AR4 estimates, mainly as a result of a more accurate estimation of the glaciers around the ice sheets by Radić and Hock (2010). IPCC AR4 used a factor of 1.2 to account for those glaciers. These different data sets result in different values for the GIC contribution; for the A1B scenario this study uses 0.10–0.24 m SLE, while in IPCC AR4 this is 0.08–0.15 m SLE (5–95% range).

The Radić and Hock data consist primarily of the WGI-XF database (Cogley, 2009a), which contains information on more than 131,000 GIC and about half of the estimated area of the world's GIC. Radić and Hock added 16 Icelandic ice caps and 47 Alaskan mountain glaciers to the Cogley data set. All available GIC are sorted into n=19 regions (Radić and Hock, 2010, their Figure 1) and m=18 size bins with upper area size 2^l km^2, $l = -3$ to 14. In addition, upscaling is performed for 10 of the 19 regions for which the inventory was not complete, where all upscaled area is assumed to be glaciers, not ice caps. Regions, size bins and upscaling are according to Radić and Hock (2010). The upscaled GIC data set finally serves as input data for the glacier model. The glacier model then computes GIC mass changes for the period 1980–1999 to 2090–2099, based on the IPCC scenarios. Eventually these volume changes are used as input for the sea-level model, which is described in Section 2.1.3 of this thesis.

Antarctic and Greenland Ice Sheet

To model the contribution of GIS and AIS to sea-level change, we need a different approach from the GIC described in the previous section. The volume-area approach is not suitable for ice sheets, due to their different size, geometry and dominating physical processes. Therefore, in IPCC AR4 (Meehl et al., 2007b, Section 10.6.4) the mass changes of the ice sheets are divided into three parts to calculate the contributions of AIS and GIS: surface mass balance (SMB) changes (accumulation and ablation), a dynamical contribution (changes in ice flow and reaction to changes in topography) and scaled-up ice sheet discharge (estimation for the imbalance due to observed ice

Table 4.1: *Empirical relations used to estimate the contributions of future ice mass changes of GIS and AIS. Constants a, b and c are dependent on ice sheet, AOGCM and scenario (J. Gregory, personal communication).* ΔT_1 *is the global mean difference between* $T_{t(2001-2099)} - T_{ave(1865-1894)}$. ΔT_2 *is the global mean difference between* $T_{t(2001-2099)} - T_{ave(1980-1999)}$. $r_1 = 0.32$ *mm/yr (Meehl et al., 2007b).*

Ice Sheet	GIS	AIS
SMB	$a + b\Delta T_1 + c\Delta T_1^2$	$a + b\Delta T_1 + c\Delta T_1^2$
Dynamical	$SMB + \frac{1}{3} * r_1$	$SMB * 0.95 + \frac{2}{3} * r_1$
Scaled-up	$\frac{1}{3} * r_1(\Delta T_2/0.63)$	$\frac{2}{3} * r_1(\Delta T_2/0.63)$

flow acceleration). Here, we briefly explain the procedures followed to calculate each of the three parts, which are identical to those applied in IPCC AR4, except for the separation of GIS and AIS contributions to be able to account for the gravitational effect. Additionally, Table 4.1 clarifies the followed procedure.

To determine future SMB changes, Gregory and Huybrechts (2006) combined annual time-series of temperature and precipitation simulated by low resolution AOGCM's, with spatial and seasonal patterns simulated by 4 high-resolution Atmosphere General Circulation Models (AGCM). This results in empirical relations of the form

$$\frac{\Delta SMB}{\Delta t} = a + b\Delta T_1 + c\Delta T_1^2. \tag{4.1}$$

describing the relation between the SMB contribution of GIS and AIS to sea-level change ($\frac{\Delta SMB}{\Delta t}$, in mm/yr) and the global temperature change with respect to pre-industrial values (ΔT_1). a, b and c are ice sheet-, model- and scenario-specific constants (Gregory and Huybrechts, 2006, J. Gregory, personal communication, 2010). Equation 4.1 is solved for all combinations of the 4 high-resolution AGCM's and the total ensemble of AOGCM's used in this study (12, 11 and 10 for respectively A1B, B1 and A2), and for the two ice sheets separately, resulting in 264 equations with different constants a, b and c. Finally, the SMB contributions of GIS and AIS for each AOGCM are calculated using the average ΔSMB of the 4 high-resolution AGCM's.

The dynamical contribution is calculated by scaling the SMB values and adding an estimate for the ice sheet contributions to sea-level change in 1993–2003. The scaling factors used in IPCC AR4 are -5% $\pm$ 5% for AIS and 0% $\pm$ 10% for GIS. Additionally the central estimate for the 1993–2003 sea-level contribution of AIS plus half that of GIS is used as scenario-independent term r_1 ($r_1 = 0.32$ mm/yr, Meehl et al., 2007b, Section 10.6.5). We need to split up the GIS and AIS contributions, because the influence on local sea-level change is dependent on the location where the land ice mass changes take place. Therefore, we assign $\frac{2}{3}$ of r_1 to AIS and $\frac{1}{3}$ of r_1 to GIS, similar to the way

Meehl et al. (2007b) constructed r_1.

To estimate the present-day ice sheet imbalance, it is assumed that the imbalance scales with the global average temperature change (Meehl et al., 2007b, Sections 10.6.5 and 10.A.5). For the calculation of the scaled-up ice sheet discharge we first assign the same fractions to r_1 as for the dynamical changes. Next, r_1 is multiplied with the future temperature change relative to that over 1980–1999 (ΔT_2) and divided by the global average temperature difference between 1865–1894 (pre-industrial) and 1993–2003 ($0.63^{\circ}C$, Meehl et al., 2007b, Section 10.A.5).

The ice sheet mass changes need to be assigned to a location to enable the calculation of a spatial pattern of sea-level change by the sea-level model, which is described in Section 2.1.3 of this thesis. For AIS, all mass change is assumed to take place on the Antarctic Peninsula and in West Antarctica (e.g. Rignot et al., 2008a), while for GIS the west coast and south part of Greenland are the assigned melt areas (e.g., Ettema et al., 2009; Rignot et al., 2008b). The mass change is distributed evenly over the area indicated with white shading in Figure 4.2, upper left panel. Distributing the mass evenly is a simplification that will probably influence the resulting pattern in sea-level change (Gomez et al., 2010). This is a refinement that needs to be addressed in future work to improve the accuracy of the estimates, if more subtle processes are included. However, in this study it was not taken into account.

4.2.2 Steric contribution

Global mean steric sea-level changes are dominated by the thermosteric part (e.g., Cazenave et al., 2009; Willis et al., 2008), since the global mean ocean salinity hardly changes over time. Therefore, it suffices to only take into account the global mean thermal expansion projected by the AOGCM's over the considered time period when calculating the steric part of the local sea-level projection. Time series of global mean thermal expansion were obtained from the CMIP3 database (Meehl et al., 2007a) and have been presented in IPCC AR4 (Their Figure 10.31). They were corrected for model drift by subtracting the nearly linear trend found in the accompanying preindustrial control run.

To this global mean component, we add the local sea-level anomalies projected by the AOGCM's associated with circulation changes due to temperature and salinity variations (which are also available from the CMIP3 database, Meehl et al., 2007a). By construction, the global mean of the sea-level anomaly field is zero. These local sea-level anomalies display large natural variability on interdecadal timescales. To filter out these slow variations, we first calculate the linear regression of local sea level over the twenty-first century at each grid point before calculating the local sea-level anomalies.

Table 4.2: *CMIP3-Models used in this study.*

AOGCM	Reference
BCCR-BCM2.0	Furevik et al. (2003)
CGCM3.1(T47)	Flato (2005)
ECHAM5/MPI-OM	Jungclaus et al. (2006)
GFDL-CM2.0	Delworth et al. (2006)
GFDL-CM2.1	Delworth et al. (2006)
GISS-EH*	Schmidt et al. (2006)
GISS-ER	Schmidt et al. (2006)
GISS-AOM$^+$	Lucarini and Russell (2002)
MRI-CGCM2.3.2	Yukimoto and Noda (2002)
MIROC3.2(hires)	K-1 model developers (2004)
NCAR-PCM	Washington et al. (2000)
UKMO-HadCM3	Gordon et al. (2000)

*Not available for A2 and B1

$^+$Not available for A2

4.2.3 Glacial isostatic adjustment (GIA)

Unless mentioned otherwise, we use the present-day GIA resulting from ICE-5G(VM2) (Peltier, 2004). In section 4.4.1 we will use the ANU model (Nakada and Lambeck, 1988, updated in 2004-2005), to illustrate the sensitivity our results to the choice of GIA model. For the time scale of this study, the sea-level changes due to GIA are almost constant; therefore, they are applied as a stationary spatial pattern.

4.2.4 Model ensemble

The sea-level estimates described in this paper are calculated using the results of simulations with the AOGCM's given in Table 4.2. These models are a subset of the World Climate Research Programme's CMIP3 multi-model dataset (Meehl et al., 2007a) used for IPCC AR4. This subset contains all models for which all required variables were available. For the selected models we consider three different emission scenarios: B1, A1B and A2, which are defined in the IPCC Special Report on Emission Scenarios (SRES, Nakicenovic and Swart, 2000). The ensemble mean global average temperature increase in 2090-2099 w.r.t. 1980-1999 is $+1.8°$C (1.1 to 2.9°C) for B1, $+2.8°$C (1.7 to 4.4°C) for A1B, and $+3.4°$C (2.0 to 5.4°C) for A2 (Meehl et al., 2007b).

The period over which we consider local sea-level change is the same as in IPCC

AR4 (Table 10.7): the difference between 1980-1999 and 2090-2099. For this period, we extract atmospheric temperature, precipitation, the global mean thermal expansion and the local sea-level anomalies due to temperature and salinity changes from the model database (Meehl et al., 2007a). For the ice sheets we need additional information on the global average temperature of the pre-industrial climate (defined as the period 1865-1894), taken from the twentieth century reference runs.

As the resolution of the different models is highly variable, the data need to be interpolated to one grid to be able to construct an ensemble mean. We choose a grid with 512 longitude points and 256 latitude points, as this is the output grid of the sea-level model (Section 2.1.3) used to model sea-level change resulting from the land ice contributions.

The size of the surface area of the ocean is model dependent. However, if a grid point is assigned to land in one model and to ocean in another, this complicates comparisons between models, and especially the calculation of an ensemble mean. Therefore, in this study, sea-level change for the ensemble mean is calculated using a universal land-ocean mask which contains ocean surface area only at those grid points where all the models have ocean points. Use of the universal mask reduces the total ocean surface area with respect to the model-specific masks, leading to minor deviations in total sea-level change in the order of 2%.

4.3 Projections of local sea-level change

4.3.1 Global mean projections

In Table 4.3 the global mean values calculated in this study are compared to the results presented in Meehl et al. (2007b, Table 10.7), for the emission scenario A1B. The Table shows that the results in this study are in line with IPCC AR4, but also that there are a few differences. Firstly, a different ensemble of AOGCM's is used for the calculations, which influences the spread in the results of all contributions, except GIA. Secondly, a different GIC data set was used because locations of land ice melt were needed to calculate the regional GIC contribution. Also, GIA was added in this study, which is a small effect globally averaged, but can be large locally. The last difference is that the scaled-up ice sheet discharge is separated for the two ice sheets in this study.

Table 4.4 lists the global mean values for the three emission scenarios of all the modelled sea-level contributions and the resulting total sea-level change, obtained using the methodology described in Section 4.2. The uncertainties presented in the table represent one standard deviation within the model ensemble. Not surprisingly, the scenario with the lowest greenhouse gas emissions, B1 (11-model ensemble), predicts the lowest sea-level rise, while the high emission A2 scenario (10-model ensemble) yields the highest estimates. Table 4.4 shows that the global average GIA is slightly positive, but very small. As GIA is a long-term effect, it is not influenced by present-day changes, and is therefore the same for all scenarios. The GIC contribute a global

Table 4.3: *Projected global average of sea-level change (m) for SRES scenario A1B between 1980-1999 and 2090-2099, comparing this study to IPCC AR4 estimates (their Table 10.7). The range given is 5–95%.*

	This study	IPCC AR4	Remarks
Steric	0.14 – 0.30	0.13 – 0.32	Different model ensemble (this study 12, IPCC AR4 16)
GIC	0.13 – 0.25	0.08 – 0.15	Regionally distributed data set
AIS	-0.08 – -0.01	-0.12 – -0.02	
GIS	0.04 – 0.08	0.01 – 0.08	
GIA	-0.001 – 0.009	–	Not computed in IPCC AR4
Sum	0.30 – 0.55	0.21 – 0.48	
Scaled-up AIS	0.04 – 0.06	–	AIS and GIS combined in
Scaled-up GIS	0.02 – 0.03	–	IPCC AR4: -0.01 – 0.13

Table 4.4: *Projected ensemble mean global average of sea-level change (m) for SRES scenarios B1 (low), A1B (middle) and A2 (high) between 1980-1999 and 2090-2099. The sum includes the steric contribution, all land ice (including scaled-up ice sheet discharge) and GIA. Contrarily to Table 4.3, the uncertainties here are 1σ between 11 models (B1), 12 models (A1B) and 10 models (A2).*

	B1	A1B	A2
Steric	0.16 ± 0.08	0.21 ± 0.09	0.27 ± 0.17
GIC	0.14 ± 0.03	0.17 ± 0.04	0.19 ± 0.04
AIS	0.01 ± 0.02	0.01 ± 0.02	0.01 ± 0.03
GIS	0.06 ± 0.01	0.08 ± 0.02	0.08 ± 0.02
GIA	0.004 ± 0.003	0.004 ± 0.003	0.004 ± 0.003
Sum	0.37 ± 0.09	0.47 ± 0.11	0.55 ± 0.17

mean volume change of 0.17 ± 0.04 m SLE for A1B, which is the dominant part of the land ice contribution. Using the IPCC AR4 approach, we find that the ice sheets (now including the estimate for the scaled-up ice sheet discharge) contribute 0.01 ± 0.02 m from AIS and 0.08 ± 0.02 m from GIS. The low value of AIS follows from a near cancellation between the negative SMB contribution and the positive value for the scaled-up ice sheet discharge. Recent literature (e.g. Rignot et al., 2008a,b, 2011; Velicogna, 2009) challenges these estimates, as current observations of the mass loss on the ice sheets indicate that this contribution might be larger. We will elaborate on this topic in the discussion section (Section 4.4.1), where the influence of a larger ice sheet contribu-

tion is demonstrated. However, here we will continue to use the IPCC AR4 ice sheet estimates, including the scaled-up ice sheet discharge, to allow for a comparison of the regional patterns to the IPCC AR4 global mean values.

Although significantly less ice is stored in GIC than in the GIS and the AIS, GIC melt still provides a relatively large contribution to sea-level change. This is caused by the higher sensitivity of GIC to climate change due to their larger mass turnover. The steric contribution has values similar to the total land ice contribution, so each accounts for about 50% of the global mean sea-level change. This implies that the total spatial pattern will depend on the steric as well as the land ice contribution, as will be shown in Section 4.3.3.

4.3.2 Spatial patterns of the different contributions

The regional patterns of the separate contributions for scenario A1B are shown in Figure 4.2. We focus on this emission scenario from now on, because it has the largest available ensemble. Between the scenarios the amplitudes change, but the patterns are very similar.

The upper left panel of Figure 4.2 shows the sea-level change resulting from mass changes of the ice sheets. Because the AIS contribution based on the IPCC AR4 estimates is very small (Table 4.4), the pattern shown in Figure 4.2 mainly results from mass changes of the GIS. The signature of the self-gravitation effect is clearly visible: a sea-level fall close to the largest melt source (GIS) and an above average sea-level rise in the Southern Hemisphere. In the upper right panel, representing the contribution of the GIC, the self-gravitation effect is also clearly visible, but now for multiple melt sources. As most ice melts in the Northern Hemisphere, sea level will rise by at least the global mean value south of the equator, with the exception of the sea level close to the Antarctic Peninsula and the Patagonian ice fields, where values are lower due to local ice mass loss. The contributions of ice sheets and GIC combined lead to a large range for the local sea-level change of -3.96 m to 0.30 m, with a global mean of 0.26 m.

The lower left panel of Figure 4.2 shows the steric contribution. The pattern displays a large spatial variability. For example, the region around AIS will experience less sea-level change than the global mean, while according to the climate models sea-level change in the Arctic Ocean will be larger than average. The steric changes range from 0.01 m to 0.48 m, with a global mean of 0.21 m. The pattern closely resembles that shown in Figure 10.32 of Meehl et al. (2007b) (note that in the latter the local sea-level change relative to the global mean is shown while here the global mean is included). This indicates that despite our smaller model ensemble (12 AOGCM's versus 16 AOGCM's in AR4), we do capture the general features of the steric pattern. The underlying causes for these spatial variations in steric sea-level change were discussed in Meehl et al. (2007b) (Section 10.6.2). For example, the relatively large steric change in the Arctic Ocean is attributed to ocean freshening, while the minimum found in the Southern Ocean is due to changes in wind stress (Landerer et al., 2007a) or small thermal expansion (Lowe and Gregory, 2006).

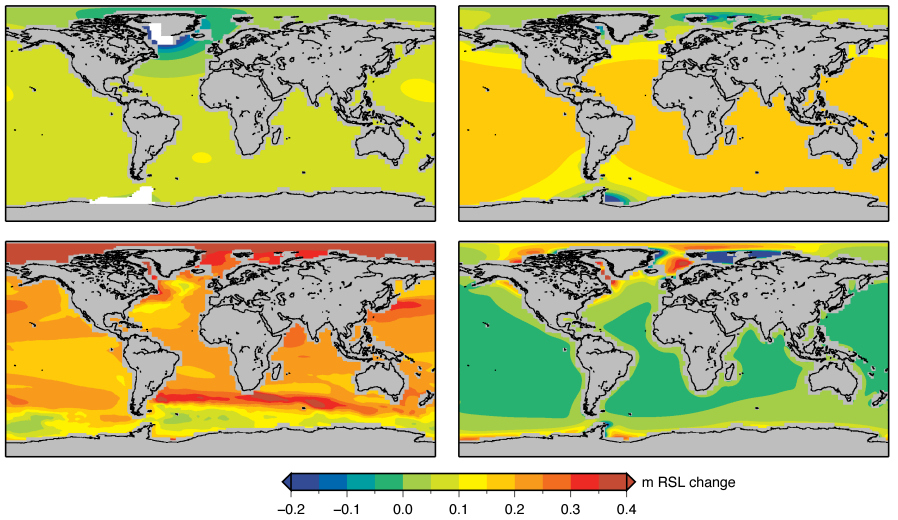

Figure 4.2: *Ensemble mean sea-level contribution (m) of ice sheets (upper left), GIC (upper right), steric changes (lower left) and GIA (lower right) for scenario A1B between 1980-1999 and 2090-2099. White shading in upper left panel indicates the mass loss regions on AIS and GIS.*

As GIA (Figure 4.2, lower right panel) is resulting from melt of the Laurentide and Fennoscandian ice sheets, the largest rates of crustal deformation due to GIA can be found in North America and Scandinavia. Changes are largest over land, but also the sea level is influenced: sea-level change values range from -0.73 m to 0.59 m, with a global mean of 0.004 m. While on average GIA is a small effect, in and near the regions previously covered by land ice the effect can still be quite large, and sometimes even dominate the other contributions (e.g. Scandinavia).

The standard deviations of the different contributions to sea-level change for the A1B ensemble are shown in Figure 4.3. The upper left panel shows the standard deviation of the ice sheet contribution, while the upper right depicts the GIC standard deviations. In both panels we find the largest uncertainties close to locations with large ice mass changes: AIS, GIS and the larger glacier areas, e.g. Svalbard. As this is where the gradients due to the self-gravitation effect are the largest, a small change in mass change will result in relatively large changes in the gradients. The middle left panel represents the σ of the steric contribution, with significantly higher values than for the land ice contributions. The largest standard deviations can be found in the Arctic Ocean, because the models disagree on the effects of Arctic freshening. To GIA we assign an average uncertainty of 20% (middle right panel), which is based on the difference between the ICE-5G(VM2)-model (Peltier, 2004) and the ANU-model (Nakada and Lambeck, 1988, updated in 2004-2005). As the GIA signal is generally quite small, this mainly results in small uncertainties. The lower panel represents the total ensemble mean standard deviation and will be discussed in Section 4.3.3.

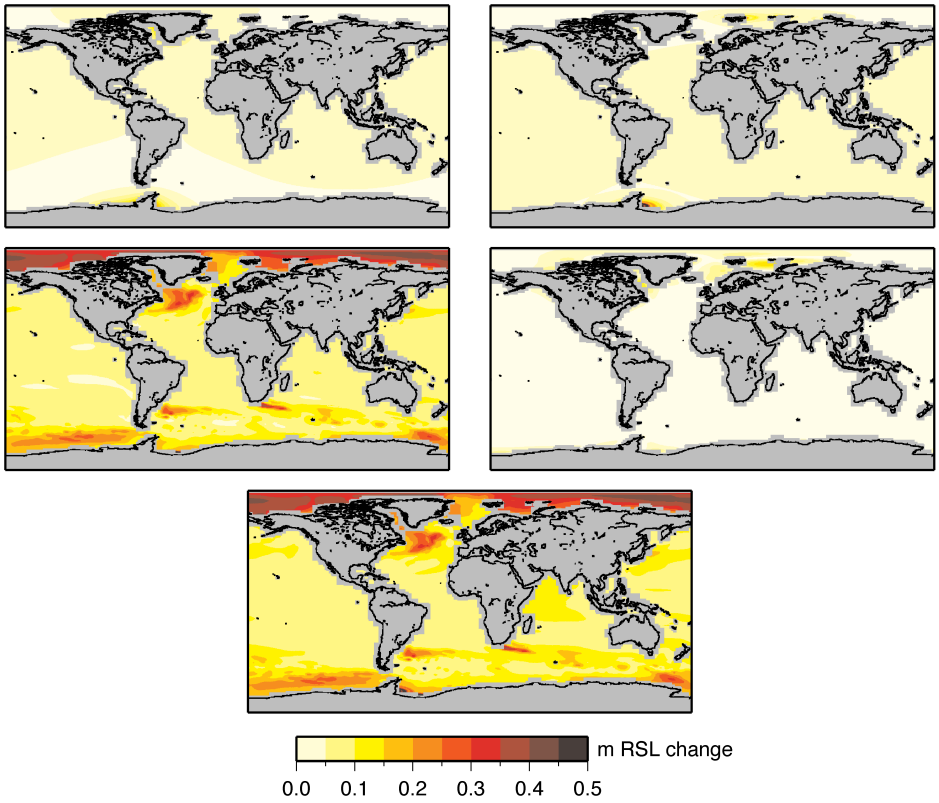

Figure 4.3: *Ensemble local standard deviation (m) of the sea-level contribution of ice sheets (upper left), GIC (upper right), steric changes (middle left), GIA (middle right) and all four contributions combined (lower centre) for scenario A1B between 1980-1999 and 2090-2099.*

4.3.3 Total projections of local sea-level change

In this section we consider the total projections for local sea-level change using the contributions calculated in the previous section. All land ice, steric and GIA contributions are added together, and the result is shown in Figure 4.4 for the three scenarios: A1B (upper panel), B1 (middle panel) and A2 (lower panel). While the global mean differs (Table 4.4), all scenarios show a similarly large spatial variability, with no significant differences in the spatial pattern. In all three panels, the spatial variability in the steric contribution has a large impact on the ensemble mean pattern. We observe for instance in all scenarios a band of relative high sea-level rise stretching from South America into the Indian Ocean. However, looking closer reveals influences of the other contributions too. The effect of Arctic freshening is less pronounced, because the steric contribution is partly balanced by the other contributions. We observe the influence of GIA for instance between Iceland and Scandinavia: the sea-level change is large since this region lies on the peripheral bulge (Peltier, 2004) and thus the Earth's surface is

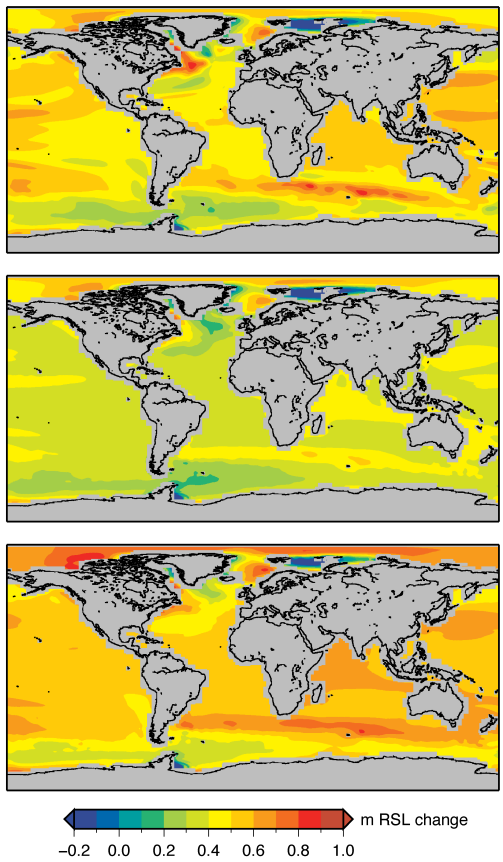

Figure 4.4: *Ensemble mean total sea-level change (m) between 1980-1999 and 2090-2099 for scenario A1B (upper, based on 12 models), B1 (middle, based on 11 models) and A2 (lower, based on 10 models).*

lowering here. Also future land ice melt influences the pattern, for instance in the Arctic Ocean, where it counteracts the influence of the steric changes, and around the Antarctic Peninsula, where a sea-level fall is projected as a result of the self-gravitation effect.

The total ensemble mean standard deviation of scenario A1B is shown in the lower panel of Figure 4.3. Here we see that the total uncertainty, when adopting the IPCC AR4 approach for the ice sheets, is dominated by uncertainties in the steric contribution, since the values of the standard deviations of land ice and GIA are significantly smaller. Hence, the largest standard deviations can be found in the Arctic Ocean and the Southern Ocean.

Figure 4.5 shows how much the projection for the local sea level deviates from the ensemble mean global mean value for scenario A1B. The figure emphasizes the large spatial variability of sea-level change, as it shows that the local values rarely equal the

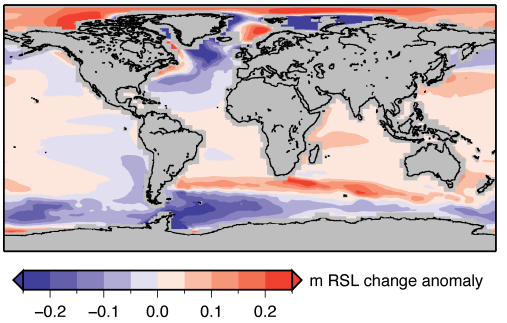

Figure 4.5: *Ensemble mean sea-level anomaly (m) w.r.t. global mean sea-level change (0.47 m) for scenario A1B between 1980-1999 and 2090-2099.*

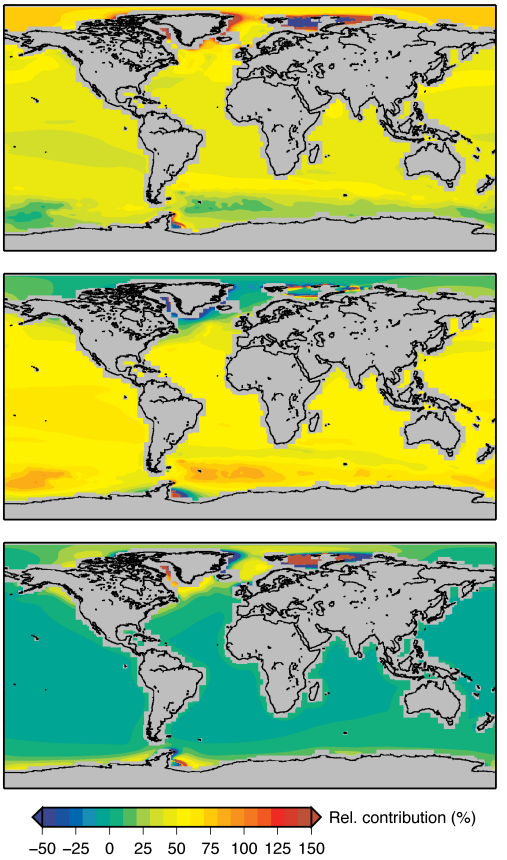

Figure 4.6: *Ratio (%) between the steric (upper), land ice (middle) and GIA (lower) contributions (Figure 4.2), and the ensemble mean sea-level change (Figure 4.4, upper panel).*

global mean value. Some regions experience a notably lower sea level, while others have extremely large sea-level rise compared to the global mean, with a pattern that is qualitatively similar for all scenarios (not shown).

In order to examine the influence of the different contributions on the total projected sea-level change and the spatial pattern, we show maps of the individual contributions as a fraction of the total value for A1B in Figure 4.6. The upper panel shows the ratio of the steric contribution, the middle panel the land ice ratio and the lower panel the GIA ratio, all relative to the total projection. There is a large region around the equator which shows very little influence of GIA and a 50%-50% contribution for land ice and steric contributions. In the Arctic Ocean, the steric contribution is slightly larger due to Arctic freshening, which is enhanced by GIA but balanced by a relatively low contribution of land ice mass loss. Around AIS there is a large band where the steric contribution has relatively little influence (10-30%), and land ice mass loss for a large part explains future sea-level change in that region (60-80%).

The ensemble mean total projection of A1B is an average of 12 AOGCM's. The total projected sea-level change for each AOGCM (for A1B) with their model-specific land-sea mask, is shown in Figure 4.7. Most AOGCM's show a pattern fairly similar to the ensemble mean, with slightly more spatial variation, which is smoothed in the ensemble mean. However, some models show overall higher values for sea-level change (MIROC3.2(hires)), while others are below the ensemble mean (NCAR-PCM and MRI-CGCM2.3.2). The differences in spatial patterns between the models arise mainly from the steric component, because the land ice contribution pattern is fairly similar for all AOGCM's as the amount of ice melt may vary depending on the temperature and precipitation change, but the locations do not change. The steric component on the other hand is largely influenced by the way small-scale processes in the ocean, like for example ocean heat uptake, are treated in the coupled models (e.g., Yin et al., 2010; Pardaens et al., 2010). Differences in amplitude between the AOGCM's, however, may be caused by steric as well as land ice mass changes, since both contributions respond to temperature changes prescribed by the AOGCM's.

4.3.4 Projections for selected coastal locations

To further illustrate the large spatial variability in sea-level change, we selected a few coastal locations and compared their local sea-level change values for the land ice, steric and GIA contributions (Figure 4.8a) and the total sea-level change (Figure 4.8b) to the global mean values. In Figure 4.8 the locations are ranked from north (Reykjavik) to south (southern tip of Chile), the first 8 locations in the Northern Hemisphere, the last 5 in the Southern Hemisphere. Additionally, the global mean is provided in panel (b) for comparison. Values are taken from the A1B ensemble mean (Figures 4.2 and 4.4).

In Figure 4.8(a), large variations can be observed for the land ice contribution. Locations like Vancouver, New York and the southern tip of Chile are below the land ice global mean of 0.25 m because they are close to large melt sources. Reykjavik

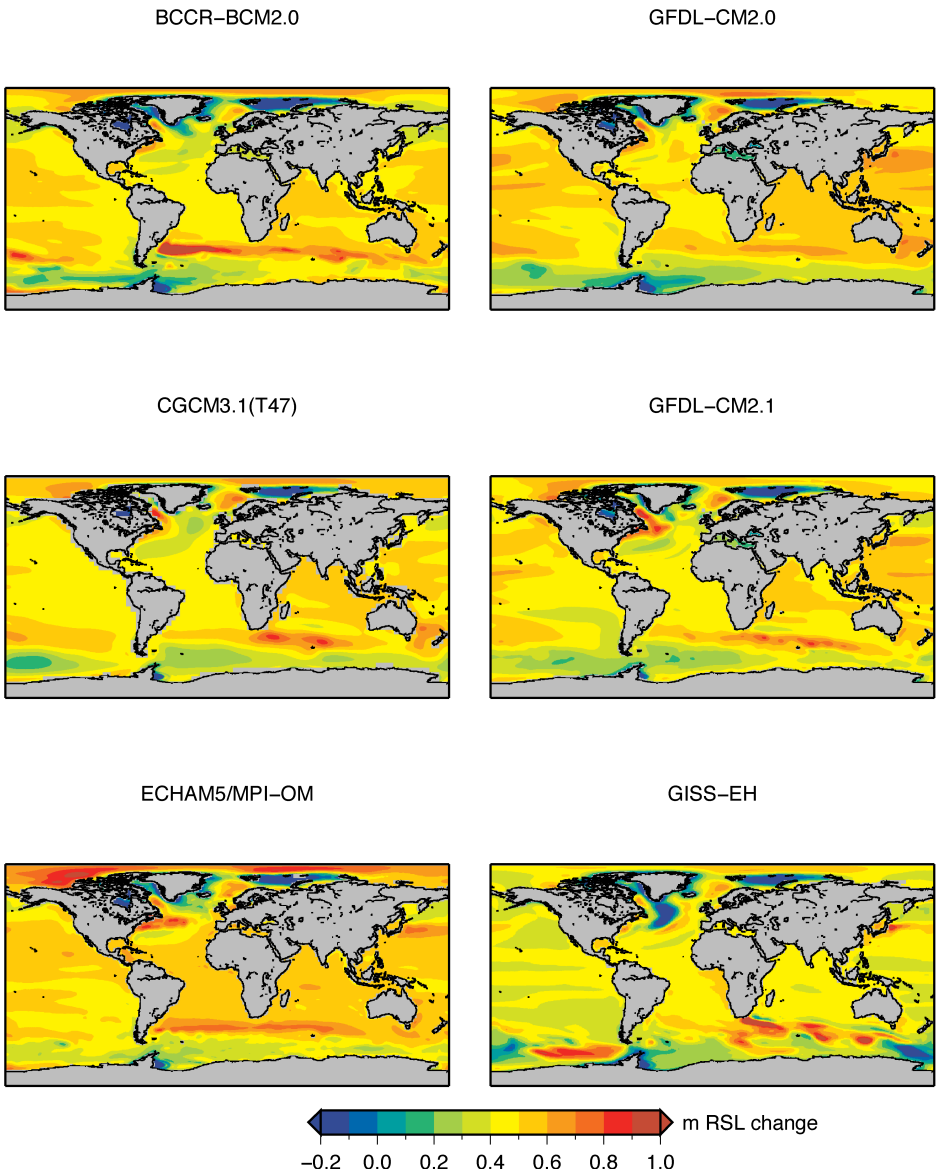

Figure 4.7: *Total sea-level change (m) between 1980-1999 and 2090-2099 for the individual AOGCM's in Table 4.2 for scenario A1B. (Continued on next page)*

even shows a negative value. On the other hand, Hawaii, Maldives and Tahiti experience values above the global mean due to their large distance from the land ice. The steric contribution shows high values for New York, Maldives and Tasmania, and low values for Miami and southern Chile, compared to the steric global mean of 0.21 m. Furthermore, in Figure 4.8(a) we see that the GIA (ICE-5G) contribution is large for

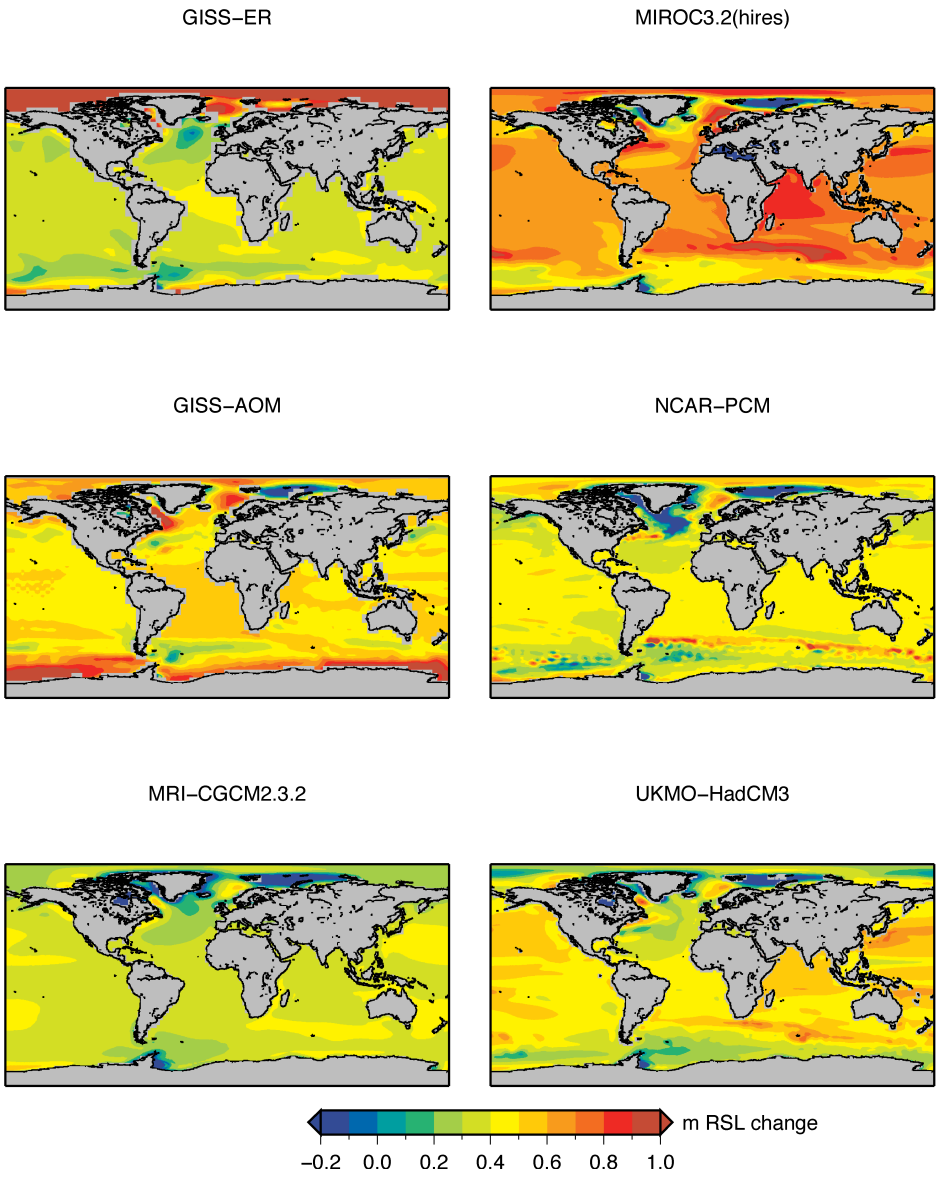

Vancouver, New York and Chile, compared to the global mean of 0.004 m. Vancouver and New York are in the peripheral bulge area, which means that these locations are still subsiding as a result of the melt of the ice sheets 20,000 years ago, resulting in a rising sea level. Reykjavik on the other hand is inside the crustal uplift area and thus experiences an sea-level fall.

The sum of the contributions is given in Figure 4.8(b), with an uncertainty of 1 standard deviation, as in Figure 4.3. All locations which are situated relatively far from

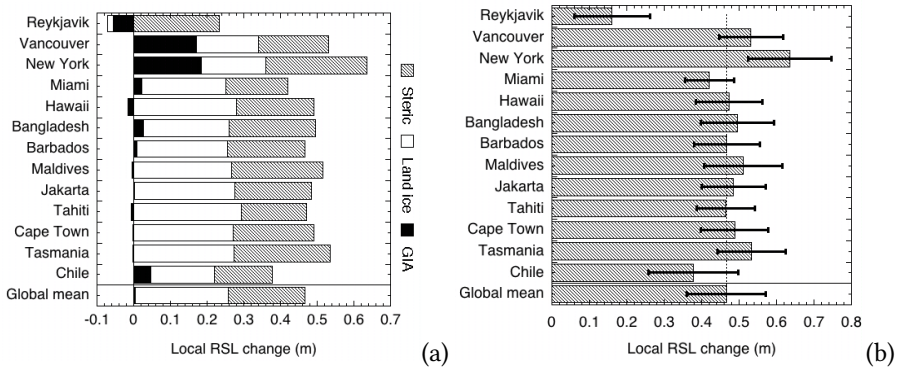

Figure 4.8: *Projection of local sea-level change (m) for selected coastal cities between 1980-1999 and 2090-2099 for scenario A1B.* **(a)** *Contributions: Steric (grey), Land ice (white) and GIA (black).* **(b)** *Total sea-level change and associated 1σ uncertainty.*

land ice melt sources experience values around or above the global mean value of 0.47 m. The largest deviations from the global mean occur in the regions closer to the ice sheets, for instance in Chile, which has a smaller land ice contribution because it is close to the Patagonian Icefields and the AIS. The results presented here illustrate that sea-level change is not just a process with large spatial variations, but also that different contributions may dominate the local sea-level change depending on the location. Therefore none of the contributions can be neglected when determining spatial patterns of total sea-level change.

4.4 Discussion of regional sea-level projections

4.4.1 Discussion of contributions included in this study

This study uses mostly the same data that were used in IPCC AR4, with the exception of the input data for the glacier model. This approach was taken to allow a comparison between the global mean values presented in IPCC AR4 and the regional patterns presented in this study.

For the GIC, a database first published in 2009 was used (Radić and Hock, 2010), because more detailed information was needed to model the regional influence of GIC on sea level. In IPCC AR4 the total volume of GIC (excluding glaciers around the GIS and the AIS) was estimated to be 0.15 (Ohmura, 2004), 0.24 (Raper and Braithwaite, 2005) and 0.37 (Dyurgerov and Meier, 2005) m SLE. These three different estimates are used throughout the AR4 report. To account for glaciers around the GIS and the AIS, the land ice contribution to sea-level change was multiplied with a factor 1.2. Here, the initial GIC volume is 0.6 m SLE, including glaciers around the GIS and the

AIS, which is larger than each of the IPCC AR4 estimates. Radić and Hock (2010) attribute these differences to the use of different methodologies and input data. As a consequence of the use of a different data set, not only the initial volume, but also the resulting projected contribution of the GIC is larger: IPCC AR4 projects a global mean contribution of GIC (including those around AIS and GIS) of 0.08 – 0.15 m SLE under the A1B scenario, while this study finds 0.10 – 0.24 m SLE (5 – 95% range).

To examine the influence of different GIC data on the regional pattern, we compare two GIC data sets, while keeping the same set-up of the model. Throughout this study we used the inventory by Radić and Hock (2010). The second data set is an inventory used by Van de Wal and Wild (2001), which contains 135 glacierized regions (Zuo and Oerlemans, 1997; Van de Wal and Wild, 2001) with an additional 10% to account for the GIC contribution of the Antarctic glaciers, as in Meehl et al. (2007b). The Van de Wal and Wild (2001) data has a smaller initial total GIC volume than the Radić and Hock (2010) data (0.50 m and 0.60 m, respectively), but we find that the contribution of GIC to future sea-level change depends on the data set rather than on the initial GIC volume, as the Van de Wal and Wild-contribution is only 0.01 m SLE larger. The main difference between the Radić and Hock data and the Van de Wal and Wild data is a larger amount of mass loss near GIS and less mass loss around AIS. This results in lower values in the Arctic Ocean and higher values (+0.02 m) in the Indian Ocean and the Southern Pacific. However, the sea-level change pattern is fairly similar to Figure 4.2 (upper right panel). Hence, we conclude that while the absolute values differ in some locations, the pattern will not change significantly when the main melt sources are situated in the same locations, which is the case for these two GIC data sets.

For the future contribution of the ice sheets, calculations were performed similar to the computations in IPCC AR4, with only one small modification. To calculate the spatial distribution of the dynamical SMB change and the scaled-up ice sheet discharge, the contributions needed to be calculated separately for each ice sheet, instead of using one value for both ice sheets combined, as in the IPCC AR4 report.

Although the results reported in IPCC AR4 were the state of the art on climate change in 2007, recent research has updated the estimates and models of different aspects regarding climate change. Nevertheless, we deliberately chose to stay as close as possible to the AR4 report in order to allow for a comparison of the spatial patterns to the well-known IPCC AR4 global mean values. To illustrate how this choice influences the results, we recalculated the sea-level change with larger estimates for the contributions of the ice sheets, as recent observations show a faster increase in mass loss than estimated in IPCC AR4 (e.g., Rignot et al., 2008a,b, 2011; Velicogna, 2009). For this example, we use a high-end estimate of 0.41 m SLE for the AIS and 0.22 m SLE for the GIS, as suggested by Katsman et al. (2011) based on a reassessment of the dynamical contribution of the ice sheets considering recent observations and expert judgement. Contrarily to the calculations done in Section 4.3, the ice sheet contribution is now fixed and thus not dependent on the temperature and precipitation provided by the climate models. This means that an ensemble spread could not be calculated for this

experiment. However, as the contribution of the ice sheets is much larger than in section 3, it will probably show larger variations for differences in climate, which would lead to a larger spread than displayed in Figure 4.3, but it is uncertain how much this would differ exactly. All the other contributions are the same as presented in Table 4.4 and Figure 4.2, the A1B scenario. Adding all the contributions now leads to a global mean sea-level change of 1.02 m SLE. The resulting anomaly with respect to the ensemble global mean sea-level change is shown in Figure 4.9. The ice sheets now account for 60% of the total sea-level change instead of only 25% in the IPCC AR4. This clearly influences the pattern in Figure 4.9, compared to Figure 4.5. The large amount of land ice melt on both ice sheets causes large sea-level fall in the regions around them. Also, the sea-level rise around the equator is much larger due to the self-gravitation effect. These effects are also shown in e.g. Bamber and Riva (2010) and Riva et al. (2010) and are a direct consequence of the gravitational attraction. The steric contribution now only accounts for 20% of the global mean instead of 45%, which means that the land ice melt is the dominant contribution. Still, features of the steric component and the GIA remain present, but less pronounced.

The example shown in Figure 4.9 illustrates the importance of using the best estimates possible when calculating regional sea-level variations, as the total pattern in sea-level change depends on the pattern from each of the contributions. Therefore, in the future, our model strategy can easily be used with better estimations for GIS mass change (e.g., Fettweis et al., 2008; Rignot et al., 2008b; Van den Broeke et al., 2009; Ettema et al., 2009), different values for AIS mass change (e.g., Rignot et al., 2008a; Bamber et al., 2009; Velicogna, 2009) or different steric fields from a new generation of climate models and improved data sets. Additionally, increasing the number of GIC described in databases and the development of global glacier models will improve the estimation of the GIC contribution to sea-level change for the next century.

For the estimate of the GIA-contribution (Section 4.2.3) we arbitrarily chose to calculate the projections based on the ICE-5G (VM2) model. We will now show the consequence of using a different GIA model, namely the ANU model (Nakada and Lambeck, 1988, updated in 2004-2005). Figure 4.10 is similar to Figure 4.8, but now the GIA contribution is from the ANU model, and only locations are shown where GIA is large. In Figure 4.10 (a) the GIA contribution according to the ANU model shows a larger sea-level rise near Reykjavik and Miami, which is substantially different from the ICE-5G GIA. Reykjavik is placed in an uplift area in the ICE-5G model, but in an area which is subsiding in the ANU-model. The region around the former ice sheets currently experiencing a sea-level rise due to GIA is much larger in the ANU-model, which explains the large values for Miami and Chile. The differences between the two models are partly caused by the ice histories used, but more importantly by different mantle viscosities, resulting in deviating present-day rates of GIA. Vancouver and New York both have a large positive contribution of GIA, resulting in an above-mean sea-level change, as shown in Figure 4.8b. The negative land ice contribution for Reykjavik is compensated by a very large positive GIA contribution, but the total sea-level change

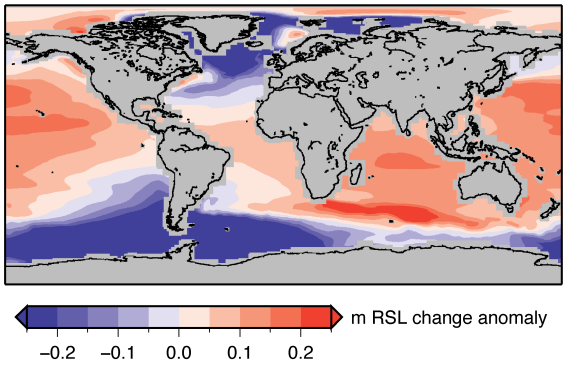

Figure 4.9: *Ensemble mean sea-level anomaly (m) w.r.t. global mean sea-level change (1.02 m) for scenario A1B between 1980-1999 and 2090-2099, for a scenario with adapted ice sheet contributions of 0.22 m for GIS and 0.41 m for AIS.*

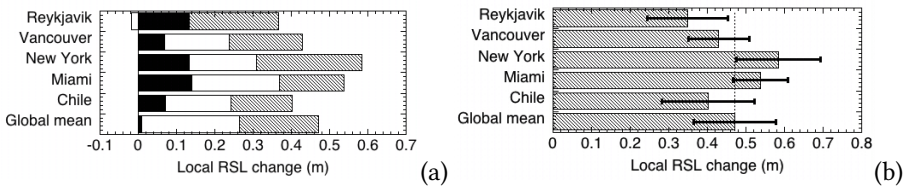

Figure 4.10: *Projection of local sea-level change (m) for selected coastal cities between 1980-1999 and 2090-2099 for scenario A1B with GIA contribution from ANU (updated version of Nakada and Lambeck, 1988).* **(a)** *Contributions: Steric (grey), Land ice (white) and GIA (black).* **(b)** *Total sea-level change and associated 1σ uncertainty.*

is still below average.

Both the global GIA models are mainly based on sea-level indicators, like sediment cores and corals, that are sparsely distributed and difficult to date accurately. Therefore, differences as in Figures 4.8 and 4.10 occur. Recent efforts that will help to reduce the current GIA uncertainty include for instance the use of space-geodesy (e.g. King et al., 2010).

4.4.2 Discussion of contributions not included in this study

A factor that influences local sea-level change but is not considered in this study is the response of the ocean circulation to land ice changes, in the form of melt water run-off being added to the ocean. In order to model the effects of freshwater addition to the ocean due to land ice melt, coupled climate models need to be equipped with an interactive land ice module. The current generation of coupled climate models does not yet have this feature and hence this effect has been omitted from the local projections presented in this study.

From dedicated numerical simulations (so-called hosing experiments) it has been known for a quite a while that the effect of melt water on the ocean circulation can be substantial (Manabe and Stouffer, 1996; Vellinga and Wood, 2002) and has notable effects on local sea level (Yin et al., 2010). However, the amount of melt water added to the ocean in these experiments is much larger than current observations of ice sheet mass loss suggest to be appropriate for the next century. Using a more realistic estimate for the imbalance of GIS, Stammer (2008) found that the added fresh water will induce sea surface height variations of a couple of centimeters after 50 years, mainly in the North Atlantic Ocean. As pointed out by Gower (2010), this is only the steric response of the global ocean circulation to freshwater forcing around GIS, as the forcing is not applied by adding fresh water but by removing salt at the ocean surface (Gower, 2010; Stammer, 2010). However, from comparative hosing experiments by Yin et al. (2010) it appears that either adding fresh water or removing salt yields very similar results with regard to regional variations in sea level. The results for global mean sea level obviously differ by the amount of fresh water that is added using the former method. Although it needs to be confirmed that this also holds for ocean freshening due to melt water originating from AIS, this indicates that it is in fact feasible to investigate the effect of melt water run-off on local sea level in a partially coupled, consistent way by applying an appropriate fresh water flux obtained from an ice sheet model. The magnitude of the response seen by Stammer (2008) suggests that this is a second-order effect for realistic ice sheet contributions. However, these type of simulations are not yet available for the time period considered in this study and hence cannot be included.

Other contributions we do not consider here are variations in terrestrial water storage, such as water impoundment behind dams (Fiedler and Conrad, 2010) or groundwater mining (Wada et al., 2010). Fiedler and Conrad (2010) report a global average sea-level fall of approximately 30 mm over the twentieth century, while Wada et al. (2010) find an average sea-level rise of 0.8 mm/yr due to groundwater mining. Although potentially important, neither of these studies provide projections for the twenty-first century.

4.4.3 Discussion of the climate model ensemble

The ensemble mean for A1B used in this study consists of 12 AOGCM's, while for the A2 and B1 scenarios an ensemble of respectively 10 and 11 AOGCM's has been used. For each scenario this is the largest ensemble for which all the required input variables are available (Section 4.2). Using the same 10 AOGCM's for all scenarios results (for A1B) in a total projected sea-level change of 0.45 ± 0.10 m instead of 0.47 ± 0.11 m, and the spatial pattern barely changes. Therefore, we considered it appropriate to use the largest available ensemble of 12 AOGCM's for the analyses presented in Section 4.3 rather than using only the overlapping AOGCM simulations.

The model spread in the total projection, which is based almost entirely on data used for the IPCC AR4 projections, is dominated by the spread in the steric changes

(Figure 4.3). In particular, in the Arctic and in the Southern Ocean the ensemble displays a large spread with a standard deviation exceeding 0.3 m. For local planning purposes, it would be beneficial if the large uncertainty in the local projection could be reduced by some form of quality control applied to the model ensemble. One example for a measure of the model skills is the ability of coupled climate models to simulate present-day dynamic sea-level patterns. Yin et al. (2010) analysed the root-mean-square difference between the observed and modelled sea-level patterns for seventeen climate models over the twentieth century, and excluded five models from their study based on this analysis. Four of these models are also part of our model ensemble (GISS-EH, GISS-AOM, MRI-CGCM2.3.2 and NCAR-PCM). An analysis of Q, defined as the difference between the ensemble mean and the model-specific steric contribution, normalized by the local standard deviation,

$$Q(x,y) = abs[SL_{steric}(x,y) - \overline{SL_{steric}(x,y)}]/\sigma(x,y) \tag{4.2}$$

reveals that GISS-EH and GISS-AOM are clearly outliers in the model ensemble in the Arctic and Southern Ocean, respectively, with values of $Q > 2.5$ over the largest part of these areas. None of the other models have Q-values comparable to this. In contrast, even though according to the analysis presented by Yin et al. (2010) they have poor skills in reproducing present-day sea-level patterns, MRI-CGCM2.3.2 and NCAR-PCM are not outliers in the model ensemble when Q is considered as a measure. This indicates that the future change in sea level they project is comparable to that of the other models.

When the four models indentified by Yin et al. (2010) are omitted from the model ensemble, the global mean contribution of the expansion and the global mean standard deviation of the steric component changes from 0.21 ± 0.09 m to 0.22 ± 0.09 m. However, the local standard deviation in the polar regions reduces considerably to sigma values of about 0.15 m rather than 0.40 m if all 12 models are included. In the Arctic, also the ensemble mean value reduces considerably.

The above analysis illustrates how large the impact of individual models on the variability can be, and hence the need for performing some type of quality control on the model results. Analyses like the one presented by Yin et al. (2010) can be a way forward to reduce the uncertainty in local projections, when the proper physical processes that cause the sea-level patterns are considered and understood (Landerer et al., 2007a; Pardaens et al., 2010).

4.5 Summary and conclusions

Sea-level change as a result of a changing climate is often regarded as a globally uniform process, with the same sea-level rise occuring everywhere. Clearly this is not the case: the spatial variability in the different contributions to relative sea-level change is very large (Figure 4.2). For governments and policy makers this is vital information

to determine whether measures have to be taken to protect coastal communities from sea-level rise.

Instead of characterizing sea-level change by a single number, we have used several models to calculate spatial distributions of the different contributions to sea-level change. As a starting point, we used the same data as in IPCC AR4, except for the GIC contribution. We coupled a volume-area model (Section 4.2.1) and estimations of ice sheet contributions (Section 4.2.1) with a sea-level model (Section 2.1.3) to compute the influence of the location and amount of melting land ice on the sea level. This was done for an ensemble of 12 coupled climate models and 3 emission scenarios with varying temperature and precipitation (Section 4.2.4). To estimate the steric contribution (changes in density and resulting changes in ocean dynamics, Section 4.2.2) we used the output from the same ensemble of coupled climate models. For the GIA, which is not influenced by the current climate but a result of climate change 20,000 years ago, we used results of a glaciation-deglaciation model to estimate the influence on sea-level change (Section 4.2.3).

In most regions, the two largest contributions are the addition of mass (the land ice component) and the changes in density (the steric component), while GIA is only large in some specific areas (Figure 4.2). The steric component shows very large spatial variations, because changes in density occur when ocean currents change, fresh water is added or atmospheric temperature changes. The land ice contribution on the other hand also shows large variations, but with a distinctive pattern due to elastic solid-earth deformation and the self-gravitation effect. Globally averaged, both the land ice contribution and the steric contribution account individually for about 50% of the sea-level change (Figure 4.6). However, considering the total projected spatial pattern reveals that all contributions included in this study, even GIA, can dominate the local sea-level change, depending on the location (Figures 4.4 and 4.8). The amplitudes of the local sea-level change differ per scenario, but the patterns are fairly similar. The spread in the local sea-level change for the projection based on the data used in IPCC AR4 is dominated by the spread in the steric contribution between the different AOGCM's, while the uncertainty in land ice contribution is largest close to the land ice melt source and fairly small otherwise (Figure 4.3). An increase in the estimation of the ice sheet contribution might also increase the spread for this contribution, but it is uncertain whether the result will be as large as the spread in the steric contribution.

The absolute values presented in this study should be interpreted carefully. In section 4.4.1 we have shown that following the approach taken by IPCC AR4 introduces a potential underestimation in the ice sheet contributions, which would influence the pattern substantially (Figure 4.9). This section also discusses the choice of GIA model, which is a small contribution when globally averaged, but can dominate sea-level change locally. Additionally, this section shows that the projections are not very sensitive to the choice of GIC data set.

We have shown with this study that it is possible to model regional variability in future sea-level change, by using a combination of spatial patterns of steric effects,

land ice melt and GIA obtained from different models. Improvements can be made, for instance by adding a coupling between ice melt and ocean dynamics or by better estimates for the land ice melt. Irrespective of the details in methodology, we think that scientific understanding now allows to discuss regional patterns rather than only the global mean values.

Acknowledgements
We would like to thank J. Gregory for providing the SMB constants and the additional expansion data, V. Radic for help with the WGI-XF data and J. G. Cogley for making this dataset available, P. Stocchi and K. Lambeck for providing the ANU model. We acknowledge the international modelling groups for providing their data for analysis, the Program for Climate Model Diagnosis and Intercomparison (PCMDI) for collecting and archiving the model data, the JSC/CLIVAR Working Group on Coupled Modelling (WGCM) and their Coupled Model Intercomparison Project (CMIP) and Climate Simulation Panel for organizing the model data analysis activity, and the IPCC WG1 TSU for technical support. We thank two anonymous reviewers for their useful comments.

CHAPTER 5

Uncertainties in the glacier contribution to sea-level change

A large part of present-day sea-level change is formed by the melt of glaciers and ice caps (GIC). This study focuses on the uncertainties in the calculation of the GIC contribution on a century timescale. The model used is based on volume-area scaling, combined with the mass balance sensitivity of the GIC. We assess different aspects that contribute to the uncertainty in the prediction of the contribution of GIC to future sea-level rise, such as (1) the volume-area scaling method (scaling factor), (2) the glacier data, (3) the climate models, and (4) the emission scenario. Additionally, a comparison of the model results to the 20th century GIC contribution is presented.

We find that small variations in the scaling factor cause significant variations in the initial volume of the glaciers, but only limited variations in the glacier volume change. If two existing glacier inventories are tuned such that the initial volume is the same, the GIC sea-level contribution over 100 yr differs by 0.027 m or 18 %. It appears that the mass balance sensitivity is also important: variations of 20 % in the mass balance sensitivity have an impact of 17 % on the resulting sea-level projections. Another important factor is the choice of the climate model, as the GIC contribution to sea-level change largely depends on the temperature and precipitation taken from climate models. Connected to this is the choice of emission scenario, used to drive the climate models. Combining all the uncertainties examined in this study leads to a total uncertainty of 0.052 m or 35 % in the GIC contribution to global mean sea level. Reducing the variance in the climate models and improving the glacier inventories will significantly reduce the uncertainty in calculating the GIC contributions, and are therefore crucial actions to improve future sea-level projections.

This chapter is based on: An assessment of uncertainties in using volume-area modelling for computing the twenty-first century glacier contribution to sea-level change, by A. B. A. Slangen and R. S. W. van de Wal, *The Cryosphere*, 5, 673–686, 2011, doi: 10.5194/tc-5-673-2011.

5.1 Introduction

Sea-level change is an important issue in the field of climate change. Currently, the largest contributions to sea-level change are the addition of mass through land ice melt and the thermal expansion of the ocean water (Bindoff et al., 2007). The land ice contribution consists of mass loss from the two large ice sheets (Greenland and Antarctica) and the glaciers and ice caps (GIC) outside the ice sheets. Both are important contributions and need further consideration for future sea-level predictions. Here we focus on the contribution of the GIC.

Over the past few years, several studies have presented estimates for the twenty-first century GIC sea-level contribution using different methods. IPCC AR4 projected a contribution of 0.08–0.15 m sea-level equivalent (SLE) for the A1B scenario (Meehl et al., 2007b), based on a range of climate models and three different values for the initial volume of all glaciers. As a follow-up on IPCC AR4, Meier et al. (2007) estimated a GIC contribution of 0.1–0.25 m SLE by 2100, where the range originates from two assumptions for the acceleration of ice loss. Another estimate was presented by Pfeffer et al. (2008), who found a GIC contribution of 0.17–0.55 m SLE by 2100, based on kinematically constrained scenarios. Bahr et al. (2009) used the accumulation area ratio (AAR) and calculated that GIC contribute 0.18 m SLE before they are in balance with the current climate. However, none of these studies provide regional estimates of GIC volume changes. The latter is done in a recent study by Radić and Hock (2011), who find a global mean contribution of 0.124 ± 0.037 m SLE. They use volume-area-length scaling to calculate regional glacier mass changes in response to climate model projections. Another study that provides regional estimates is Slangen et al. (2012, Chapter 4), who use volume-area scaling and arrive at a GIC contribution of 0.17 ± 0.04 m SLE.

The current study does not aim at improving the estimate of the GIC sea-level contribution as most of the above studies do, but at providing insight into the uncertainties of the GIC contribution.

The model used here is based on the volume-area scaling method, which builds on concepts developed by Bahr et al. (1997) and was applied for sea-level projections by Van de Wal and Wild (2001) and Slangen et al. (2012, Chapter 4). The model uses the volume-area relation in combination with a relation for the mass balance sensitivity of the glaciers and the amount of precipitation, and is described in Section 2.1.1 of this thesis. The present study uses the same approach and data as the Slangen et al. (2012) study, with the only difference that Antarctic glaciers are excluded here to enable a comparison to the older inventory used by Van de Wal and Wild (2001). This leads to a lower value for the total GIC contribution to sea-level change than in Slangen et al. (2012, Chapter 4).

Details of the model set-up and the data used in this study are presented in Section 5.2. A comparison of the model results for the past GIC contribution and a description of the reference experiment is presented in Section 5.3. In Section 5.4, which forms the core of this paper, the sensitivity studies are described. We distinguish uncertain-

ties related to the volume-area scaling method (Section 5.4.1), the glacier data (Section 5.4.2), the choice of climate model (Section 5.4.3), and the choice of emission scenario (Section 5.4.4). Finally, in Section 5.5, a summary of the findings in the previous sections is presented.

5.2 Data and methods

5.2.1 The volume-area model

The volume-area model that is used in this study is described in Section 2.1.1 of this thesis. For glaciers, γ in Equation 2.1 is set to 1.375 (Bahr, 1997; Chen and Ohmura, 1990). For c, Van de Wal and Wild (2001) used a value of $0.12\,\mathrm{m}^{3-2\gamma}$ to obtain a total GIC volume of 0.50 m SLE including GIC surrounding Antarctica and Greenland. Radić and Hock (2010) use a value of $0.2055\,\mathrm{m}^{3-2\gamma}$ and arrive at 0.60 m SLE for their glacier inventory. Here we vary c from 0.05 to $0.30\,\mathrm{m}^{3-2\gamma}$ in the sensitivity analysis (Section 5.4.1), and use $0.2055\,\mathrm{m}^{3-2\gamma}$ as the reference value. For ice caps, γ is set to 1.25 and c to $1.7026\,\mathrm{m}^{3-2\gamma}$, assuming an ice cap with a circular base (Paterson, 1994). These ice cap values are kept constant throughout the study, because variations in c of $\pm 25\,\%$ were found to lead to very small variations of $\pm 0.5\,\%$ in the sea-level contribution.

All values for initial volume (V_i) and the GIC contribution to sea-level change (δV) shown in the next sections are, unless explicitly mentioned, mean values of calculations with temperature and precipitation scenarios obtained from 12 AOGCM's (Meehl et al., 2007a). The set of AOGCM's will be referred to as the model ensemble, and will be more thoroughly described in Section 5.2.3.

The imbalance of the GIC with climate is accounted for by starting the calculations in 1865, and applying a global temperature increase of $0.7\,^\circ\mathrm{C}\,100\,\mathrm{yr}^{-1}$ over the period 1865–1990 (Trenberth et al., 2007). The importance of the imbalance of the GIC with climate is tested in Section 5.4.1, by applying data of Zuo and Oerlemans (1997) (Z97), which cover the period 1865–1990. For this reason we adopt 1990 as the starting year for the future contribution. The starting volume and area in 1865 are calculated iteratively, such that the modelled volume and area in 1990 agree with the glacier inventory. The model calculations are continued for another 100 yr after 1990, which results in a total of 225 modelled years. Future volume changes are therefore defined as the difference between 1990 and 2090.

5.2.2 Two glacier inventories

In this study, two glacier inventories are used, in order to estimate the uncertainty related to the choice of inventory. The first and default glacier inventory is an extended version of the WGI-XF (Cogley, 2009a), which has a World Glacier Inventory core (WGI, National Snow and Ice Data Center, 1999), and is combined with Icelandic and Alaskan data (Radić and Hock, 2010). The GIC are divided into 19 large regions, of which two are located around Antarctica. As the second inventory (described below)

does not contain any Antarctic data, the two Antarctic regions of this inventory will be excluded from this comparison. Of the remaining 17 regions, 7 regions have an incomplete glacier inventory. To complete these regions, an upscaling procedure is performed as described in Radić and Hock (2010). Then, to obtain the new number of glaciers per size bin, we divide the upscaled area by the average area in the size bin before upscaling. It is assumed that the entire upscaled area consists of glaciers, which slightly changes the ratio of glaciers and ice caps. However, tests show that this influence is negligibly small. We sort the remaining 17 regions into 14 regions as shown in Table 5.1. Using these 14 regions of Z97 facilitates a comparison of Radić and Hock (2010) data with the second glacier inventory. The total area in the Radić and Hock (2010) data set is 568 709 km^2. Each region has a size distribution in 18 size classes, ranging from $< 2^{-3}\,\mathrm{km}^{-2}$ to 2^{13}–$2^{14}\,\mathrm{km}^{-2}$. We will from now on refer to this glacier inventory as R10.

The second inventory used in this study also has a WGI core, but uses an older version than the R10 data set. Furthermore, the treatment of data-sparse regions differs from R10. This inventory consists of 135 regions, of which 100 regions are the main glaciated regions outside the two major ice sheets (Oerlemans, 1993, Z97), and 35 regions are located around the Greenland ice sheet (Van de Wal and Wild, 2001). The 135 regions are also merged into 14 large regions, as shown in Table 5.1. The total glaciated area in this data set is 597 613 km^2. For 41 of the 135 glaciated regions a size distribution is available in 15 size classes (from 2^{-6}–$2^{-5}\,\mathrm{km}^{-2}$ to $\geq 2^{9}\,\mathrm{km}^{-2}$). For the 35 regions on Greenland it is assumed that all glaciers are in the largest possible size class. The remaining 59 regions are assigned the average size distribution of the 41 regions which have a size distribution. From now on we will refer to this glacier inventory as W01.

As the GIC contribution to sea level is dominated by the large size classes we prefer the R10 data set as the reference inventory, since it has a better subdivision of the large classes than the W01 data set. Nevertheless, we will also use the W01 data to show how differences in the inventory, upscaling and area binning contribute to the uncertainty in the calculation of the GIC sea-level contribution. It also allows for a comparison of the recent inventory to earlier results (Section 5.4.2).

In Figure 5.1 it can be seen that the division of glacier area over the regions is similar for both inventories. However, as the volume-area relation is non-linear, the volume also depends on the size distribution of the glaciers in each region and thus the volume will not necessarily be equal for both data sets. These differences in the initial volume in 1990 (V_{i}) are a potential source of uncertainty and will be addressed in Section 5.4.

Table 5.1: *Regions and initial volume in 1990 (km^3) used in this study.*

This study	Region name (R10)	Volume (km^3)	Region name, number (W01)	Volume (km^3)
1 Arctic Canada	Arctic Canada	81 943	North Canada, 1–6	63 149
2 Alaska	Alaska/W. Canada/W. US	30 519	Alaska/Rocky Mountains, 7–30	21 802
3 Iceland	Iceland	4558	Iceland, 53–57	2191
4 Svalbard	Svalbard	10 199	Svalbard, 58	6995
5 Scandinavia	Scandinavia	222	Scandinavia, 62–63	155
6 Russian Arctic	Franz Jos./N. Zemlya/S. Zemlya	17 658	Franz Josef, 59–61	11 134
7 East Russia	North and East Asia	168	East Russia, 88–93	351
8 Central Europe	Central Europe	192	Central Europe, 64–65	130
9 South Russia	Caucasus	88	South Russia, 66–69	374
10 Central Asia	High Mountain Asia	12 536	Central Asia, 70–87	24 514
11 South America	South America I/II	7570	South America, 31–52	14 873
12 Africa	–	0	South Africa, 94–96	0.2
13 New Zealand	New Zealand	82	New Zealand, 98–100	219
14 Greenland	Greenland	16 099	Greenland, 101–135	36 398

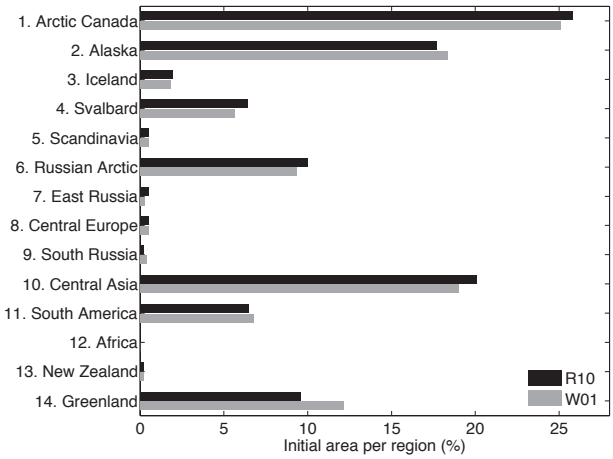

Figure 5.1: *Relative initial GIC area per region for the two glacier inventories, R10 in black, W01 in grey.*

5.2.3 Twelve climate models

The glacier model requires information on atmospheric temperature and precipitation to calculate the glacier contribution to sea-level change. These values are taken from the results of simulations with AOGCM's, of which the names and references are presented in Table 5.2. These models are a subset of the World Climate Research Programme's CMIP3 multi-model data set (Meehl et al., 2007a) used for IPCC AR4. This subset contains 12 models and was also used by Slangen et al. (2012, Chapter 4 in this thesis). In this study we mainly consider the emission scenario A1B, as defined in the IPCC Special Report on Emission Scenarios (Nakicenovic and Swart, 2000). In Section 5.4.4, the uncertainty resulting from the choice of emission scenario will be discussed, by using scenarios B1 and A2. The ensemble mean global average temperature increase in 2090–2099 w.r.t. 1980–1999 is $+2.8$ °C (1.7 to 4.4 °C) for the A1B scenario, $+1.8$°C (1.1 to 2.9°C) for B1, and $+3.4$°C (2.0 to 5.4°C) for A2 (Meehl et al., 2007b).

As the resolution of the different climate models is highly variable, the data are bilinearly interpolated to one grid to be able to construct an ensemble mean. We choose a grid with 512 longitude points and 256 latitude points, as this is the grid used in the sea-level model that calculates the sea-level patterns resulting from land ice mass changes.

In order to apply the ensemble mean climate forcing to the two glacier inventories R10 and W01 we use temperature and precipitation differences between 1980–2000 and 2090–2099. The values at each of the 135 locations of the W01 data set are averaged over the 14 regions as defined in Table 5.1. These mean values are used as forcing for the volume-area model. This procedure is necessary as the locations of the upscaled GIC in R10 are only known by region.

Table 5.2: *CMIP3-Models used in this study.*

Model name	Reference
BCCR-BCM2.0	Furevik et al. (2003)
CGCM3.1(T47)	Flato (2005)
ECHAM5/MPI-OM	Jungclaus et al. (2006)
GFDL-CM2.0	Delworth et al. (2006)
GFDL-CM2.1	Delworth et al. (2006)
GISS-EH	Schmidt et al. (2006)
GISS-ER	Schmidt et al. (2006)
GISS-AOM	Lucarini and Russell (2002)
MRI-CGCM2.3.2	Yukimoto and Noda (2002)
MIROC3.2(hires)	K-1 model developers (2004)
NCAR-PCM	Washington et al. (2000)
UKMO-HadCM3	Gordon et al. (2000)

5.3 Reference experiment and past sea-level contribution

5.3.1 Reference experiment

A reference experiment is defined for the remainder of this study, using the R10 glacier inventory. The reference V_i in 1990 is calculated using Equation 2.1, with $c = 0.2055\,\mathrm{m}^{3-2\gamma}$ and $\gamma = 1.375$, which are the values proposed by R10. This results in a V_i of $1.8122 \times 10^{14}\,\mathrm{m}^3$, or 0.50 m SLE. Note that ice caps are included using $c = 1.7026\,\mathrm{m}^{3-2\gamma}$ and $\gamma = 1.25$. These ice cap values are kept constant throughout this study, and variations on model parameters will only be performed on the glacier part, which is the largest contribution: 89 % glacier area vs. 11 % ice cap area. The value of 0.50 m SLE is lower than the original value by R10 (0.60 m SLE), because glaciers around Antarctica are excluded as they are not explicitly located in R10 and only taken into account by a scaling consideration in W01. Using the settings as described in Section 5.2.1, we compute a sea-level contribution for 1990–2090 (δV) of 0.149 ± 0.022 m SLE for the reference experiment.

To compare the results for the two glacier inventories, the total V_i of the W01 inventory is tuned such that it equals the total V_i of the reference experiment R10, by varying the scaling factor c in Equation 2.1. The value found for W01 is $c = 0.144\,\mathrm{m}^{3-2\gamma}$. This value for c is slightly larger than the original value adopted by W01 of $0.12\,\mathrm{m}^{3-2\gamma}$, which would yield a V_i of 0.42 m SLE for all glaciers except the Antarctic region, and 0.5 m SLE including glaciers around Antarctica and Greenland. With a c of $0.144\,\mathrm{m}^{3-2\gamma}$ and all other settings as in the reference experiment, we find

for the W01 glacier inventory a δV of 0.176 ± 0.025 m SLE.

Using the two glacier inventories thus leads to a difference of 0.027 m SLE in δV, which is quite large: 18 % difference with respect to the R10 reference inventory. The reason for this difference will be analysed in Section 5.4.2.

5.3.2 Past sea-level contribution

The model is set up such that a steady state with the prevailing climate is assumed before 1865, after which a temperature perturbation of $0.7\ ^{\circ}\mathrm{C}\,100\,\mathrm{yr}^{-1}$ is applied for the period 1865–1990. By imposing this temperature perturbation it is ensured that GIC are not in a steady state in 1990, which is very important for future projections (Z97, Van de Wal and Wild, 2001). Other methods to account for the imbalance with climate are for instance by modelling the accumulation area ratio (e.g. Bahr et al., 2009) or the equilibrium-line altitude (e.g. Raper and Braithwaite, 2006). The influence of the choice of temperature perturbation will be shown in Section 5.4.1.

For the reference experiment, the 1865–1990 GIC sea-level contribution is 0.057 m for the R10 data and 0.064 m for the W01 data. In Figure 5.2 the modelled sea-level contributions of R10 and W01 (blue and red line, respectively) are compared to the pentadal mass balance series of Cogley (2009b) (green line) and the estimated GIC contribution of Leclercq et al. (2011) (black line). The latter is a global reconstruction of glacier length records back to 1800 using volume-length scaling (Bahr et al., 1997; Oerlemans et al., 2007). Note that the total area differs between the data sets: Cogley (2009b) uses 785 000 km^2, Leclercq et al. (2011) use 704 000 km^2 (both include Antarctic glaciers), W01 has a surface area of 597 613 km^2 and R10 is the smallest with 568 709 km^2 (both R10 and W01 exclude Antarctic glaciers).

The data of Cogley (2009b) are available from 1950 onwards. In Figure 5.2 the Cogley data shows pentadal variability, which is not present in W01 and R10 because a uniform temperature increase was applied. The model results are also compared to the values of Leclercq et al. (2011), who find a contribution of 0.078 ± 0.022 m for the period 1865–1990. R10 and W01 show a smaller increase for the 1865–1925 period than Leclercq et al. (2011), which is probably caused by a different history before 1865. The volume-area model assumes all glaciers to be in balance with climate before 1865, whereas the Leclercq et al. data are already in imbalance in 1865 (Leclercq et al., 2011, their Figure 6). Nevertheless, the period after 1925 shows a cumulative sea-level contribution similar to our experiments, which indicates that applying the imbalance of $0.7\ ^{\circ}\mathrm{C}\,100\,\mathrm{yr}^{-1}$ for the 1865–1990 period is appropriate when calculating the contribution from 1990–2090.

5.4 Sensitivity experiments

A set of sensitivity experiments is described in this section. First, the model set-up is investigated, by varying some of the model parameters. The three experiments that

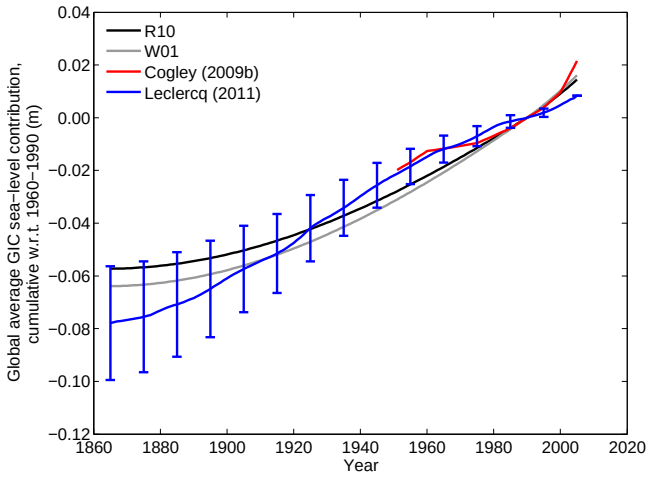

Figure 5.2: *Global average GIC sea-level contribution (m) relative to 1990.*

will be discussed are the mass balance sensitivity (Section 5.4.1), the scaling factor c in Equation 2.1 (Section 5.4.1) and the imbalance histories (Section 5.4.1). Next, the input of the model, i.e. the glacier data, is discussed in Section 5.4.2. Finally, the twelve climate models (Section 5.4.3) and the influence of different emission scenarios are discussed (Section 5.4.4).

5.4.1 Glaciological analytical uncertainty

Mass balance sensitivity

The mass balance sensitivity of a glacier indicates how the mass balance responds to changes in temperature and precipitation. Oerlemans and Fortuin (1992) found that it strongly depends on the amount of precipitation the glacier receives in a year. We therefore use Equations 2.3 and 2.4 to relate mass balance sensitivity to precipitation, as proposed by Z97. The mass balance sensitivity relation is a parameterisation based on mass balance observations on 12 glaciers described in Oerlemans and Fortuin (1992) and Oerlemans (1994), which has been confirmed by Braithwaite and Raper (2002). However, the mass balance sensitivity may vary between different climate zones, and those 12 glaciers possibly are not representative for the entire distribution of GIC on Earth. Hence, we study the effect of the uncertainty in the mass balance sensitivity.

To test the consequences of variations in the mass balance sensitivity, we apply a variation of $\pm 20\,\%$, which is considered a fair estimate of the uncertainty due to the limited data set used to derive the sensitivity. Additionally, the precipitation used to calculate the mass balance sensitivity is varied by $\pm 20\,\%$.

Varying the total mass balance sensitivity by $\pm 20\,\%$ leads to a deviation of $17\,\%$ in the future sea-level contribution. Varying the precipitation rate by $\pm 20\,\%$ leads

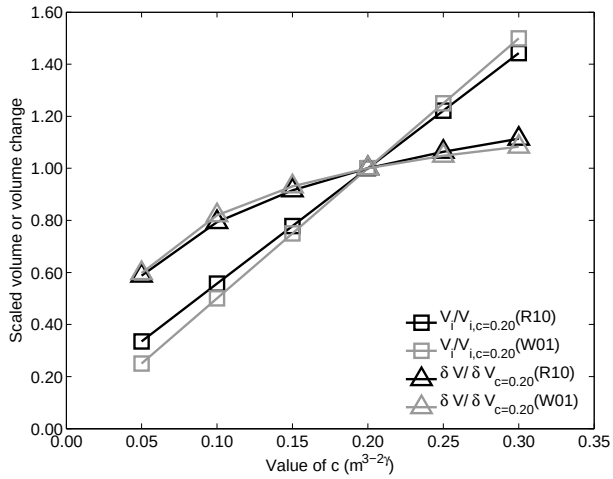

Figure 5.3: *Initial GIC volume (V_i) relative to $V_{\mathrm{i},c=0.20}$, and 1990–2090 GIC sea-level contribution (δV) relative to $\delta V_{c=0.20}$. R10 in black, W01 in grey.*

to smaller changes in δV of 12 %, since variations in precipitation rate are related to variations in mass balance sensitivity through Equations 2.3 and 2.4. Thus, differences in precipitation rate are less important than variations in the mass balance sensitivity itself given a range of variation of 20 %. With respect to the reference experiment, varying the mass balance sensitivity by ± 20 % leads to a deviation of 0.026 m SLE in the projected sea-level change.

Scaling factor c

In this second sensitivity experiment, the scaling factor c in Equation 2.1 is varied by a range of 0.05 to 0.30 $\mathrm{m}^{3-2\gamma}$. This influences not only the 1990–2090 contribution of GIC to sea-level change (δV), but also the initial volume in 1990 (V_i), because both are calculated by applying the volume-area relation (Equation 2.1) to the glacier data.

The results in terms of V_i and δV for variations in the scaling factor c are shown in Figure 5.3. In this figure, the values obtained for V_i and δV with $c = 0.20\,\mathrm{m}^{3-2\gamma}$ are taken as reference values, and the quantities shown are V_i and δV relative to these reference values for a range of values of c: $\frac{V_\mathrm{i}}{V_{\mathrm{i},c=0.20}}$ and $\frac{\delta V}{\delta V_{c=0.20}}$. Figure 5.3 shows that the scaled V_i increases linearly with c, for both the R01 and the W01 glacier inventory. However, the scaled δV shows a different, less sensitive, response than the scaled V_i to an increase in c. If values for c are varied by $\pm 0.05\,\mathrm{m}^{3-2\gamma}$ (25 %), V_i changes by 25 %, while δV varies by only 9 % (0.014 m SLE). This means that small deviations in c will not have a large influence on the modelled contribution of GIC to sea-level change. This is encouraging since c is poorly constrained and may therefore vary between glaciers and regions, which is reflected by the different values that can be found in the literature (e.g. Bahr, 1997; Chen and Ohmura, 1990).

The cause of the different response of V_i and δV to variations in c can be explained by the fact that GIC in a changing climate generally do not reach a new equilibrium state in 100 yr time, except smaller glaciers, which may disappear completely. This is illustrated in Figure 5.4, where the volume evolution in time for a few glacier size classes is shown. The figure also shows that the GIC in the larger size classes are still in the transition phase of adjusting to climate change. In the volume-area approach, GIC can only reach a new equilibrium by disappearing, unlike the methods of Raper and Braithwaite (2006) or Radić and Hock (2011), which can reach a new equilibrium over time. However, these methods require more information on the GICs hypsometry, which is not available for all glaciers. Additionally, larger glaciers will not reach an intermediate equilibrium within 100 yr, and therefore the volume-area method provides sufficient results for this period.

Figure 5.4 suggests that the volume evolution in time can be described by an *arccotan* function. This is the case for all glacier size classes separately, but also for the total GIC volume. Hence, the evolution of volume with time (t, t_0 =1865) can be written as:

$$V^* = \frac{\pi}{2} + arccotan\ \frac{t\text{-}D}{E}, \tag{5.1}$$

where V^* is $\frac{V_t}{V_0}$, D is the year where V_t is 0, and E is a mathematical constant describing the fit without any specific physical interpretation. Equation 5.1 is only valid for $t < D$. As an example, fits have been made for the R10 data set of the total modelled GIC volume for 1865–2090, for different values of c. The parameters resulting from the fits are shown in Table 5.3. From the Table it appears that, while D and E both increase for larger V_i, D/E is more or less constant. The derivative of Equation 5.1 reads:

$$\frac{\delta V^*}{\delta t} = \frac{1}{1 + t_*^2} \tag{5.2}$$

with t_* being (t-D)/E. As E ranges from 200 to 270, this implies that for the first 200 yr differences in the volume loss over time are small. We indeed see that when c is varied by $\pm$25 %, the δV^* between 125 and 225 yr varies by only 10 %. As a consequence, the exact value of c is not that important within the time frame considered.

We have performed a similar sensitivity study on the other parameter in Equation 2.1, γ. Available estimates for γ are 1.375 (Bahr, 1997), used in this study, and 1.36 (Bahr et al., 1997). The range over which γ is tested is based on the difference between the two estimates: 1.345 to 1.405 with steps of 0.015. From this we also find that V_i is more sensitive to the choice of the scaling exponent γ than δV, which is fairly insensitive to variations in γ.

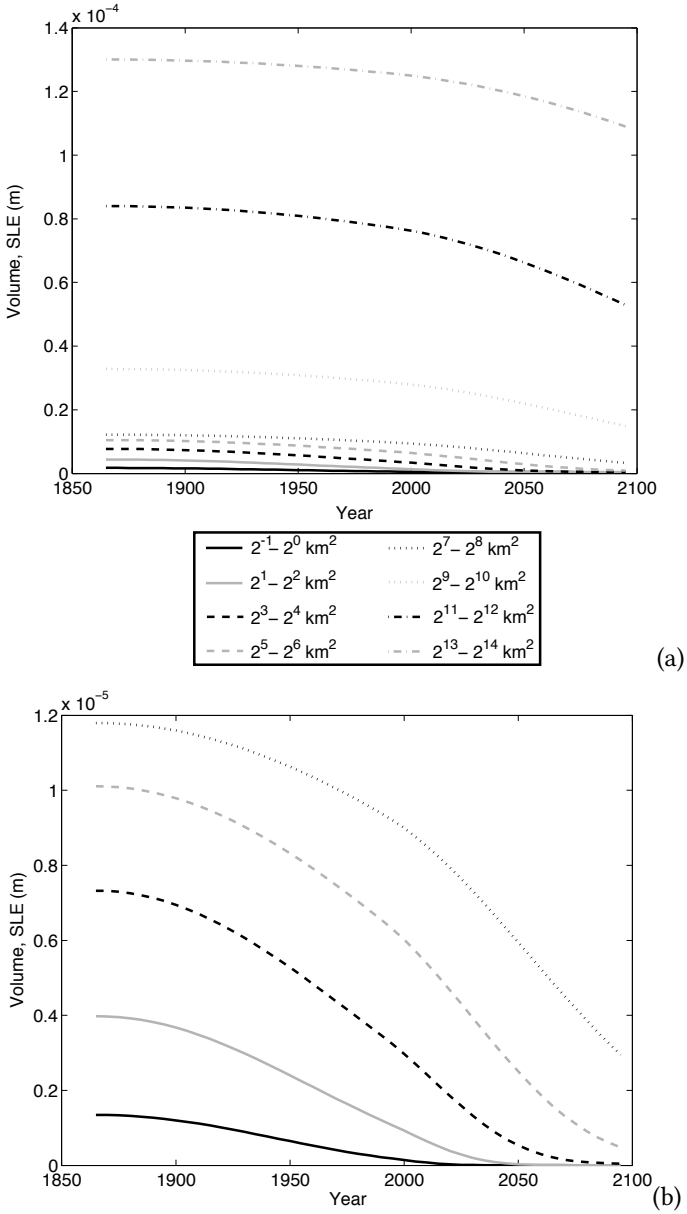

Figure 5.4: *Volume evolution (m) in time for* **(a)** *every second size class for reference experiment R10 and* **(b)** *close-up of the smallest 5 size classes in* **(a)**.

Table 5.3: *Results of fits on the evolution of V (Equation 5.1) for 3 values of c (Equation 2.1), using the R10 data. $V_{t=0\ \mathrm{yr}}$ represents the 1865 volume, $V_{t=125\ \mathrm{yr}}$ the 1990 volume, $V_{t=225\ \mathrm{yr}}$ the 2090 volume, D and E are fitted constants in yr. SLE is calculated assuming an ocean area of 3.62×10^8 km^2.*

	Small V_i $c = 0.1$	Medium V_i $c = 0.15$	Large V_i $c = 0.2$
$V_{t=0\ \mathrm{yr}}$ (SLE m)	0.33	0.44	0.54
$V_{t=0\ \mathrm{yr}}$ $(10^5\ \mathrm{km}^3)$	1.22	1.58	1.97
$V_{t=125\ \mathrm{yr}}$ $(10^5\ \mathrm{km}^3)$	0.99	1.39	1.78
$V_{t=225\ \mathrm{yr}}$ $(10^5\ \mathrm{km}^3)$	0.61	0.95	1.30
D (yr)	338	402	454
E (yr)	204	240	270
D/E	1.66	1.68	1.68
Volume loss $(10^5\ \mathrm{km}^3)$	0.38	0.44	0.48

Imbalance in 1990

Throughout this study, the 1990 imbalance of the GIC is simulated by imposing a temperature change of $0.7\ ^\circ\mathrm{C}\,100\,\mathrm{yr}^{-1}$ for the period 1865–1990, which is in line with the IPCC AR4 estimate (see Table 3.2 in Trenberth et al., 2007). However, in this section we will impose a range of different options for the imbalance on the R10 data to quantify their influence on the future sea-level change.

The first option we explore is to calculate the GIC contribution without an imbalance. This means that the glacier model starts its calculations in 1990, which clearly influences the resulting contribution (Figure 5.5, light blue line) with a difference as large as 39 % from the reference experiment ($0.7\ ^\circ\mathrm{C}\,100\,\mathrm{yr}^{-1}$, black line). However, it is not very realistic to assume that GIC are currently in balance with climate, and this option shows how important it is to include an imbalance, as it has a large influence on the future sea-level contribution (compare e.g. Z97).

As a second test, the rate of temperature change for 1865–1990 is varied: $0.6\ ^\circ\mathrm{C}\,100\,\mathrm{yr}^{-1}$ (Figure 5.5, magenta line) and $0.8\ ^\circ\mathrm{C}\,100\,\mathrm{yr}^{-1}$ (green line). For the sea-level contribution before 1990 this results in deviations of about ± 0.01 m from the reference in 1865. However, for the future sea-level contribution the differences are in the order of ± 0.005 m, which is about 4 %. This indicates that the exact value of the rate of temperature change is not a large source of uncertainty for the future contribution, as long as the value chosen is close to the observations.

Another factor that influences the volume change is the precipitation. Increasing the initial precipitation rate in 1990 leads to a larger contribution from the GIC to sea-level change, because the mass-balance sensitivity highly depends on the precipitation

rate and will consequently increase. This makes GIC more sensitive to temperature changes. We find that an increase of 10 % in the precipitation rate in 1990 combined with a temperature change of $0.6\ ^{\circ}\mathrm{C}\,100\,\mathrm{yr}^{-1}$ for the imbalance leads to a similar sea-level contribution by 2090 as a temperature increase of $0.7\ ^{\circ}\mathrm{C}\,100\,\mathrm{yr}^{-1}$. The same holds for a temperature change of $0.8\ ^{\circ}\mathrm{C}\,100\,\mathrm{yr}^{-1}$ combined with a precipitation decrease of 10 %.

To test the influence of regional variations, we now prescribe a temperature change for each region separately, similar to the way the modelled climate changes are used for the 1990–2090 period (see Section 5.2.3). We test two options: for the first we use a compilation of historical temperatures from Z97 (Figure 5.5, dark blue line); for the second we take the regional temperatures from the 20th century climate model runs (20C3M, Figure 5.5, red line). Figure 5.5 shows that for the 1990–2090 contribution the Z97 data are very close to the $0.7\ ^{\circ}\mathrm{C}\,100\,\mathrm{yr}^{-1}$ option and the 20C3M data result in a slightly smaller contribution. For the 1865–1990 contribution, the difference is larger, 0.01 m for Z97 and 0.02 m for the climate models. This indicates that taking regional values for the temperature change over the past, despite having influence on the past contribution, does not have a large impact on the future contribution.

As can be seen in Figure 5.5, the different options for the imbalance show larger deviations in the past volume change than in the future contribution. The past contribution acts as a spin-up period, and starts with all glaciers in balance with climate. Depending on the prescribed climate, the glaciers are brought in imbalance with climate, leading to relatively large deviations from the reference run. For the future contribution however, the climate is taken from the AOGCM's, so the only difference is the initial imbalance in 1990. It appears that this leads to differences in the past being more pronounced than in the future contribution.

Summarising, we find that if an imbalance is included (all options except "no imbalance"), the average deviation in the future contribution is 0.009 m SLE, provided that the temperature increase between 1865 and 1990 is around $0.7\ ^{\circ}\mathrm{C}\,100\,\mathrm{yr}^{-1}$.

5.4.2 Glaciological data uncertainty

Choice of inventory

In this section we consider the importance of the geometrical input to the model and its influence on the resulting GIC sea-level contribution (δV). We compare the two glacier inventories using the reference experiment settings as defined in Section 5.3.1. As mentioned before, the initial area per region (Figure 5.1) is quite similar for both glacier inventories. Furthermore, since the experiment considered here is the reference experiment, also V_{i} is similar. However, V_{i} is not divided equally over the different regions. In Figure 5.6 it can be seen that there are substantial differences between the two inventories. In Central Asia, South America and Greenland the regional V_{i} in R10 is smaller than the V_{i} in W01, while the opposite is true for Canada, Alaska and the Russian Arctic.

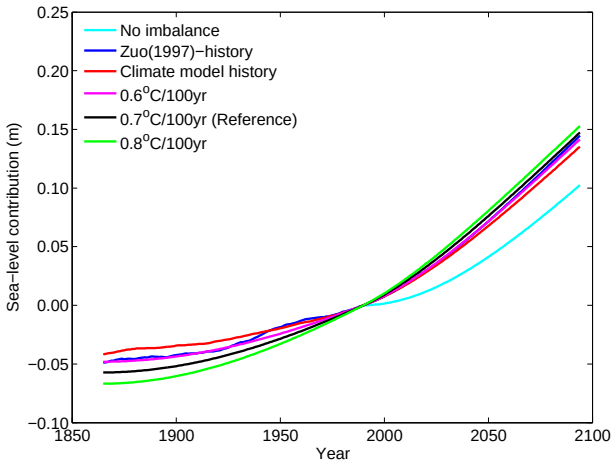

Figure 5.5: *GIC sea-level contribution (m) for different imbalance options, R10 glacier inventory.*

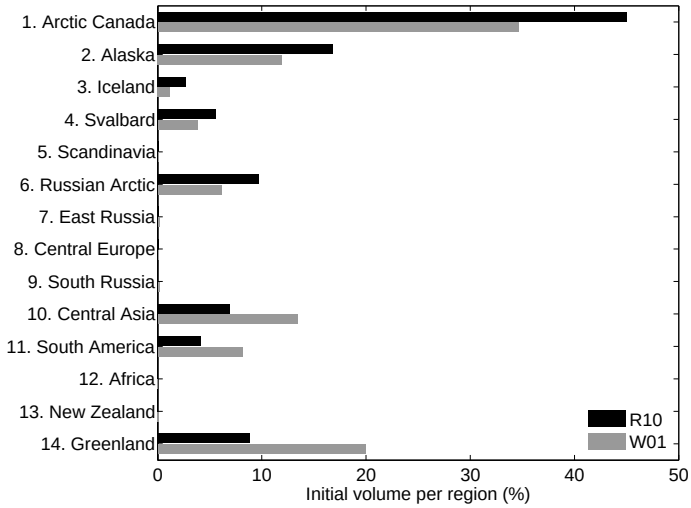

Figure 5.6: *Initial GIC volume per region relative to V_i for the two inventories ($V_{\mathrm{i,R10}} = V_{\mathrm{i,W01}}$).*

To explain the cause of these differences, we focus on Arctic Canada and Central Asia. Arctic Canada occupies 25 % of the initial area in both data sets, but the V_i differs substantially (10 % more in R10). Figure 5.7a shows how the total area is divided over the size bins: the largest W01 size bin ($> 2^9\,\mathrm{km}^2$) contains most of the W01 area, where the R10 size bins (until $> 2^{14}\,\mathrm{km}^2$) allow for a more precise classification of these larger GIC. To calculate the volume of the GIC, the average area in the size bins

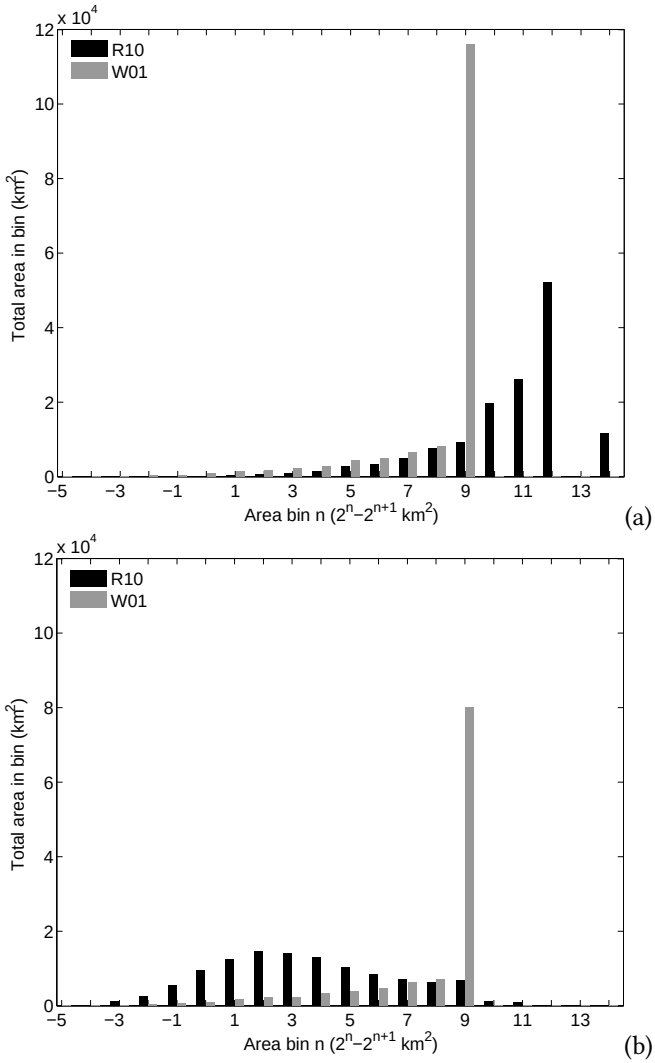

Figure 5.7: *Initial (1990) GIC area (km^2) per size bin for* **(a)** *Arctic Canada and* **(b)** *Central Asia. R10 uses size bins -3 (all GIC with area $< 2^{-2}$ km^2) to 14 ($> 2^{14}$ km^2), W01 uses size bins -5 ($< 2^{-4}$ km^2) to 9 ($> 2^9$ km^2).*

is used. In the volume-area relation, volume increases with the 1.375 power of the area, which means that the larger size bins of R10 result in a larger volume, explaining the different V_i for this region. As a second example, the size bins for Central Asia are shown in Figure 5.7b. In this case, W01 classifies more GIC into the largest size bin than R10, which leads to a higher V_i for the W01 data. Hence, differences in V_i per region are often caused by differences in the classification of GIC in size bins. These classification differences are not only the result of the increased number of glaciers in

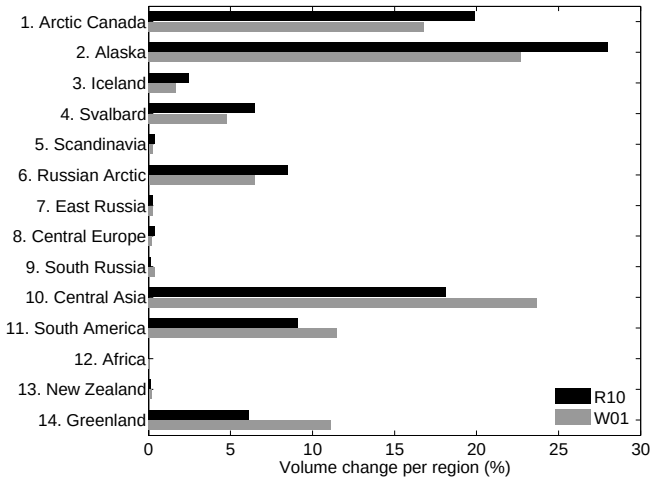

Figure 5.8: *GIC sea-level contribution per region relative to total δV.*

the R10 data set, but also due to the division of large ice bodies into smaller glaciers.

The R10 reference experiment yields a δV of 0.149 ± 0.022 m SLE, while using W01 results in 0.176 ± 0.025 m SLE, which is a difference of 0.027 m SLE. The uncertainty represents one σ uncertainty among the 12 climate models, and will be further discussed in Section 5.4.3. Figure 5.8 shows the ensemble mean δV per region relative to V_i for both glacier inventories. The larger differences (>1 %) between the two inventories are in regions with significant contributions; Arctic Canada, Alaska, Svalbard, the Russian Arctic, Central Asia, South America and Greenland. So, although the V_i is the same, the regional contributions of V_i and δV differ significantly. This is important when local sea-level change is the key interest rather than the global average sea-level change.

The relative values in Figures 5.6 and 5.8 show how the mass change is divided over the regions, but not how this relates to the V_i per region. Therefore, V_i and the GIC volume change are presented in m SLE per region in Figure 5.9. This immediately shows the largest glaciated regions and the regions with the highest mass loss. The V_i of R10 is clearly larger in Arctic Canada, Alaska, Iceland, Svalbard and the Russian Arctic, while W01 shows larger values in Central Asia, South America and Greenland. The total δV is larger for the W01 data, which is mainly caused by differences in Central Asia, South America and Greenland. This can again be explained by the way GIC are classified into size classes in the two inventories.

For each of the two data sets, the sea-level change pattern resulting from the ice mass changes is computed with a sea-level model (Schotman, 2008). This model calculates a gravitationally consistent field of sea-level change while accounting for rotational processes. For more information on the model, the reader is referred to Slangen et al. (2012). The model results are shown in Figure 5.10a, where the percentage pre-

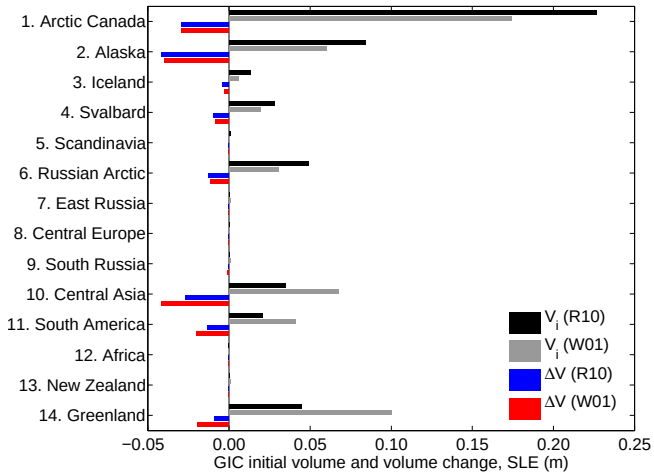

Figure 5.9: *GIC initial volume (V_i) and volume change per region (δV), SLE (m).*

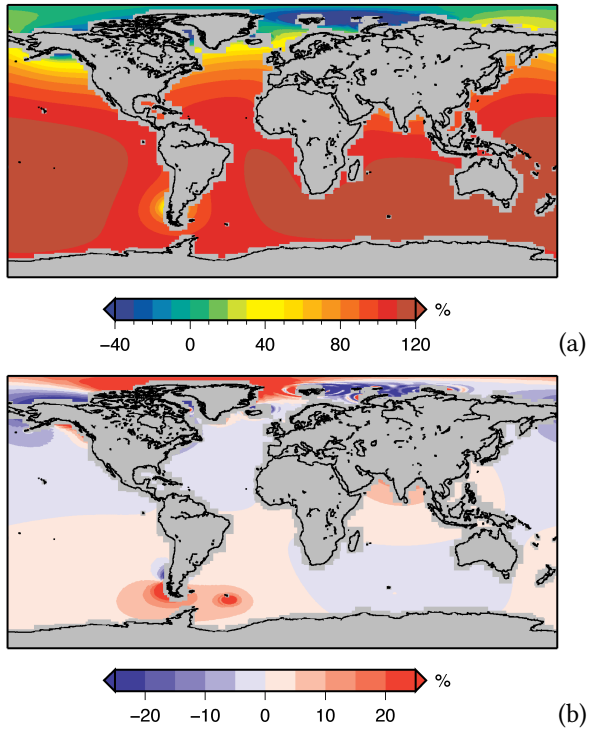

Figure 5.10: (a) *Local sea-level change (1990–2090) relative to the ensemble global mean sea-level change (%) (R10, global average 0.149 m).* **(b)** *Difference in relative sea-level change (%) (R10–W01).*

sented is $\frac{\delta V_{\text{local}}}{\delta V_{\text{globalmean}}} \cdot 100\,\%$, which is the local sea-level change due to GIC relative to the global mean sea-level change due to GIC. In the figure, values below zero imply a sea-level fall, values between 0 and 100 % imply a sea-level rise below the R10 global average, and values above 100 % indicate a sea-level rise larger than the global average. Figure 5.10a shows that, except for Patagonia, the Southern Hemisphere will experience a sea-level rise greater than average, the Northern Hemisphere a rise less than average and parts of the Arctic region will even experience a sea-level fall from the contribution of GIC. This is because most glaciers are situated around the Arctic, where the largest decrease in ice mass will be and thus the largest changes in the gravitational field. Differences further inland, such as in Central Asia, only have a minor effect.

In Figure 5.10b the differences in the sea-level change pattern between R10 and W01 are shown in percentages. A positive value indicates that R10 has a larger relative sea-level change, while a negative value implies a larger relative sea-level change for W01. Regions with substantial differences between the two inventories are Patagonia and the high Arctic, where the largest differences in sea-level pattern can be found close to the largest melt sources. This is a consequence of the non-linear pattern of the gravitational adjustment with a strong response close to the source of mass change and a gradual transition in the far field. Consequently, further away from the melting ice the patterns of R10 and W01 are very similar.

Data uncertainty

While in the previous section two inventories were compared, this section will consider the measurement uncertainties of each of the glacier inventories. These uncertainties are for instance due to the data being obtained from various sources, or not all regions being complete. To show how this influences the GIC sea-level contribution, we vary the initial GIC area by an arbitrarily chosen $\pm 10\,\%$. For R10, this results in variations in the GIC contribution of ± 0.017 m, while for W01 it is ± 0.019 m. This is a deviation of 11 % with respect to the reference value, which is substantial. This shows that it is of great importance that the glacier inventories are completed with the highest possible accuracy.

5.4.3 Climate model uncertainty

The ensemble mean sea-level change (1990–2090) calculated for the reference experiment is 0.149 ± 0.022 m SLE for R10 and 0.176 ± 0.025 m SLE for W01. These uncertainties are based on the spread in the climate models used for the calculations (Section 5.2.3). In this section we consider the δV for the twelve climate models individually. In Figure 5.11, δV is shown for each climate model and both glacier inventories separately. The dashed line indicates the ensemble mean value of each inventory. The figure shows that there are large differences among the climate models, yielding GIC contributions in the range of 0.12 to 0.22 m SLE. These differences are caused by vari-

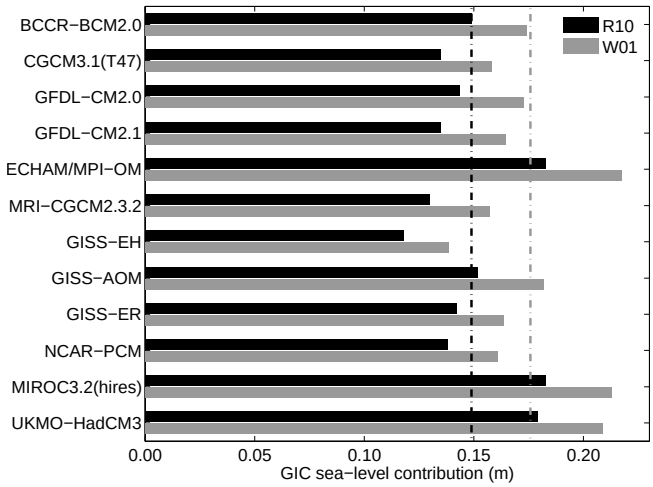

Figure 5.11: *GIC sea-level contribution (m) for the 12 climate models and the two glacier inventories (1990-2090). Dashed lines represent model mean contribution for each inventory.*

ations in temperature and precipitation patterns of the climate models. All models consistently present larger contributions for the W01 data set than for R10, due to differences in the classification of the GIC in size bins. The difference between the highest and the lowest climate model is 0.065 m (R10) and 0.079 m (W01), the largest absolute deviation from the ensemble mean is 0.034 m (R10) and 0.042 m (W01). The average absolute deviation from the ensemble mean for both data sets combined is 0.018 m or 12 %. Clearly, the choice of climate model has a significant impact on the resulting GIC contribution. It is therefore important to use a large ensemble and not to rely on a single climate model as long as we cannot prove one to be superior to the others.

5.4.4 Emission scenario uncertainty

Closely connected to the choice of climate model is the emission scenario that is chosen to drive the climate model. Throughout this study, the A1B scenario has been used. However, depending on the socio-economic developments in the next century, the actual emissions might be higher or lower than in the A1B scenario, which will of course influence the temperature change and the amount of GIC melt and thus the sea-level contribution. Therefore, we also show the GIC sea-level contribution resulting from calculations with the A2 and B1 scenarios (Nakicenovic and Swart, 2000). The A2 and B1 model ensembles are slightly smaller than the A1B scenario, as not all AOGCM's are available for these scenarios. In the A2 ensemble, GISS-EH and GISS-AOM are not available, leading to a ensemble size of 10 models. For B1, GISS-EH is not available, thus leading to an ensemble size of 11 models. The resulting GIC contribution to sea-level change, using the R10 inventory, is 0.168 ± 0.021 m SLE for A2 and 0.128 ± 0.018 m SLE for B1. It is not surprising that the warmer A2 scenario

yields a higher GIC contribution than the cooler B1 scenario. These results show that the choice of emission scenario is an important factor, as the deviation from the A1B scenario is on average 0.020 m SLE or 13 %.

5.5 Conclusions

This study examined sources of uncertainty in the computation of the future sea-level contribution of melting GIC with a volume-area model. Four sources of uncertainty were examined in Section 5.4, being the analytical uncertainty (Section 5.4.1), the data uncertainty (Section 5.4.2), the choice of climate model (Section 5.4.3), and the choice of emission scenario (Section 5.4.4). The results of the sensitivity studies are summarised in Table 5.4, which shows the applied variations and the resulting ensemble mean deviations from the reference experiment for δV.

In Section 5.4.1, the mass balance sensitivity was varied by $\pm 20\,\%$, which led to a variation of $\pm 17\,\%$ or 0.026 m SLE in the GIC contribution to sea-level change. Thus, variations in mass balance sensitivity have a notable effect on the GIC sea-level contribution. This means that if the applied sensitivity is not representative for a global approach, it will introduce a significant error in the calculated sea-level contribution.

The influence of changes in scaling factor c was examined in Section 5.4.1. It appeared that small variations in c cause significant variations in the V_i in 1990 (25 %), but only limited changes in the future contribution to sea-level change. For a range of $\pm 0.05\,\mathrm{m}^{3-2\gamma}$, δV varied by only $\pm 9\,\%$ or 0.014 m. The remarkable difference in sensitivity between V_i and δV can be explained by considering the time scale of interest (100 yr) and the response time of a glacier to a changing climate.

As glaciers are currently not in balance with climate, a temperature history has to be prescribed, for which several options were explored in Section 5.4.1. It appeared that it is important to include an imbalance, as excluding it leads to a systematic underestimation of the future sea-level contribution. The various options for a temperature history for the period 1865–1990 did not result in large deviations; the average difference is only 0.009 m SLE for the future contribution.

If the two glacier inventories are tuned such that the V_i is the same, the δV over 100 yr differs by 0.027 m. An important difference between the two data sets is the way the area is divided into size bins, which leads to differences in the contribution of some regions. As R10 has a more complete inventory in for instance Central Asia and Greenland, where differences between W01 and R10 are the largest, R10 probably gives a better indication of the GIC contribution than the older W01 data. The differences between these data sets indicate that it is very important to obtain information on the missing glaciers in the glacier inventories, especially in underrepresented but largely glaciated areas, such as Alaska, Arctic Canada and Antarctica.

Despite the differences in global mean values and among the different regions, we found that for the majority of the ocean surface there are only minor differences in the modelled sea-level change patterns between the two glacier inventories (Figure 5.10b).

Table 5.4: *Summary of the differences in δV found with the sensitivity studies.*

Sensitivity test	Section	Variation	Difference (m)	Difference (%)
Mass balance sensitivity	5.4.1	$\pm 20\,\%$	0.026	17
Scaling factor c	5.4.1	$\pm 25\,\%$	0.014	9
Imbalance in 1990	5.4.1	5 options	0.009	5
Choice of inventory	5.4.2	2 datasets	0.027	18
Data uncertainty	5.4.2	$\pm 10\,\%$	0.017	11
Choice of climate model	5.4.3	12 models	0.018	12
Choice of emission scenario	5.4.4	3 scenarios	0.020	13
Total uncertainty			0.052	35
No Imbalance	5.4.1	no imbalance	0.058	39

The largest differences in the pattern occur close to the melt areas, such as in the Arctic region. Further away from the GIC, the sea-level change is above the global average due to the self-gravitation effect, and differences between results obtained with the two inventories are small.

Due to the partially incomplete inventories and the various data sources that contribute to the inventories, there is a measurement uncertainty. Section 5.4.2 showed that variations of $\pm 10\,\%$ in the initial area lead to changes of $\pm 11\,\%$ in the GIC contribution to sea-level change. This high sensitivity indicates that it is very important that the data in the inventories is as accurate as possible.

Section 5.4.3 showed that the choice of global climate model can lead to large differences in the GIC contribution. It is best to use an ensemble where possible, as this will reduce the influence of outliers in the climate models. Another way to reduce the uncertainty due to climate models would be to use AOGCM's with a smaller grid, such that smaller glacierised areas will be better represented in the climate model, because currently the grid size of the climate model is often larger than the size of the glacierised area (Randall et al., 2007). Additionally, glaciers are found in mountainous areas, which are poorly resolved by climate models. Therefore, the climate model yields a temperature and precipitation change that is possibly not representative for the glacierised area. Improving the climate models with an elevation-dependent correction will significantly reduce the uncertainty in calculating the GIC contributions and is therefore a crucial action for future work.

To simulate how the climate change depends on socio-economic developments in the future, various emission scenarios have been developed (Nakicenovic and Swart, 2000). In Section 5.4.4 a few of these scenarios were tested to determine the influence on calculations of the GIC contribution. It was found that the emission scenario

uncertainty is of the same order as the climate model uncertainty.

An example of an uncertainty that could not be accounted for is the response of calving glaciers and tide-water glaciers to a warming climate. As indicated by Radić and Hock (2011) and references therein, the scarcity of estimates and complexity of the mechanisms do not allow for a good estimate of the contribution of these glaciers on a global scale. Therefore, the uncertainties presented here only concern the contribution to sea-level change as a response to surface mass balance changes.

Combining the uncertainties obtained with the sensitivity experiments in this study, we arrive at a total uncertainty of 0.052 m on a contribution of 0.149 m when using the volume-area approach, which is 35 %. The sea-level rise estimates of Meehl et al. (2007b), Meier et al. (2007), Pfeffer et al. (2008) and Radić and Hock (2011) mentioned in the introduction all fall at least partly within this range. The Meehl et al. (2007b) estimate is slightly lower than our contribution, which might be caused by our initial GIC volume estimate being higher than their highest volume estimate: 0.50 m SLE vs. 0.37 m SLE. Radić and Hock (2011) use the same data set as in this study (R10), but find a lower contribution while they include Antarctica. They perform a different evaluation of the volume changes, because instead of grouping the glaciers into 14 regions, each glacier is modelled separately. Also, they use a volume-area-length approach instead of volume-area scaling. The difference between their result and this study is therefore also an illustration of the uncertainty due to differences of analytical method. However, the main uncertainties in their method are the same as those described in this study: a mass balance sensitivity based on few glaciers, an incomplete glacier database and the use of global climate models for temperature and precipitation. These points should therefore be the targets when aiming at improving the estimate of the GIC contribution to sea-level change.

Acknowledgements

We would like to thank P. Leclercq, R. Giesen, J. G. Cogley and an anonymous reviewer for their helpful comments and suggestions. We also thank NSIDC, WGMS, V. Radic and J. G. Cogley for collecting, archiving and providing the glacier inventories. We acknowledge the international modelling groups for providing their data for analysis, the Program for Climate Model Diagnosis and Intercomparison (PCMDI) for collecting and archiving the model data, the JSC/CLIVAR Working Group on Coupled Modelling (WGCM) and their Coupled Model Intercomparison Project (CMIP) and Climate Simulation Panel for organizing the model data analysis activity, and the IPCC WG1 TSU for technical support.

CHAPTER 6

Projecting twenty-first century regional sea-level changes

Sea-level rise is one of the most important consequences of a warming climate, affecting many densely populated coastal communities (Nicholls and Cazenave, 2010). Estimating the spatial variability of sea-level change is a pressing topic in sea-level research (Milne et al., 2009), since local information is essential for adequate coastal management. Regional variations of substantial magnitude can be caused by, for instance, gravitational effects resulting from land ice mass changes (Mitrovica et al., 2001), ocean density variations and associated changes in ocean dynamics (Yin et al., 2010) and Glacial Isostatic Adjustment (GIA) (Peltier, 2004). An increased scientific understanding of these processes now allows us to progress from global mean projections to regional patterns (Slangen et al., 2012, Chapter 4 of this thesis). In this study we show regional projections of twenty-first century sea-level change. We present results for a moderate (RCP4.5) and a warm (RCP8.5) climate change scenario, based on state-of-the-art CMIP5 climate model output (Taylor et al., 2011), combined with model- and observation-based contributions of land ice (Meehl et al., 2007b; Katsman et al., 2011, Chapter 4 of this thesis) and the contribution of GIA (Peltier, 2004) to sea-level change. While the two scenarios yield global mean changes of 0.35 ± 0.08 m and 0.68 ± 0.11 m respectively, regional changes reach values of up to 30% above the global mean in equatorial regions, and up to 50% below the global mean in the Arctic region. We show that, depending on the location studied and the scenario applied, all individual components can dominate local sea-level change. This implies that it is crucial to carefully consider regional variations of all components rather than just global mean values.

This chapter is based on: Projecting twenty-first century regional sea-level changes, by A. B. A. Slangen, M. Carson, C. A. Katsman, R. S. W. van de Wal, A. Köhl, L. L. A. Vermeersen and D. Stammer, *In preparation.*

6.1 Introduction

We present regional sea-level change projections for the end of the twenty-first century, based on the latest climate model simulations assembled in the WRCP's Fifth Coupled Model Intercomparison Project (CMIP5) (Taylor et al., 2011). A set of simulations from 12 climate models (see Section 6.5.1) is used, applying the newly defined Representative Concentration Pathways (RCP) (Meinshausen et al., 2011). From these we use the RCP4.5 and RCP8.5 scenarios, associated with global mean twenty-first century temperature changes of, respectively 1.2–2.7°C and 2.7–5.7°C. The moderate RCP4.5 scenario is paired with a moderate estimate of ice sheet mass loss (Meehl et al., 2007b; Slangen et al., 2012) and yields a global mean sea-level rise of 0.35±0.08 m between 1986–2005 and 2081–2100, while the warmer RCP8.5 scenario, combined with higher ice sheet mass loss (Pfeffer et al., 2008; Katsman et al., 2011), yields a global mean rise of 0.68±0.11 m. This pairing is done to show that, given these climate model simulations and this range of ice sheet variations, there is a considerable regional spread in projected sea-level change. The sea-level contributions considered are land ice changes, steric/dynamic variations, and Glacial Isostatic Adjustment (GIA). For RCP4.5, the land ice and the steric/dynamic contribution account for 51% and 49% of the global mean sea-level change, respectively, while for RCP8.5 these values are 63% and 37% (Table 6.1). In both scenarios, the global mean GIA contribution is small, but it can be significant or even dominant on regional scales. The regional pattern of sea-level change due to land ice changes is calculated by solving the sea-level equation including gravitational, rotational and viscoelastic deformation effects (Schotman and Vermeersen, 2005, Section 2.1.3). The pattern from the global mean steric plus dynamic topography contribution, here called "steric/dynamic", is computed using the CMIP5 climate model simulations. The GIA contribution results from the ICE5G(VM2) model (Peltier, 2004, Section 2.3).

6.2 Methods

The climate model data were extracted from the CMIP5 database (Taylor et al., 2011) on March 1st 2012 (see Section 6.5.1). The data include 2 m air temperature, precipitation, global mean steric and the regional sea surface height above geoid. All the data are interpolated on a $1^\circ \times 1^\circ$ grid.

The land ice contribution consists of two parts: the glaciers and ice caps (GIC), and the ice sheets. The GIC contribution is computed using temperature and precipitation data from the CMIP5 database (Taylor et al., 2011). For the glacier mass loss projection we used a model based on volume-area considerations (Bahr et al., 1997; Van de Wal and Wild, 2001), which requires temperature, precipitation and a glacier area inventory (Radić and Hock, 2010) as input. See Section 2.1.1 and Chapter 5 in this thesis for model details and a quantification of uncertainties.

For the ice sheet contribution, a moderate and a high estimate are used. For the

Table 6.1: *Projected ensemble mean (12 climate models) global average sea-level change (m) for the RCP4.5 scenario with moderate ice sheet contribution and RCP8.5 with high ice sheet contribution over the period from 1986–2005 to 2081–2100. The ice sheet contribution is constructed by adding the surface mass balance (SMB, see Section 6.5.2) estimates and the dynamical (dyn) estimates of the Greenland ice sheet (Gre) and the Antarctic ice sheet (Ant). The variance represents 1σ in the model ensemble.*

	RCP4.5		RCP8.5	
Glaciers and ice caps		0.14 ± 0.03		0.22 ± 0.04
Ice sheets		0.04 ± 0.06		0.21 ± 0.08
- Ant (SMB)	-0.07 ± 0.05		-0.09 ± 0.05	
- Ant (dyn)	0.05 ± 0.01		0.13 ± 0.05	
- Gre (SMB)	0.04 ± 0.03		0.08 ± 0.03	
- Gre (dyn)	0.02 ± 0.01		0.09 ± 0.03	
Steric/dynamic		0.17 ± 0.05		0.25 ± 0.07
GIA		0.00 ± 0.00		0.00 ± 0.00
Total		0.35 ± 0.08		0.68 ± 0.11

moderate estimate, values are adapted from the Intergovernmental Panel on Climate Change Fourth Assessment Report (IPCC AR4) (Meehl et al., 2007b), considering contributions from ice sheet surface mass balance changes (SMB, see Section 6.5.2) and a dynamical response based on the extrapolation of observations up to 2007. For Antarctica this yields a near-zero contribution, while Greenland contributes 0.06±0.03 m (Table 6.1). However, given that the understanding of recently observed dynamic ice sheet behaviour is still limited (Rignot et al., 2008b; Pritchard et al., 2009; Velicogna, 2009), and that the present generation of ice sheet models may not adequately simulate ocean-ice interactions, we also consider an estimate with a larger ice-dynamical component. This estimate is based on attempts to quantify the dynamical contributions by combining recent observations and expert judgement rather than using ice sheet model simulations (Katsman et al., 2011). For Antarctica, a dynamical contribution of 0.13±0.05 m is added to the SMB, while the Greenland ice sheet contribution is doubled using 0.09±0.03 m for the dynamics (Table 6.1). These values for the dynamical contribution are in line with independently derived estimates based on changes in discharge in potentially vulnerable areas (Pfeffer et al., 2008). Although the dynamical response of the ice sheets is not directly connected to atmospheric temperature fluctuations, we choose here to link the moderate estimate to RCP4.5 and the higher estimate to RCP8.5. This is done to span a range of possible variations and explore the consequences for the regional sea-level patterns (Figures 6.1a and 6.1b), but by no means suggests that one dynamical scenario is more likely to occur in response to a

certain emission scenario than the other. To obtain a measure for the variance of the ice sheet contribution in the climate model ensemble, the variance in the contribution of the GIC near the ice sheets is scaled with the ice sheet estimates, resulting in the values presented in Table 6.1.

The sea-level pattern resulting from all ice mass changes is computed using a sea-level model (Schotman and Vermeersen, 2005) which solves the sea-level equation (Farrell and Clark, 1976) by considering changes in the Earth's gravitational field from ice mass changes, resulting solid-earth deformation and changes in the Earth's rotation vector (Mitrovica et al., 2001).

The CMIP5 contribution is constructed by taking the sea surface height above geoid, and constraining the global mean to be the global steric average sea surface height at each time step. All data were corrected for model drift by subtracting the linear trend in the timeseries of the accompanying pre-industrial control run (Gregory et al., 2001; Katsman et al., 2008).

The sea-level pattern resulting from GIA is taken from model simulations with the ICE5G(VM2) model (Peltier, 2004). It is assumed to be constant over the time scale of this study and it is the same for both RCP scenarios. Other existing GIA scenarios will contribute values to present-day relative sea-level change that will hardly differ. This is due to the fact that all GIA models are constrained by relative sea-revel curves in the first place. GIA models differ mainly in Late-Pleistocene ice sheet scenarios and in earth rheological models, not in present-day relative sea-level estimates.

6.3 Regional sea-level projections

The patterns in Figures 6.1a and 6.1b show the result of gravitational, rotational and viscoelastic deformation effects (Mitrovica et al., 2001; Kopp et al., 2010) due to the redistribution of land ice mass from GIC and ice sheets. This pattern is characterised by a sea-level fall near main ice loss regions and above-average sea-level rise at low latitudes. This is illustrated in Figure 6.2, where the projected land ice contribution (blue) is negative in the Arctic Ocean, below average in the North Atlantic Ocean, and above average in the Equatorial Pacific Ocean. The RCP4.5 pattern (Figure 6.1a) reflects that melting of the Greenland ice sheet and of the GIC at high northern latitudes dominates the ice mass loss for this scenario, while Antarctica only contributes by its peripheral glaciers around the Antarctic Peninsula. The pattern for RCP8.5 (Figure 6.1b) is quite similar but with higher values, as the ice sheet contribution is five times as large as for RCP4.5 (Table 6.1), while the GIC contribution is only 50% larger. This results in values of over 0.50 m in equatorial regions, compared to 0.25 m in RCP4.5.

The steric/dynamic sea-level patterns show much more small-scale variability than the land ice contribution patterns due to local oceanic temperature and salinity variations associated with circulation changes (Figures 6.1c and 6.1d). Regional variations range from 0.00 to 0.38 m for RCP4.5 (global mean 0.17 ± 0.05 m), and from -0.03 to 0.56 m for RCP8.5 (global mean 0.25 ± 0.07 m). Larger than average steric/dynamic

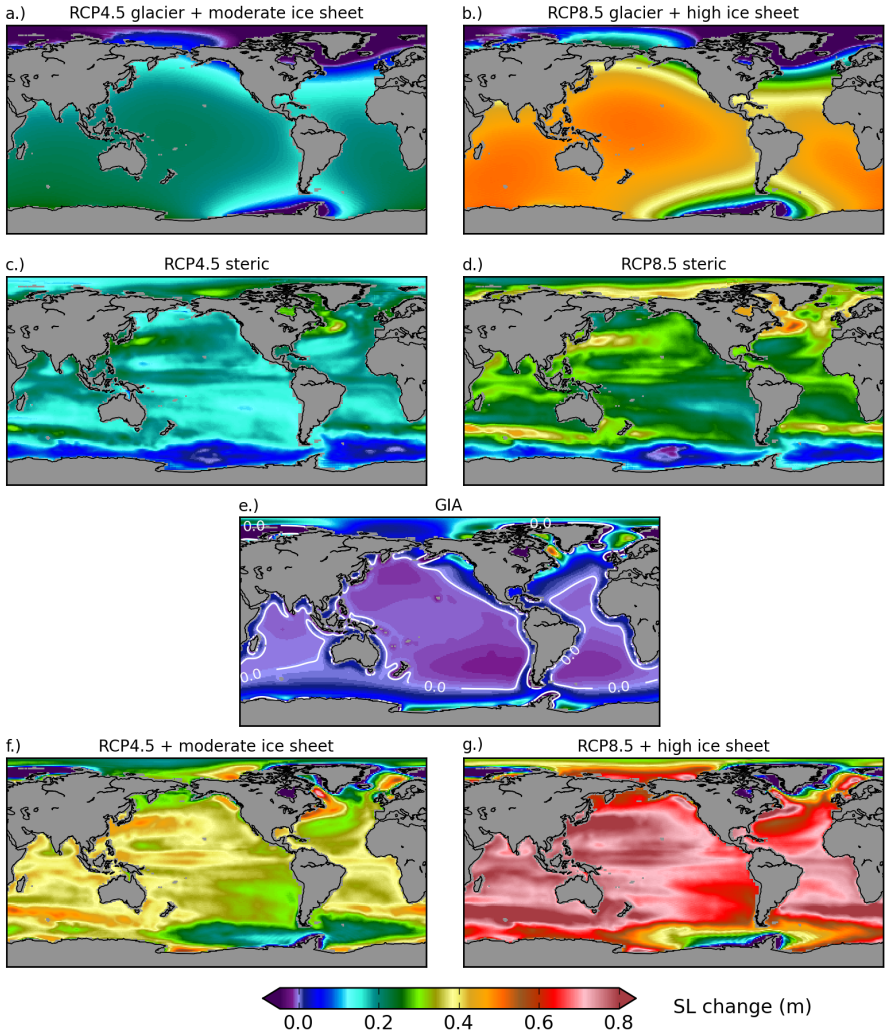

Figure 6.1: *Ensemble mean sea-level change patterns. Projected ensemble mean (12 climate models) relative sea-level change patterns (m) over the period from 1986–2005 to 2081–2100;* **(a)** *RCP4.5 GIC + moderate ice sheet estimate,* **(b)** *RCP8.5 GIC + high ice sheet estimate,* **(c)** *RCP4.5 global steric plus dynamic topography contribution,* **(d)** *RCP8.5 global steric plus dynamic topography contribution,* **(e)** *GIA contribution,* **(f)** *total projection of RCP4.5 + moderate ice sheet (a+c+e),* **(g)** *total projection of RCP8.5 + high ice sheet (b+d+e). Accompanying ensemble global mean values are shown in Table 6.1.*

sea-level rise is projected for the North Atlantic Ocean (Figure 6.2, red), while the Indian-Antarctic Basin displays a dipole pattern, probably associated with changes in the Antarctic Circumpolar Current (ACC) (Meehl et al., 2007b). Changes in the strength of the ACC vary between models, but can account for the limited sea-level

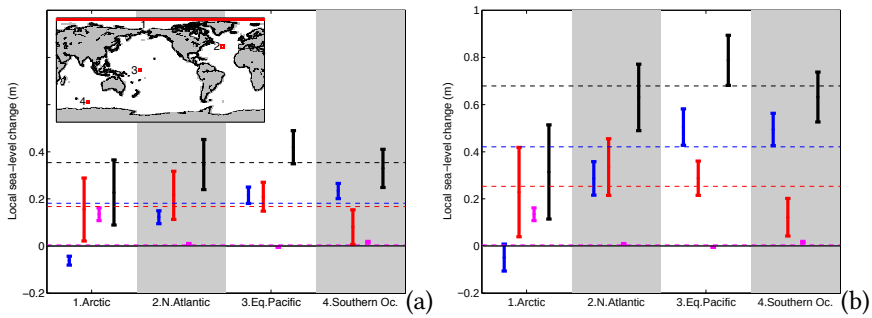

Figure 6.2: *Regional sea-level contributions. Projected ensemble mean (12 climate models) regional average sea-level change contributions of land ice (blue), global steric plus dynamic topography (red), GIA (magenta) and total (black) for specific regions for* **(a)** *RCP4.5 + moderate ice sheet estimate* **(b)** *RCP8.5 + high ice sheet estimate. Error bars indicate 1 σ in the model ensemble, dashed lines indicate the global mean. Regions as indicated in the map are 1. Arctic Ocean (all longitudes; 87.5-88.5° N), 2. North Atlantic Ocean (35.5-39.5° W; 38.5-42.5° N), 3. Equatorial Pacific Ocean (177.5-181.5° E; 1.5° S-2.5° N) and 4. Indian-Antarctic Basin (87.5-91.5° E; 53.5-57.5° S).*

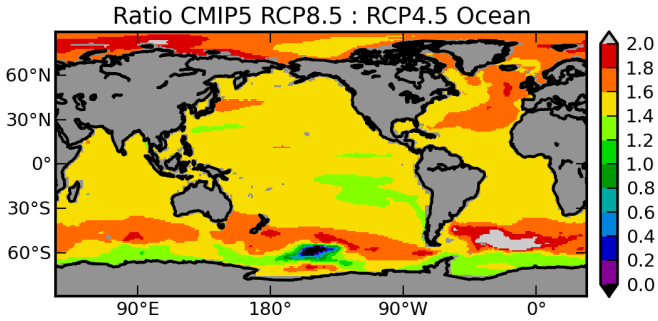

Figure 6.3: *Ratio (-) of the CMIP5 model ensemble steric/dynamic contributions between RCP8.5 and RCP4.5.*

rise around Antarctica. Additionally, thermal expansion is weaker in the cold polar waters. The global mean steric/dynamic contributions differ mostly by a factor 1.5 between the RCP scenarios (Table 6.1 and Figure 6.3), and scale with the global mean temperature change (Perrette et al., 2012), in contrast to the dynamical ice sheet contributions.

Not only changes in the mass or density of the ocean are important for sea-level change, but also vertical deformation due to long-term GIA (Peltier, 2004, Figure 6.1e). Although the GIA contribution is mostly small (Figure 6.2, magenta), it plays an important role near regions where large ice sheets used to be. This contribution is not

influenced by the chosen climate scenario nor by any present-day ice mass variations, and is therefore the same for RCP4.5 and RCP8.5.

In the total sea-level change patterns of both scenarios (Figure 6.1f and Figure 6.1g), we observe high variability from the steric/dynamic contribution, but also a sea-level fall resulting from land ice melt around for instance Greenland, as well as changes resulting from GIA in the Russian Arctic. Although values are larger for RCP8.5, the relative deviation from the global mean is fairly similar for both scenarios (Figure 6.4), with values that are 50% lower around the ice sheets and up to 30% higher in a broad band around the equator. Some striking differences can be noted around North America. RCP4.5 (Figure 6.4a) shows a strong positive anomaly west of Canada, which is caused primarily by GIA. Since GIA does not change while the other contributions increase, this is less pronounced for RCP8.5 (Figure 6.4b). At the east coast of the North American continent we also observe a positive anomaly, caused by GIA in the north and the steric/dynamic component in the south. Since only the steric/dynamic contribution increases, the strongest positive anomaly shifts southward in RCP8.5.

Figure 6.5 shows that the distribution of the local sea-level change is skewed. The distribution has a larger tail towards lower values and an upper limit that is cut off by the gravitational effect, which has a maximum value of 25% above the global mean in the far field. For both scenarios, projected local values deviate more than 10% from the global mean for over 50% of the ocean surface, and deviate more than 25% in almost 10% of the ocean.

Focusing on specific regions (Figure 6.2) shows that the large variations in the total are due to the combined variations in each of the components. In the Arctic Ocean, the total change is below average for both scenarios; only 0.23 m for RCP4.5 and 0.31 m for RCP8.5 (Figure 6.2, black). This is caused by a below-average land ice contribution, which is not compensated by the positive GIA contribution of 0.13 m. In the North Atlantic Ocean, the total change is close to the global mean, as the smaller land ice contribution (65% of the global mean) due to the vicinity of Greenland is partly compensated by the steric/dynamic contribution. In the Equatorial Pacific Ocean, changes are projected to reach values almost 30% above the global mean, because both the land ice and the steric/dynamic contribution are above average (Figure 6.2). The Indian-Antarctic Basin total on the other hand is slightly below the global mean, due to a 50% lower steric/dynamic contribution, which is not compensated by the above-average land ice contribution.

6.4 Discussion and conclusions

While previous work (Slangen et al., 2012, Chapter 4 of this thesis) focused on obtaining a first estimate of the regional patterns in sea-level change connected to the global mean values as presented in the IPCC AR4 report (Meehl et al., 2007b), we here present state-of-the-art estimates of regional sea-level variations by using results from the CMIP5 database (Taylor et al., 2011) which contains simulations of the latest

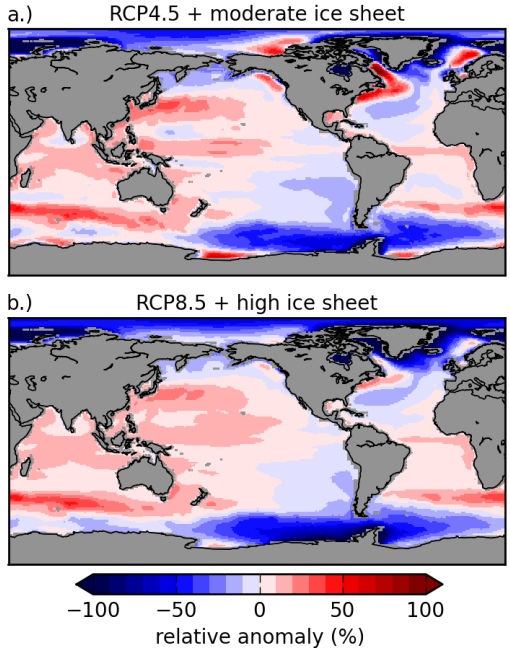

Figure 6.4: *Relative sea-level anomalies. Projected ensemble mean (12 climate models) sea-level change anomaly relative to the total global mean change (%) over the period from 1986–2005 to 2081–2100 for* **(a)** *RCP4.5 + moderate ice sheet estimate, global mean is 0.35±0.08 m* **(b)** *RCP8.5 + high ice sheet estimate, global mean is 0.68±0.11 m.*

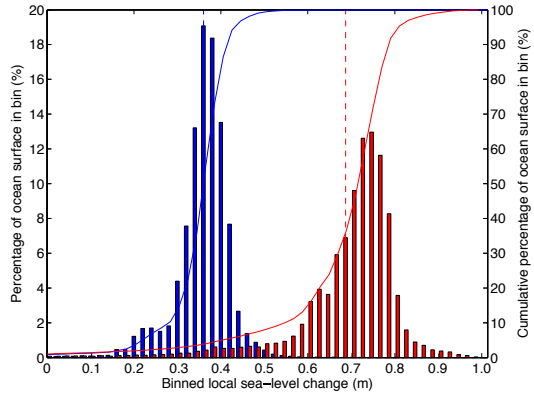

Figure 6.5: *Histogram of the binned local sea-level change (% of the total ocean surface). RCP4.5 in blue, RCP8.5 in red. Vertical dotted lines indicate the global mean, solid lines the cumulative percentage (right axis). Binwidth is 0.02 m. Percentage of ocean surface with less than 0 m sea-level change (not shown) is 0.87% (RCP4.5) and 1.02% (RCP8.5), there are no values over 1.0 m.*

generation of climate models (see Section 6.5.3 for a comparison). However, the climate model ensemble is only one of the many factors that determine local sea-level change. In addition, patterns depend strongly on accurate estimates for ice sheet and GIC mass changes. While 50-year long model simulations are carried out for Greenland melting (Stammer et al., 2011), projections up to 2100 for both ice sheets are not yet available. Including the release of fresh water from land ice melt and the feedback on ocean dynamics might affect the projections. Another contribution to sea-level change arises from changes in continental water storage (Chao et al., 2008; Wada et al., 2010; Konikow, 2011). A recent publication (Wada et al., 2012) projected a groundwater contribution of around 8 ± 3 cm by 2100 based on SRES scenarios. This component can also be included into regional sea-level projections once those calculations are carried out for the CMIP5 model ensemble.

Our results show that local sea-level changes deviate more than 25% from the global mean projection for as much as 10% of the ocean area, indicating that spatial variations are very large. For planning purposes it is very important to know these local values, and it is therefore crucial to carefully consider the regional patterns of the separate contributions, because each can dominate local sea-level change.

6.5 Supplementary information

6.5.1 Climate model ensemble

The ensemble of climate models from the CMIP5 database (Taylor et al., 2011) (http://cmip-pcmdi.llnl.gov/cmip5/), which was used in this study, consists of 12 models (Table 6.2). These models were chosen because they provide all necessary data on March 1st 2012. Figure 6.6 shows for all 12 climate models the climate model dependent components, i.e. the combined steric/dynamic and GIC contributions. This clearly indicates that there is a large amount of variability between the different climate models, both in amplitude and in pattern. For instance, while canESM2, NorESM1, HadGEM2-ES and IPSL CM5A-LR overall yield larger values, changes in CNRM-CM5, MRI CGCM3 and INM_CM4 are smaller. The spread between the models is expressed as a standard deviation in Table 6.1. See Section 6.5.3 for a further analysis of the steric component.

Table 6.2: *CMIP5-models (Taylor et al., 2011) used in this study.*

AOGCM	Institution
BCC-CSM1.1	Beijing Climate Center, China Meteorological Administration
CanESM2	Canadian Centre for Climate Modelling and Analysis
CNRM-CM5	Centre National de Recherches Meteorologiques
GFDL-ESM2M	NOAA Geophysical Fluid Dynamics Laboratory
GISS-E2-R	NASA Goddard Institute for Space Studies
HadGEM2-ES	Met Office Hadley Centre
INM-CM4	Institute for Numerical Mathematics
IPSL-CM5A-LR	Institut Pierre-Simon Laplace
MIROC5	AORI (University of Tokyo), NIES, JAMSTEC
MPI-ESM-LR	Max Planck Institute for Meteorology (MPI-M)
MRI-CGCM3	Meteorological Research Institute
NorESM1-M	Norwegian Climate Centre

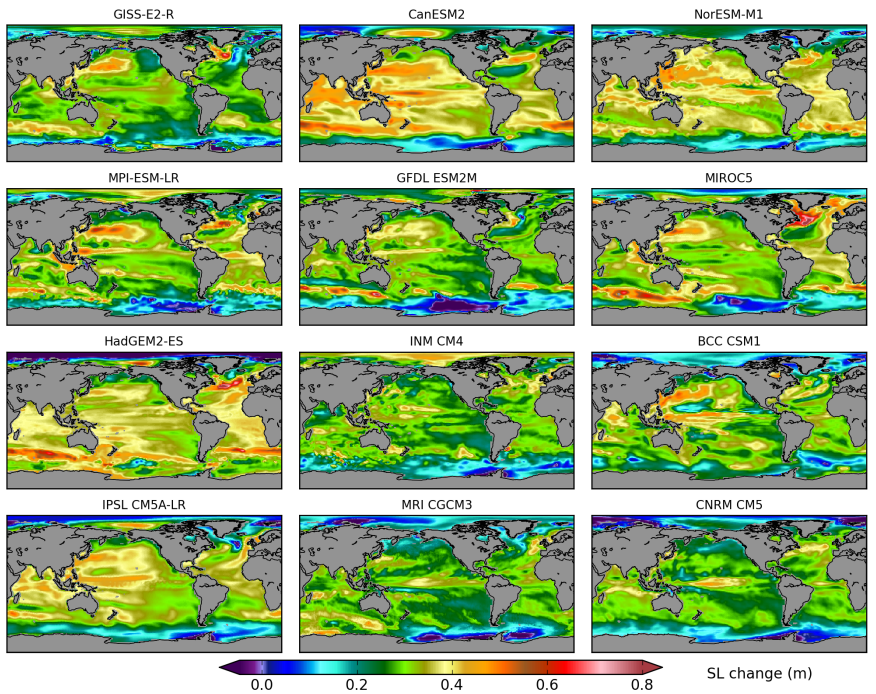

Figure 6.6: *Individual climate model projections. Projected relative sea-level change patterns (m) from the combined global steric plus dynamic topography and GIC contributions for RCP4.5 over the period from 1986–2005 to 2081–2100 for each individual climate model (Table 6.2).*

6.5.2 The SMB-contribution of the ice sheets

The contribution of the ice sheets to sea-level change can be subdivided into a surface mass balance (SMB) part and a dynamical (dyn) part. Since there are no modelling results available yet for the ice sheets that use RCP scenarios, we based our SMB estimate on IPCC AR4 (Meehl et al., 2007b) results. First, the SMB estimates were plotted as a function of the temperature change as projected by the SRES scenarios. Then, linear fits were derived, as shown in Figure 6.7. This results in Equation 6.1 for Greenland and Equation 6.2 for Antarctica, with $\delta\mathrm{SMB}$ in m sea-level change and $\delta\mathrm{T}_{\mathrm{atm}}$ in degrees C.

$$\delta\mathrm{SMB}_{\mathrm{Greenland}} = 0.0163 \times \delta\mathrm{T}_{\mathrm{atm}} - 0.0016 \tag{6.1}$$

$$\delta\mathrm{SMB}_{\mathrm{Antarctica}} = -0.0106 \times \delta\mathrm{T}_{\mathrm{atm}} - 0.0412 \tag{6.2}$$

With a global mean temperature change of 1.2–2.7°C for RCP4.5 and 2.7–5.7°C for RCP8.5, the SMB estimates for Greenland and Antarctica could be computed, as presented in Table 6.1. This also accounts for the effect that SRES scenarios are slightly different from the RCP scenarios in terms of temperature change.

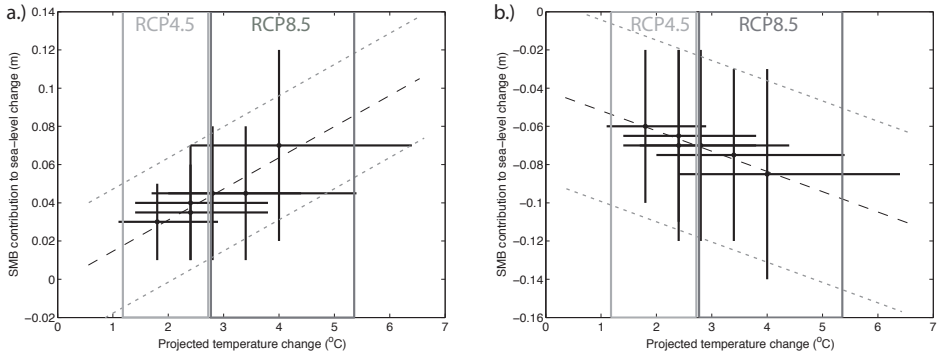

Figure 6.7: *SMB change contribution (m) as a function of temperature change (°C) by the end of the 21st century derived from 6 SRES scenarios, for* **(a)** *Greenland and* **(b)** *Antarctica. Uncertainties are the 5 to 95% ranges (Meehl et al., 2007b, Table 10.7).*

6.5.3 Comparison to previously published regional estimates

The methodology used in this study is based on previous work (Slangen et al., 2012, Chapter 4 of this thesis), hereafter referred to as S12, but there are some important differences. Here we use the newest climate model output from the CMIP5 data base (Taylor et al., 2011) rather than those from the CMIP3 data base (Meehl et al., 2007a) as used by S12. Apart from using newer model results, the general goal of the study is different. While S12 aimed at providing regional fields for the global values as presented in IPCC AR4, this study aims at providing state-of-the-art fields using new insights

Table 6.3: *Projected ensemble mean (12 models) global average sea-level change (m) for the CMIP3 SRES A1B scenario from Slangen et al. (2012) and CMIP5 RCP4.5 from this study (as in Table 6.1). S12 values are scaled by a factor 95/105 to correct for the different length of the time period considered in the two studies (105 yrs in S12 versus 95 yrs in this study). The variance represents 1σ in the model ensemble.*

	A1B	RCP4.5
GIC	0.15 ± 0.04	0.14 ± 0.03
AIS	0.01 ± 0.02	-0.02 ± 0.05
GIS	0.07 ± 0.02	0.06 ± 0.03
Steric	0.19 ± 0.08	0.17 ± 0.05
GIA	0.00 ± 0.00	0.00 ± 0.00
Sum	0.43 ± 0.10	0.35 ± 0.08

and simulations from the latest generation of climate models. In CMIP5, all climate models apply the newly defined RCP scenarios (Meinshausen et al., 2011), while S12 used CMIP3 model results based on SRES scenarios (Nakicenovic and Swart, 2000). This section compares the sea-level projection based on the SRES A1B scenario from S12 to the one based on the RCP4.5 scenario from the current study. Note that the A1B ensemble projects a temperature change of 2.8–4.2°C, while RCP4.5 projects a lower range of 1.2–2.7°C by 2100. The global mean values for various components contributions to sea-level rise are given in Table 6.3 for the A1B scenario as well as for the RCP4.5 scenario for easy comparison.

The use of the new climate model ensemble influences both the steric contribution and the GIC contribution. For the steric component, the overall pattern is quite similar between SRES A1B and RCP4.5, although the values in RCP4.5 are generally lower because the global mean temperature increase is smaller. The most prominent difference in the steric component is the decrease in the ensemble spread in the Arctic Ocean (Figure 6.8). In CMIP3, some models projected Arctic freshening while others did not, leading to a large spread in this region. In CMIP5, there is still some disagreement between the ensemble members with respect to the timing of the reduction of the sea ice, but less than in CMIP3, leading to a smaller variance. For the SRES A1B ensemble, the steric rise in the Arctic was projected to be 0.1-0.2 m above the global mean (Figure 10.32 in Meehl et al., 2007b). For the RCP4.5 ensemble it is close to the global mean (Figure 6.2), and the models tend to agree more on this result (Figure 6.6) than was the case for the SRES A1B ensemble (Pardaens et al., 2011). We speculate that this can be attributed to the improved resolution of the climate models (for the SRES A1B ensemble, the outliers seem to be the models with the lowest resolution (Pardaens et al., 2011)) and/or recent efforts to improve the sea ice modules in climate models triggered by model deficiencies that came to light when simulating recent changes in Arctic sea ice cover (Stroeve et al., 2007).

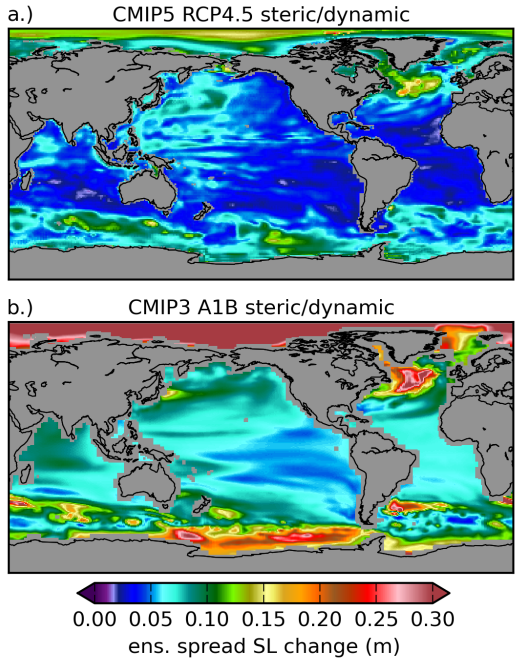

Figure 6.8: *Ensemble standard deviation (m) of the global steric plus dynamic topography contribution to sea-level change for* **(a)** *CMIP5-RCP4.5* **(b)** *CMIP3-SRES A1B.*

Also in the Southern Ocean the variance in the steric contribution was large in the SRES A1B ensemble and has been reduced in the RCP4.5 ensemble. In this region, the steric contribution is projected to display a dipole pattern with smaller than average rise along the Antarctic continent and a larger than average rise further to the north (Figure 6.1c, Figure 10.32 in Meehl et al., 2007b), which has been linked to shifts in the Antarctic Circumpolar Current (Gregory et al., 2001; Suzuki et al., 2005; Landerer et al., 2007b). Apparently, the substantial model disagreement on this aspect has been reduced between the CMIP3 climate models (Pardaens et al., 2011) and the current generation of climate models.

The GIC contribution is calculated using temperature and precipitation data from the climate model ensemble. Not only the global mean temperature change is smaller in RCP4.5 compared to SRES A1B, also the local temperature rise in the individual regions considered for GIC melt is lower. The precipitation change is not structurally different between the two scenarios, and might thus have a positive effect in one mountain region and a negative effect in the other, causing very small differences in the pattern. As a consequence of the smaller temperature increase the GIC contribution to sea-level change is lower in the RCP4.5 scenario of the CMIP5 ensemble (Table 6.3).

An additional benefit of the new CMIP5 ensemble is the general increase in the resolution of the climate models. This improves the amount of detail in which the

ocean circulation can be represented and hence the resolution of the projection, as it is constructed for a land-sea mask given by the combined masks of the models in the ensemble (see S12 for details). As a result of the improved model resolution, the ocean area covered by this combined land-sea mask increased from 80% to 90% of the actual ocean area. The improvement of the land-ocean mask can clearly be seen when comparing the two panels in Figure 6.8.

Finally, this study used a different approach to obtain estimates for the ice sheet contributions. Firstly, the SMB component and the dynamical component are considered separately. While the SMB component is based on the IPCC AR4 values (Meehl et al., 2007b), the dynamical component is treated differently than was done in S12. Two scenarios were used: a moderate scenario based on IPCC AR4 (Meehl et al., 2007b) and S12, and a scenario with a larger contribution based on ice-dynamical considerations (Pfeffer et al., 2008; Katsman et al., 2011). This yields a wider range for the ice sheet contribution than in S12, which provides insight in the possible changes in sea level arising from various ice sheet mass variations.

Acknowledgements

We acknowledge the World Climate Research Programme's (WRCP) Working Group on Coupled Modelling (WGCM), which is responsible for CMIP, and we thank the climate modelling groups listed in Table 6.2 for producing and making available their model output. Many thanks to M. Carson for making Figures 6.1, 6.3, 6.4, 6.6 and 6.8.

CHAPTER 7

Summary, conclusions and outlook

7.1 Summary and conclusions

The research in this thesis focuses on the modelling of regional patterns in relative sea-level change. The main processes contributing to sea-level change are mass change (land ice melt and terrestrial exchange), volume change, and solid-earth deformation. The main theory and tools used to model these processes and their regional patterns were described in Chapter 2.

In Chapter 3, the theory posed in Chapter 2 has been tested for data covering the period 1961–2003. Modelled patterns of sea-level trends over this period were compared to tide gauge observations. The contributions that were included in this chapter are changes in land ice, the steric change, GIA, terrestrial exchange -groundwater and dams- and a correction for atmospheric pressure changes. The observations used are tide gauge observations, which provide timeseries of monthly mean relative sea level. To compare the observations to the modelled changes, we zoomed in on 17 regions around the world. A qualitative analysis showed that the models perform quite well in most regions, although in some regions the high variability in the observations could not be explained by the models, such as in the Mediterranean. This might be solved by improving the steric contribution, which is the only component with a high variability. There is room for improvement as the uncertainties for this component are large towards the earlier part of the period and data coverage is limited for the Southern Hemisphere. A more quantitative test shows that the comparison of the 17 regional observation means to 17 regional model means yields an R^2-value of 0.54. Statistically it was shown that both the models and the observations can be based on the same normal distribution, although the standard deviation in the observation is clearly larger

than the standard deviation in the modelled sea-level rise. A possible explanation for this higher variability in the observations could be in small-scale coastal processes, for instance related to sediment transport, that are not present in the modelled contributions. Varying the data sets used for each of the contributions, whether changing one or more component at a time, does not cause a significant overall improvement in the explained variability over all regions. Locally there are improvements possible, but an improvement in one region will generally lead to a decrease of explained variability in another region. This indicates that the different solutions for the contributions each have their strengths and weaknesses. Overall, the ability of the models to at least partly explain these local observations indicates that the level of understanding of the processes that cause sea-level change is such that these models can also be used for the projection of future regional sea-level changes.

While Chapter 3 focused on the past, the remaining Chapters 4 to 6 were directed towards future projections of regional sea-level changes. Information on future local sea-level changes is vital for governments and policy makers to determine which measures have to be taken to protect coastal communities. In Chapter 4, a first step was taken towards 21^{st} century regional sea-level projections. The main goal in this chapter was to show the regional patterns of the global mean values as presented in IPCC AR4 (Meehl et al., 2007b). For this, the output from 12 CMIP3 AOGCM's and 3 emission scenarios -A1B, A2 and B1- has been used to project the regional contributions of land ice mass changes and steric changes. This was combined with the local sea-level contribution from GIA based on the ICE5G glaciation-deglaciation model (Peltier, 2004). The glacier contributions were computed with a volume-area glacier model, the ice sheets values were based on IPCC AR4. The changes in land ice mass were fed into a sea-level model which computed the gravitationally and rotationally consistent regional sea-level pattern. The steric pattern was derived from the same AOGCM ensemble. The total pattern revealed a highly variable regional pattern, with values deviating up to 70% from the global mean, which locally may be dominated by each of the three contributions. Most of the high variability was caused by the steric contribution, while land ice melt caused a distinct pattern due to elastic solid-earth deformation and the self-gravitation effect, and GIA dominated in typical uplift regions such as Scandinavia. Between the emission scenarios, the amplitudes of the local sea-level change were found to vary, but the patterns are fairly similar. The study in this chapter was the first to combine regional patterns from land ice melt, steric change and GIA, and used them to make future sea-level projections. However, it was found that there are large uncertainties associated with each contribution.

Chapter 5 focused on the uncertainties in the glacier contribution to sea-level change, and more specifically those associated with the use of the volume-area model. The chapter examined four sources of uncertainty: the analytical uncertainty, the data uncertainty, the choice of climate model, and the choice of emission scenario. The analytical uncertainty included the mass balance sensitivity, the scaling factor and the present-day imbalance of glaciers with climate. We concluded that the mass balance

sensitivity has the largest effect on the computation of the glacier contribution. To test the importance of the uncertainty in the data, we examined the response of the glacier contribution to a different glacier inventory and to uncertainties in the measurements. It was found that quite large differences occur when comparing two possibilities for the glacier inventories, which describe the initial area of the glaciers. Furthermore, it appeared that the choice of climate model and emission scenario can lead to quite large differences in the glacier contribution to sea-level change. The use of an ensemble of climate models did reduce the influence of outliers and decreased the uncertainty associated with the choice of climate model. Also, the use of smaller grids in climate models might improve the results in the relatively small, mountainous glacierised areas. The combined uncertainty of all the experiments examined in the chapter is 35%. The uncertainties in the mass balance sensitivity and the choice of inventory are found to be the largest contributors to this combined uncertainty. These are therefore important points for improving the estimate of the glacier contribution to sea-level change.

In Chapter 6, the methodology described in Chapter 4 was used to provide up-to-date regional sea-level projections using more recent models and data. These projections are based on AOGCM data from 12 models in the CMIP5 model database, which are the current (summer 2012) state-of-the-art climate simulations. The projections were computed for two RCP climate scenarios: the moderate RCP4.5 scenario with a global mean temperature increase of 0.8–2.7°C between 2000 and 2100, and the warmer RCP8.5 scenario with a 2.7–5.7°C warming. The output from the climate models was used to compute the steric/dynamic contribution to regional sea-level change and to compute the glacier contribution using temperature and precipitation changes. These scenarios were then coupled to two ice sheet scenarios to account for the large uncertainty in the present-day ice sheet contribution: a moderate estimate and a high estimate. Similar to Chapter 4, the GIA contribution was added. The addition of all these contributions yields regional deviations of as much as 30 % above and 50 % below the global mean values. The chapter has also shown that all individual components can dominate sea-level change, depending on the location and the climate scenario. In the total regional sea-level pattern, we observed that in as much as 10 % of the ocean area, the regional values differ more than 25% from the global mean values. These results indicate that it is important to include all these components and their regional patterns to get a complete view of future sea-level change.

7.2 Outlook

This thesis treated the modelling of regional patterns in sea-level change in recent past and future. One thing that is clear from both the observations and the models is that sea-level change is certainly not a uniform process, and that regional deviations from the global mean can be large. Observations also show that sea level is rising in most locations. However, there are many remaining questions that need to be solved.

In Chapter 3 we learned that the past observations can still not be explained by

models in all details. Especially the large local variability in the tide gauge observations cannot be explained with the current set of models and available data of the past half century. The difference between direct observations and models might be caused by a missing process or by coastal influences that are not included in these models. The use of satellite measurements in addition to tide gauge observations may decrease the influence of coastal effects, and may yield more insight into possible missing processes. As the length of the satellite altimetry measurement timeseries grows each year, this becomes an increasingly interesting dataset to study the influence of climate change on regional sea-level change. It might also be interesting to focus on the influence of coastal processes such as sediment transport and long-term tidal effects on sea-level change, but this requires models with much smaller spatial resolutions.

For the projection of future sea-level changes, there are uncertainties in basically each of the components, of which some are expected to improve in the near future. It is therefore crucial to study and refine each of the different contributions to obtain more accurate projections. For instance the inventories used for the glacier contribution will become more accurate due to the use of satellite imagery in the determination of the glacier area, and a new glacier inventory is expected to be available in the autumn of 2012. It is also important to realise that, while the glacier contribution is currently one of the larger contributions to sea-level rise, the majority of the smaller glaciers may melt away in the coming century, and is thus not an infinite source of sea-level rise (see Figure 5.4 in this thesis). Of major concern are the future contributions of the two large ice sheets, since they store an amount of freshwater that is equal to 65 meters global mean sea-level rise. It is not expected that this will all melt within the coming centuries, but the current melt rates of the large ice sheets do indicate an increasing contribution to sea-level change. The dynamical response of the ice sheets, especially those parts that are located on downward inland slopes, is still poorly understood and introduces a large uncertainty in this contribution to sea-level change. However, much research in the cryospheric community is focusing on this subject, which will hopefully result in a better understanding of the processes governing mass changes on the ice sheets (e.g., Rignot et al., 2011; Pritchard et al., 2012, Ice2Sea project, SeaRISE project). It is expected that the steric contribution will keep on increasing, as is presently the case. An uncertainty in this contribution is the response of the deep ocean to a warming climate. The ARGO network (Gould et al., 2004), launched in 1999, now contains around 3,000 floats continuously measuring ocean temperature and conductivity up to a depth of 2 km. Expanding these timeseries will hopefully lead to a better understanding of this component.

A component that was not yet included in our sea-level projections in Chapters 4 and 6 is the terrestrial exchange contribution. However, Wada et al. (2012) recently published an estimate of the future contribution of groundwater depletion to sea-level change. This study projects a groundwater depletion contribution of approximately 8 cm global mean sea-level rise by 2100 based on SRES emission scenarios. This is a significant contribution, and therefore it will need to be included in future regional

sea-level projections.

A contribution that could not yet be included is the response of the ocean circulation to the addition of freshwater through the runoff of meltwater into the ocean. To include this, model resolutions need to be much smaller, and the possibility of turbulent mixing in the ocean needs to be included. Models of this type are computationally very expensive and therefore currently not yet included in the ocean part of the current ensemble of climate models. However, it is expected that this will be added, thereby allowing for a better representation of ocean dynamical changes through freshwater input.

Other challenges for the future include the change of extreme events, such as storms and floods, and their influence on regional sea-level change. For this, storm setup models will need to be coupled to regional sea-level models. Information on these events is valuable for coastal protection purposes, since coastal defenses need to be able to withstand especially these more extreme conditions.

Despite the relatively large uncertainties just mentioned, the work presented in this thesis provides important insights on the processes that contribute to regional variations in sea-level change. Currently, much research is being done on refining the knowledge that will help to significantly improve the regional projections of the different contributions. We expect that these combined efforts will lead to a better and more complete understanding of regional sea-level changes.

List of acronyms

AIS Antarctic Ice Sheet

AGCM Atmosphere General Circulation Model

AOGCM Atmosphere-Ocean coupled General Circulation Model

CMIP3 Third Coupled Model Intercomparison Project

CMIP5 Fifth Coupled Model Intercomparison Project

ELA Equilibrium Line Altitude

EOF Empirical Orthogonal Function

GIA Glacial Isostatic Adjustment

GIC Glaciers and Ice Caps

GIS Greenland Ice Sheet

GOCE Gravity field and steady-state Ocean Circulation Explorer

GRACE Gravity Recovery And Climate Experiment

IB Inverse Barometer

IPCC AR4 Intergovernmental Panel on Climate Change Fourth Assessment Report

LGM Last Glacial Maximum

PREM Preliminary Reference Earth Model

PSMSL Permanent Service for Mean Sea Level

RACMO Regional Atmospheric Climate MOdel

RCP Representative Concentration Pathways

RLR Revised Local Reference

RSL Relative Sea Level

SLE Sea-Level Equivalent

SMB Surface Mass Balance

SRES Special Report on Emission Scenarios

WGI World Glacier Inventory

WCRP World Climate Research Programme

Bibliography

Antonov, J. I., S. Levitus and T. P. Boyer, 2002. Steric sea level variations during 1957-1994: Importance of salinity, *J. Geophys. Res.*, **107**(C12), 8013, doi:10.1029/2001JC000964.

Antonov, J. I., S. Levitus and T. P. Boyer, 2005. Thermosteric sea level rise, 1955-2003, *Geophys. Res. Lett.*, **32**, L12602.

Baart, F., P. H. A. J. M. van Gelder, J. de Ronde, M. van Koningsveld and B. Wouters, 2012. The Effect of the 18.6-Year Lunar Nodal Cycle on Regional Sea-Level Rise Estimates, *J. Coast. Res.*, **28**(2), 511–516.

Bahr, D. B., 1997. Global distributions of glacier properties: A stochastic scaling paradigm, *Water Resour. Res.*, **33**(7), 1669–1679.

Bahr, D. B., M. B. Dyurgerov and M. F. Meier, 2009. Sea-level rise from glaciers and ice caps: A lower bound, *Geophys. Res. Lett.*, **36**, 4.

Bahr, D. B., M. F. Meier and S. D. Peckham, 1997. The physical basis of glacier volume-area scaling, *J. Geophys. Res.*, **102**(B9), 20355–20362.

Bamber, J. and R. Riva, 2010. The sea level fingerprint of recent ice mass fluxes, *The Cryosphere*, **4**, 621–627.

Bamber, J. L., R. E. M. Riva, L. L. A. Vermeersen and A. M. LeBrocq, 2009. Reassessment of the Potential Sea-Level Rise from a Collapse of the West Antarctic Ice Sheet, *Science*, **324**, 901–903.

Bindoff, N. L., J. Willebrand, V. Artale, A. Cazenave, J. Gregory, S. Gulev, K. Hanawa, C. Le Quéré, S. Levitus, Y. Nojiri, C. K. Shum, L. D. Talley and A. Unnikrishnan, 2007. Observations: Oceanic Climate Change and Sea Level. In: Climate Change 2007: The Physical Science Basis. Contribution of Working Group I to the Fourth Assessment Report of the Intergovernmental Panel on Climate Change [Solomon, S., D. Qin, M. Manning, Z. Chen, M. Marquis, K.B. Averyt, M. Tignor and H.L. Miller (eds.)], Cambridge University Press, Cambridge, U. K. and New York, NY. USA.

Bintanja, R. and R. S. W. van de Wal, 2008. North American ice-sheet dynamics and the onset of 100,000-year glacial cycles, *Nature*, **454**, 869–872.

Bogdanov, V. I., M. Yu. Medvedev, V. A. Solodov, Yu. A. Trapeznikov, G. A. Troshkov and A. A. Trubitsina, 2000. Mean monthly series of sea level observations (1777-1993) at the Kronstadt gauge, *Reports of the Finnish Geodetic Institute*, **1**, 34.

Braithwaite, R. J. and S. C. B. Raper, 2002. Glaciers and their contribution to sea level change, *Phys. Chem. Earth*, **27**, 1445–1454.

Cazenave, A., K. Dominh, S. Guinehut, E. Berthier, W. Llovel, G. Ramilien, M. Ablain and G. Larnicol, 2009. Sea level budget over 2003-2008. A reevaluation from GRACE space gravimetry, satellite altimetry and ARGO, *Glob. Planet. Change*, **65**, 83–88.

Cazenave, A. and R. S. Nerem, 2004. Present-day sea level change: observations and causes, *Rev. Geophys.*, **42**(RG3001).

Chao, B. F., Y. H. Wu and Y. S. Li, 2008. Impact of Artificial Reservoir Water Impoundment on Global Sea Level, *Science*, **320**, 212–214.

Chappell, J., 1983. Evidence for smoothly falling sea levels relative to north Queensland, Australia, during the past 6000 years, *Nature*, **302**, 406–408.

Chappell, J. and N. J. Shackleton, 1986. Oxygen isotopes and sea level, *Nature*, **324**, 137–140.

Chen, J. and A. Ohmura, 1990. Estimation of Alpine glacier water resources and their change since the 1870's, *IAHS*, **193**, 127–135.

Church, J. A., D. Roemmich, C. M. Domingues, J. K. Willis, N. J. White, J. E. Gilson, D. Stammer, A. Köhl, D. P. Chambers, F. W. Landerer, J. Marotzke, J. M. Gregory, T. Suzuki, A. Cazenave and P.-Y. Le Traon, 2010. Ocean Temperature and Salinity Contributions to Global and Regional Sea-Level Change. In: Understanding Sea-Level Rise and Variability[J. A. Church and P. L. Woodworth and T. Aarup and W. S. Wilson (eds.)], Blackwell Publishing Ltd., 1st ed.

Church, J. A. and N. J. White, 2006. A 20th century acceleration in global sea-level rise, *Geophys. Res. Lett.*, **33**, L01602.

Church, J. A. and N. J. White, 2011. Sea-Level Rise from the Late 19th to the Early 21st Century, *Surv. Geophys.*.

Church, J. A., N. J. White, R. Coleman, K. Lambeck and J. X. Mitrovica, 2004. Estimates of the regional distribution of Sea Level Rise over the 1950-2000 Period, *J. Clim.*, **17**, 2609–2625.

Church, J. A., N. J. White, L. F. Konikow, C. M. Domingues, J. G. Cogley, E. Rignot, J. M. Gregory, M. R. van den Broeke, A. J. Monaghan and I. Velicogna, 2011. Revisiting the Earth's sea-level and energy budgets from 1961 to 2008, *Geophys. Res. Lett.*, **38**(L18601).

Cogley, J. G., 2009a. A more complete version of the World Glacier Inventory, *Ann. Glaciol.*, **50**, 32–38.

Cogley, J. G., 2009b. Geodetic and direct mass-balance measurements: comparison and joint analysis, *Ann. Glaciol.*, **50**(50), 96–100.

De Boer, B., R. S. W. van de Wal, L. J. Lourens and R. Bintanja, 2011. Transient nature of the Earth's climate and the implications on the interpretation of benthic $\delta^{18}O$ records, *Palaeogeography, Palaeoclimatology, Palaeoecology*, **335-336**, 4–11.

Delworth, T. L., A. J. Broccoli, A. Rosati, R. J. Stouffer, V. Balaji, J. A. Beesley, W. F. Cooke, K. W. Dixon, J. Dunne, K. A. Dunne, J. W. Durachta, K. L. Findell, P. Ginoux, A. Gnanadesikan, C. T. Gordon, S. M. Griffies, R. Gudgel, M. J. Harrison, I. M. Held, R. S. Hemler, L. W. Horowitz, S. A. Klein, T. R. Knutson, P. J. Kushner, A. R. Langenhorst, H.-C. Lee, S-J Lin, J. Lu, S. L. Malyshev, P. C. D. Milly, V. Ramaswamy, J. Russell, M. D. Schwarzkopf, E. Shevliakova, J. J. Sirutis, M. J. Spelman, W. F. Stern, M. Winton, A. T. Wittenberg, B. Wyman, F. Zeng and R. Zhang, 2006. GFDL's CM2 Global Coupled Climate Models. Part I: Formulation and Simulation Characteristics, *J. Clim.*, **19**, 643–674.

Domingues, C. M., J. A. Church, N. J. White, P. J. Gleckler, S. E. Wijffels, P. M. Barker and J. R. Dunn, 2008. Improved estimates of upper-ocean warming and multi-decadal sea-level rise, *Nature*, **453**, 1090–1094.

Douglas, B. C., 2001. Sea level change in the era of the recording tide gauges. In: Sea level change in the era of the recording tide gauges [B. C. Douglas and M. S. Kearney and S. P. Leatherman (eds.)], Elsevier, New York.

Dyurgerov, M. B. and M. F. Meier, 2005. Glaciers and the Changing Earth System: A 2004 Snapshot, *Tech. rep.*, Inst. of Arct. and Alp. Res., Univ. of Colo., Boulder, occas Pap No 58.

Dziewonski, A. M. and D. L. Anderson, 1981. Preliminary reference Earth model, *Phys Earth Planet Inter*, **25**, 297–356.

Ekman, M., 1988. The world's longest continuous series of sea level observations, *Pure appl. geophys.*, **127**(73-77).

Ettema, Janneke, Michiel R. van den Broeke, Erik van Meijgaard, Willem Jan van de Berg, Jonathan L. Bamber, Jason E. Box and Roger C. Bales, 2009. Higher surface mass balance of the Greenland ice sheet revealed by high-resolution climate modeling, *Geophys. Res. Lett.*, **36**(12).

Fairbanks, R. G., 1989. A 17,000-year glacio-eustatic sea level record: influence of glacial melting rates on the Younger Dryas event and deep-ocean circulation, *Nature*, **342**, 637–642.

Farrell, W. E. and J. A. Clark, 1976. On Postglacial Sea Level, *Geophys. J. R. Astron. Soc.*, **46**, 647–667.

Fettweis, X., E. Hanna, H. Gallée, P. Huybrechts and M. Erpicum, 2008. Estimation of the Greenland ice sheet

surface mass balance for the 20th and 21st centuries, *The Cryosphere*, **2**(2), 117–129.

Fiedler, J. W. and C. P. Conrad, 2010. Spatial variability of sea level rise due to water impoundment behind dams, *Geophys. Res. Lett.*, **37**(L12603).

Flato, G. M., 2005. The third generation coupled global climate model (CGCM3).

Furevik, T., M. Bentsen, H. Drange, N. Kvamsto and A. Sorteberg, 2003. Description and evaluation of the Bergen climate model: ARPEGE coupled with MICOM, *Clim. Dyn.*, **21**, 27–51.

Gomez, N., J. X. Mitrovica, M. E. Tamisiea and P. U. Clark, 2010. A new projection of sea level change in response to collapse of marine sectors of the Antarctic Ice Sheet, *Geophys. J. Int.*, **180**, 623–634.

Gomis, D., S. Ruiz, M. G. Sotillo, E. Alvarez-Fanjul and J. Terradas, 2008. Low frequency Mediterranean sealevel variability: The contribution of atmospheric pressure and wind, *Glob. Planet. Change*, **63**(2-3), 215–229.

Gordon, C., C. Cooper, C. A. Senior, H. T. Banks, J. M. Gregory, T. C. Johns, J. F. B. Mitchell and R. A. Wood, 2000. The simulation of SST, sea ice extents and ocean heat transports in a version of the Hadley Centre coupled model without flux adjustments, *Clim. Dyn.*, **16**, 147–168.

Gould, J., D. Roemmich, S. Wijffels, H. Freeland, M. Ignaszewsky, X. Jianping, S. Pouliquen, Y. Desaubier, U. Send, K. Radhakrishnan, K. Takeuchi, K. Kim, M. Danchenkov, P. Sutton, B. King, B. Owens and S. Riser, 2004. Argo profiling floats bring new era of in situ ocean observations, *Eos*, **85**(19), 179, 190–191.

Gouretski, V. and K. P. Koltermann, 2007. How much is the ocean really warming?, *Geophys. Res. Lett.*, **34**(L01610).

Gower, J. F. R., 2010. Comment on "Response of the global ocean to Greenland and Antarctic ice melting" by D. Stammer, *J. Geophys. Res.*, **115**(C10).

Gregory, J. M., J. A. Church, G. J. Boer, K. W. Dixon, G. M. Flato, D. R. Jackett, J. A. Lowe, S. P. O'Farrell, E. Roeckner, G. L. Russell, R. J. Stouffer and M. Winton, 2001. Comparison of results from several AOGCMs for global and regional sea level change 1900-2100, *Clim. Dyn.*, **18**, 225–240.

Gregory, J. M. and P. Huybrechts, 2006. Ice-sheet contributions to future sea-level change, *Phil. Trans. R. Soc. A*, **364**(doi:10.1098/rsta.2006.1796), 1709–1731.

Gregory, J. M. and J. Oerlemans, 1998. Simulated future sea-level rise due to glacier melt based on regionally and seasonally resolved temperature changes, *Nature*, **391**, 474–476.

Gregory, J. M., N. J. White, J. A. Church, M. F. P. Bierkens, J. E. Box, M. R. van den Broeke, J. G. Cogley, X. Fettweis, E. Hanna, P. Huybrechts, L. F. Konikow, P. W. Leclercq, B. Marzeion, J. Oerlemans, M. E. Tamisiea, Y. Wada, L. M. Wake and R. S. W. Van de Wal, 2012. Twentieth-century global-mean sea-level rise: is the whole greater than the sum of the parts?, submitted.

Haskell, N.A., 1935. The motion of a fluid under a surface load 1, *Physics*, **6**, 265–269.

Heyworth, A. and C. Kidson, 1982. Sea-level changes in southwest England and Wales, *Proc. Geol. Assoc.*, **93**(91).

Holgate, S. J. and P. L. Woodworth, 2004. Evidence for enhanced coastal sea level rise during the 1990s, *Geophys. Res. Lett.*, **31**, L07305.

Howat, I. M., Y. Ann, I. Joughin, M. R. van den Broeke, J. T. M. Lenaerts and B. Smith, 2011. Mass balance of Greenland's three largest outlet glaciers, 2000–2010, *Geophys. Res. Lett.*, **38**(L12501).

Ishii, M. and M. Kimoto, 2009. Reevaluation of Historical Ocean Heat Content Variations with Time-Variying XBT and MBT Depth Bias Corrections, *J. Oceanogr.*, **65**, 287–299.

Jungclaus, J. H., N. Keenlyside, M. Botzet, H. Haak, J. J. Luo, M. Latif, J. Marotzke, U. Mikolajewicz and E. Roeckner, 2006. Ocean circulation and tropical variability in the coupled model ECHAM5/MPI-OM, *J. Clim.*, **19**, 3952–3972.

K-1 model developers, 2004. K-1 coupled model (MIROC) description, *Tech rep 1*, Center for Climate System Research, University of Tokyo.

Katsman, Caroline, Wilco Hazeleger, Sybren Drijfhout, Geert van Oldenborgh and Gerrit Burgers, 2008. Climate scenarios of sea level rise for the northeast Atlantic Ocean: a study including the effects of ocean dynamics and gravity changes induced by ice melt, *Clim. Change*, **91**(3), 351–374.

Katsman, Caroline A., A. Sterl, J. J. Beersma, H. W. van den Brink, J. A. Church, W. Hazeleger, R. E Kopp, D. Kroon, J. Kwadijk, R. Lammersen, J. Lowe, M. Oppenheimer, H.-P. Plag, J. Ridley, H. von Storch, D. G. Vaughan, P. Vellinga, L. L. A. Vermeersen, R. S. W. van de Wal and R. Weisse, 2011. Exploring high-

end scenarios for local sea level rise to develop flood protection strategies for a low-lying delta—the Netherlands as an example, *Clim. Change*, **109**, 617–645.

King, M.A., Z. Altamimi, J. Boehm, M. Bos, R. Dach, P. Elosegui, F. Fund, M. Hernández-Pajares, D. Lavallée, P.J. Mendes Cerveira, N. Penna, R.E.M. Riva, P. Steigenberger, T. van Dam, L. Vittuari, S. Williams and P. Willis, 2010. Improved Constraints to Models of Glacial Isostatic Adjustment: A Review of the Contribution of Ground-based Geodetic Observations, *Surv. Geophys.*, **31**(5), 465–507.

Konikow, L. F., 2011. Contribution of global groundwater depletion since 1900 to sea-level rise, *Geophys. Res. Lett.*, **38**(L17401).

Kopp, R. E., J. X. Mitrovica, S. M. Griffies, J. Yin, C. C. Hay and R. J. Stouffer, 2010. The impact of Greenland melt on local sea levels: a partially coupled analysis of dynamic and static equilibrium effects in idealized water-hosing experiments, *Clim. Change*, **103**, 619–625.

Lambeck, K. and J. Chappell, 2001. Sea Level Change Through the Last Glacial Cycle, *Science*, **292**(5517), 679–686.

Lambeck, K., C. D. Woodroffe, F. Antonioli, M. Anzidei, W. Roland Gehrels, J. Laborel and A. J. Wright, 2010. Paleoenvironmental Records, Geophysical Modeling, and Reconstruction of Sea-Level Trends and Variability on Centennial and Longer Timescales. In: Understanding Sea-Level Rise and Variability [J. A. Church and P. L. Woodworth and T. Aarup and W. S. Wilson (eds.)], Blackwell Publishing Ltd., 1st ed.

Landerer, Felix W., Johann H. Jungclaus and Jochem Marotzke, 2007a. Ocean bottom pressure changes lead to a decreasing length-of-day in a warming climate, *Geophys. Res. Lett.*, **34**.

Landerer, F. W., J. H. Jungclaus and J. Marotzke, 2007b. Regional dynamic and steric sea level change in response to the IPCC-A1B scenario, *J. Phys. Oceanogr.*, **37**(296-312).

Leclercq, P. W. and J. Oerlemans, 2012. Global and hemispheric temperature reconstruction from glacier length fluctuations, *Clim. Dyn.*, **38**(5-6), 1065–1079.

Leclercq, P. W., J. Oerlemans and J. G. Cogley, 2011. Estimating the Glacier Contribution to Sea-Level Rise for the Period 1800–2005, *Surv. Geophys.*.

Lemke, P., J. Ren, R. B. Alley, I. Allison, J. Carrasco, G. Flato, Y. Fujii, G. Kaser, P. Mote, R. H. Thomas and T. Zhang, 2007. Observations: Changes in Snow, Ice and Frozen Ground. In: Climate Change 2007: The Physical Science Basis. Contribution of Working Group I to the Fourth Assessment Report of the Intergovernmental Panel on Climate Change [Solomon, S., D. Qin, M. Manning, Z. Chen, M. Marquis, K.B. Averyt, M. Tignor and H.L. Miller (eds.)], Cambridge University Press, Cambridge, U. K. and New York, NY. USA.

Lenaerts, J. T. M., M. R. van den Broeke, W. J. van de Berg, E. van Meijgaard and P. Kuipers Munneke, 2012. A new, high resolution surface mass balance map of Antarctica (1979-2010) based on regional climate modeling, *Geophys. Res. Lett.*, **39**(L04501).

Levitus, S., J. Antonov and T. Boyer, 2005. Warming of the World Ocean, 1955-2003, *Geophys. Res. Lett.*, **32**, 4.

Levitus, S., J. I. Antonov, T. P. Boyer, O. K. Baranova, H. E. Garcia, R. A. Locarnini, A. V. Mishonov, J. R. Reagan, D. Seidov, E. S. Yarosh and M. M. Zweng, 2012. World ocean heat content and thermosteric sea level change (0-2000 m), 1955-2010, *Geophys. Res. Lett.*, **39**(L10603).

Levitus, S., J. I. Antonov, T. P. Boyer, R. A. Locarnini, H. E. Garcia and A. V. Mishonov, 2009. Global ocean heat content 1955-2008 in light of recently revealed instrumentation problems, *Geophys. Res. Lett.*, **36**, L07608.

Lidén, R., 1938. Den senkvartära strandförskjutningens förlopp och kronologi i Ångermanland, *Geol. Foren. Furhandl.*, **60**(397).

Lorbacher, K., S. J. Marsland, J. A. Church, S. M. Griffies and D. Stammer, 2012. Rapid barotropic sea level rise from ice sheet melting, *J. Geophys. Res.*, **117**(C06003).

Lowe, J. A. and J. M. Gregory, 2006. Understanding projections of sea level rise in a Hadley Centre coupled climate model, *J. Geophys. Res.*, **111**(C11014, doi:10.1029/2005JC003421).

Lucarini, L. and G. L. Russell, 2002. Comparison of mean climate trends in the northern hemisphere between National Centers for Environmental Prediction and two atmosphere-ocean model forced runs, *J. Geophys. Res.*, **107 (D15)**, 4269, doi:10.1029/2001JD001247.

Manabe, S. and R. J. Stouffer, 1996. Simulation of abrupt climate change induced by freshwater input to the

North Atlantic Ocean, *Nature*, **378**, 165–167.

Meehl, G. A., C. Covey, T. Delworth, M. Latif, B. McAvaney, J. F. B. Mitchell, R. J. Stouffer and K. E. Taylor, 2007a. The WCRP CMIP3 multi-model dataset: A new era in climate change research, *Bull. Am. Meteorol. Soc.*, **88**, 1383–1394.

Meehl, G. A., T. F. Stocker, W. D. Collins, P. Friedlingstein, A.T. Gaye, J.M. Gregory, A. Kitoh, R. Knutti, J.M. Murphy, A. Noda, S.C.B. Raper, I.G. Watterson, A.J. Weaver and Z.-C. Zhao, 2007b. Global Climate Projections. In: Climate Change 2007: The Physical Science Basis. Contribution of Working Group I to the Fourth Assessment Report of the Intergovernmental Panel on Climate Change [Solomon, S., D. Qin, M. Manning, Z. Chen, M. Marquis, K.B. Averyt, M. Tignor and H.L. Miller (eds.)], Cambridge University Press, Cambridge, U. K. and New York, NY. USA.

Meier, M. F., M. B. Dyurgerov, U. K. Rick, S. O'Neel, W. T. Pfeffer, R. S. Anderson, S. P. Anderson and A. F. Glazovsky, 2007. Glaciers Dominate Eustatic Sea-Level Rise in the 21st Century, *Science*, **317**, 1064–1067.

Meinshausen, M., S. J. Smith, K. Calvin, J. S. Daniel, M. L. T. Kainuma, J-F. Lamarque, K. Matsumoto, S. A. Montzka, S. C. B. Raper, K. Riahi, A. Thomson, G. J. M. Velders and D. P. P. van Vuuren, 2011. The RCP greenhouse gas concentrations and their extensions from 1765 to 2300, *Clim. Change*, **109**, 210–241.

Milanković, M., 1930. Mathematische Klimalehre und Astronomische Theorie der Klimaschwankungen. Handbuch der Klimalogie Band 1, Borntrager, Berlin.

Millard, R. C., O.I Mamayev, N.P. Fofonoff, J. M. Gieskes, E. Lafond, E. L. Lewis, F. J. Millero, S. Morcis, R. Perkin, A. Poisson and J. L. Reid, 1987. International oceanographic tables, *Unesco tech. pap. mar. sci.*, **4**.

Miller, L. and B. C. Douglas, 2004. Mass and volume contributions to twentieth-century global sea level rise, *Nature*, **428**, 406–409.

Milly, P. C. D., A. Cazenave, J. S. Famiglietti, V. Gornitz, K. Laval, D. P. Lettenmaier, D. L. Sahagian, J. M. Wahr and C. R. Wilson, 2010. Terrestrial Water-Storage Contributions to Sea-Level Rise and Variability. In: Understanding Sea-Level Rise and Variability [J. A. Church and P. L. Woodworth and T. Aarup and W. S. Wilson (eds.)], Blackwell Publishing Ltd., 1st ed.

Milne, G. A., W. Roland Gehrels, C. W. Hughes and M. E. Tamisiea, 2009. Identifying the causes of sea-level change, *Nat. Geosc.*, **2**, 471–478.

Milne, G. A. and J. X. Mitrovica, 1998. Postglacial sea-level change on a rotating Earth, *Geophys. J. Int.*, **133**, 1–19.

Mitrovica, J. X., N. Gomez and P. U. Clark, 2009. The Sea-Level Fingerprint of West Antarctic Collapse, *Science*, **323**, 753.

Mitrovica, J. X. and W. R. Peltier, 1991. On Postglacial Geoid Subsidence Over the Equatorial Oceans, *J. Geophys. Res.*, **96**(B12), 20053–20071.

Mitrovica, J. X., M. E. Tamisiea, J. L. Davis and G. A. Milne, 2001. Recent mass balance of polar ice sheets inferred from patterns of global sea-level change, *Nature*, **409**, 1026–1029.

Moore, J. C., S. Jevrejeva and A. Grinsted, 2011. The historical global sea-level budget, *Ann. Glaciol.*, **52**(59).

Mound, J. E. and J. X. Mitrovica, 1998. True Polar Wander as a Mechanism for Second-Order Sea-Level Variations, *Science*, **279**, 534–537.

Nakada, M. and K. Lambeck, 1988. The melting history of the late Pleistocene Antarctic ice sheet, *Nature*, **333**, 36–40.

Nakicenovic, N. and R. Swart, eds., 2000. Emission Scenarios, Cambridge University Press, Cambridge, U. K.

National Snow and Ice Data Center, 1999, updated 2009. World glacier inventory, World Glacier Monitoring Service and National Snow and Ice Data Center/World Data Center for Glaciology. Boulder, CO.

Nicholls, R. J. and A. Cazenave, 2010. Sea-Level Rise and Its Impact on Coastal Zones, *Science*, **328**(5985), 1517–1520.

Oerlemans, J., 1993. Modelling of glacier mass balance, In: Ice in the climate system [W.R. Peltier (ed.)], Nato ASI Series I 12.

Oerlemans, J., 1994. Quantifying global warming from the retreat of glaciers, *Science*, **264**, 243–245.

Oerlemans, J., M. B. Dyurgerov and R. S. W. van de Wal, 2007. Reconstructing the glacier contribution to sea-level rise back to 1850, *The Cryosphere*, **1**, 59–65.

Oerlemans, J. and J. P. F. Fortuin, 1992. Sensitivity of Glaciers and Small Ice Caps to Greenhouse Warming,

Science, **258**(5079), 115–117.

Oerlemans, J. and B. K. Reichert, 2000. Relating glacier mass balance to meteorological data by using a seasonal sensitivity characteristic, *J. Glaciol.*, **46**, 1–6.

Ohmura, A., 2004. Cryosphere during the twentieth century. In: The State of the Planet: Frontiers and Challenges in Geophysics [R. S. J. Sparks and C. J. Hawkesworth (eds.)], AGU, Washington, D. C., vol. 150 of *Geophys. Monogr. Ser.*, 239–257.

Pardaens, A. K., J. M. Gregory and J. A. Lowe, 2010. A model study of factors influencing projected changes in regional sea level over the twenty-first century, *Clim. Dyn.*.

Pardaens, A. K., J. A. Lowe, S. Brown, R. J. Nicholls and D. de Gusmao, 2011. SeaâĂŘlevel rise and impacts projections under a future scenario with large greenhouse gas emission reductions, *Geophys. Res. Lett.*, **38**(L12604).

Paterson, W. S. B., 1994. The physics of Glaciers (3rd edn.), Pergamon, Oxford, U.K.

Peltier, W.R., 2004. Global Glacial Isostasy and the Surface of the Ice-Age Earth: The ICE-5G (VM2) Model and GRACE, *Annu. Rev. Earth Planet. Sci.*, **32**, 111–149.

Peltier, W. R., 2001. Global Glacial Isostatic Adjustment and Modern Instrumental Records of Relative Sea Level History. In: Sea Level Rise [B.C. Douglas, M.S. Kearney and S.P. Leatherman (eds.)], Academic press.

Perrette, M., F. Landerer, R. Riva, K. Frieler and M. Meinshausen, 2012. Probabilistic projection of sea-level change along the world's coastlines, *Earth Syst. Dynam. Discuss.*, **3**, 357–389.

Pfeffer, W. T., J. T. Harper and S. O'Neel, 2008. Kinematic Constraints on Glacier Contributions to 21st-Century Sea-Level Rise, *Science*, **321**(1340).

Pirazzoli, P. A., 2005. A review of possible eustatic, isostatic and tectonic contributions in eight late-Holocene relative sea-level histories from the Mediterranean area, *Quartenary Science Reviews*, **24**(18-19), 1989–2001.

Pritchard, H. D., R. J. Arthern, D. G. Vaughan and L. A. Edwards, 2009. Extensive dynamic thinning on the margins of the Greenland and Antarctic ice sheets, *Nature*, **461**(7266), 971–975.

Pritchard, H. D., S. R. M. Ligtenberg, H. A. Fricker, D. G. Vaughan, M. R. van den Broeke and L. Padman, 2012. Antarctic ice-sheet loss driven by basal melting of ice shelves, *Nature*, **484**(7395).

Purkey, S. G. and G. C. Johnson, 2010. Warming of Global Abyssal and Deep Southern Ocean Waters between the 1990s and 2000s: Contributions to Global Heat and Sea Level Rise Budgets, *J. Clim.*, **23**, 6336–6351.

Radić, V. and R. Hock, 2010. Regional and global volumes of glaciers derived from statistical upscaling of glacier inventory data, *J. Geophys. Res.*, **115**(F01010).

Radić, V. and R. Hock, 2011. Regionally differentiated contribution of mountain glaciers and ice caps to future sea-level rise, *Nat. Geosc.*, **4**.

Radić, V., R. Hock and J. Oerlemans, 2007. Volume-area scaling vs flowline modelling in glacier volume projections, *Ann. Glaciol.*, **46**, 234–240.

Radić, V., R. Hock and J. Oerlemans, 2008. Analysis of scaling methods in deriving future volume evolutions of valley glaciers, *J Glaciol*, **54**(187), 601–612.

Randall, D. A., R. A. Wood, S. Bony, R. Colman, T. Fichefet, J. Fyfe, V. Kattsov, A. Pitman, J. Shukla, J. Srinivasan, R. J. Stouffer, A. Sumi and K. E. Taylor, 2007. Climate Models and Their Evaluation. In: Climate Change 2007: The Physical Science Basis. Contribution of Working Group I to the Fourth Assessment Report of the Intergovernmental Panel on Climate Change [Solomon, S., D. Qin, M. Manning, Z. Chen, M. Marquis, K.B. Averyt, M.Tignor and H.L. Miller (eds.)]., Cambridge University Press, Cambridge, U. K. and New York, NY. USA.

Raper, S. C. B. and R. J. Braithwaite, 2005. The potential for sea level rise: New estimates from glacier and ice cap area and volume distributions, *Geophys. Res. Lett.*, **32**(L05502).

Raper, S. C. B. and R. J. Braithwaite, 2006. Low sea level rise projections from mountain glaciers and icecaps under global warming, *Nature*, **439**, 311–313.

Rignot, Eric, Jonathan L. Bamber, Michiel R. van den Broeke, Curt Davis, Yonghong Li, Willem Jan van de Berg and Erik van Meijgaard, 2008a. Recent Antarctic ice mass loss from radar interferometry and regional climate modelling, *Nat. Geosc.*, **1**(2), 106–110.

Rignot, E., J. E. Box, E. Burgess and E. Hanna, 2008b. Mass balance of the Greenland ice sheet from 1958 to 2007, *Geophys. Res. Lett.*, **35**(20).

Rignot, E., I. Velicogna, M. R. van den Broeke, A. Monaghan and J. Lenaerts, 2011. Acceleration of the contribution of the Greenland and Antarctic ice sheets to sea level rise, *Geophys. Res. Lett.*, **38**(L05503).

Riva, R. E. M., J. L. Bamber, D. A. Lavallée and B. Wouters, 2010. Sea-level fingerprint of continental water and ice mass change from GRACE, *Geophys. Res. Lett.*, **37**(L19605).

Ross, J. C., 1854. On the effect of the pressure of the atmosphere on the mean level of the ocean, *Phil. Trans. R. Soc.*, **144**, 285–296.

Schmidt, G. A., R. Ruedy, J. E. Hansen, I. Aleinov, N. Bell, M. Bauer, S. Bauer, B. Cairns, V. Canuto, Y. Cheng, A. Del Genio, G. Faluvegi, A. D. Friend, T. M. Hall, Y. Hu, M. Kelley, N. Y. Kiang, D. Koch, A. A. Lacis, J. Lerner, K. K. Lo, R. L. Miller, L. Nazarenko, V. Oinas, J. Perlwitz, D. Rind, A. Romanou, G. L. Russell, M. Sato, D. T. Shindell, P. H. Stone, S. Sun, N. Tausnev, D. Thresher and M. S. Yao, 2006. Present day atmospheric simulations using GISS ModelE: Comparison to in-situ, satellite and reanalysis data, *J. Clim.*, **19**, 153–192.

Schotman, H. H. A., 2008. Shallow-Earth Rheology from Glacial Isostasy and Satellite Gravity, PhD thesis, TU Delft.

Schotman, H. H. A. and L. L. A. Vermeersen, 2005. Sensitivity of glacial isostatic adjustment models with shallow low-viscosity earth layers to the ice-load history in relation to the performance of GOCE and GRACE, *Earth and Planetary Science Letters*, **236**, 828–844.

Slangen, A. B. A., C. A. Katsman, R. S. W. van de Wal, L. L. A. Vermeersen and R. E. M. Riva, 2012. Towards regional projections of twenty-first century sea-level change based on IPCC SRES scenarios, *Clim. Dyn.*, **38**(5-6), 1191–1209.

Solomon, S., D. Qin, M. Manning, Z. Chen, M. Marquis, K.B. Averyt, M. Tignor and H.L. Miller, eds., 2007. Climate Change 2007: The Physical Science Basis. Contribution of Working Group I to the Fourth Assessment Report of the Intergovernmental Panel on Climate Change, Cambridge University Press, Cambridge, U. K. and New York, NY. USA.

Stammer, D., 2008. Response of the global ocean to Greenland and Antarctic ice melting, *J. Geophys. Res.*, **113**(C06022).

Stammer, D., 2010. Reply to comment by J. F. R. Gower on ";Response of the global ocean to Greenland and Antarctic ice melting";, *J. Geophys. Res.*, **115**(C10).

Stammer, D., N. Agarwal, P. Herrmann, A. Köhl and C. R. Mechoso, 2011. Response of a Coupled Ocean–Atmosphere Model to Greenland Ice Melting, *Surv. Geophys.*, **32**, 621–642.

Steffen, K., R. H. Thomas, E. Rignot, J. G. Cogley, M. B. Dyurgerov, S. C. B. Raper, P. Huybrechts and E. Hanna, 2010. Cryospheric Contributions to Sea-level Rise and Variability. In: Understanding Sea-Level Rise and Variability [J. A. Church and P. L. Woodworth and T. Aarup and W. S. Wilson (eds.)], Blackwell Publishing Ltd., 1st ed.

Stroeve, J., M. M. Holland, W. Meier, T. Scambos and M. Serreze, 2007. Arctic sea ice decline: Faster than forecast, *Geophys. Res. Lett.*, **34**(L09501).

Suzuki, T., H. Hasumi, T. T. Sakamoto, T. Nishimura, A. Abe-Ouchi, T. Segawa, N. Okada, A. Oka and S. Emori, 2005. Projection of future sea level and its variability in a high-resolution climate model: ocean processes and greenland and antarctic ice-melt contribu- tions , *Geophys. Res. Lett.*.

Taylor, K., R. J. Stouffer and G. A. Meehl, 2011. An overview of CMIP5 and the experiment design, *Bull. Am. Meteorol. Soc.*.

Trenberth, K. E., P.D. Jones, P. Ambenje, R. Bojariu, D. Easterling, A. Klein Tank, D. Parker, F. Rahimzadeh, J.A. Renwick, M. Rusticucci, B. Soden and P. Zhai, 2007. Observations: Surface and Atmospheric Climate Change. In: Climate Change 2007: The Physical Science Basis. Contribution of Working Group I to the Fourth Assessment Report of the Intergovernmental Panel on Climate Change [Solomon, S., D. Qin, M. Manning, Z. Chen, M. Marquis, K.B. Averyt, M. Tignor and H.L. Miller (eds.)], Cambridge University Press, Cambridge, U. K. and New York, NY. USA.

Tsimplis, M., G. Spada, M. Marcos and N. Flemming, 2011. Multi-decadal sealevel trends and land movements in the MediterraneanSea with estimates of factors perturbing tide gauge data and cumulative uncertainties, *Glob. Planet. Change*, **76**(1-2), 63–76.

Van de Wal, R. S. W. and M. Wild, 2001. Modelling the response of glaciers to climate change by applying volume-area scaling in combination with a high resolution GCM, *Clim. Dyn.*, **18**, 359–366.

Van den Broeke, M., J. Bamber, J. Ettema, E. Rignot, E. Schrama, W.J. van de Berg, E. van Meijgaard, I. Velicogna and B. Wouters, 2009. Partitioning Recent Greenland Mass Loss, *Science*, **326**(5955), 984–986.

Van Veen, J., 1945. Bestaat er een geologische bodemdaling te Amsterdam sedert 1700?, *Tijdschrift Koninklijk Nederlandsch Aardrijkskundig Genootschap*, **2e reeks**(deel LXII).

Vaughan, D. G., 2008. West Antarctic Ice Sheet collapse – the fall and rise of a paradigm, *Clim. Change.*, **91**, 65–79.

Velicogna, I., 2009. Increasing rates of ice mass loss from the Greenland and Antarctic ice sheets revealed by GRACE, *Geophys. Res. Lett.*, **36**.

Vellinga, M. and R. A. Wood, 2002. Global climatic impacts of a collapse of the Atlantic thermohaline circulation, *Clim. Change.*, **54**, 251–267.

Vermeersen, L. L. A. and R. Sabadini, 1999. Polar wander, sea-level variations and ice age cycles, *Surv. Geophys.*, **20**, 415–440.

Vermeersen, L. L. A. and H. H. A. Schotman, 2009. Constraints on Glacial Isostatic Adjustment from GOCE and Sea Level Data, *Pure appl. geophys.*, **166**, 1261–1281.

Vorren, K. D. and D. Moe, 1986. The early Holocene climate and sea-level changes in Lofoten and Vesterålen, North Norway, *Norsk Geol. Tidd.*, **66**(135).

Wada, Y., L. P. H. van Beek, C. M. van Kempen, J. W. T. M. Reckman, S. Vasak and M. F. P. Bierkens, 2010. Global depletion of groundwater resources, *Geophys. Res. Lett.*.

Wada, Y., L. P. H. van Beek, F. C. Sperna Weiland, B. F. Chao, Y-H. Wu and M. F. P. Bierkens, 2012. Past and future contribution of global groundwater depletion to sea-level rise, *Geophys. Res. Lett.*, **39**(L09402).

Washington, W. M., J. W. Weatherly, G. A. Meehl, A. J. Semtner Jr, T.W.. Bettge, A.P. Craig, W.G. Strand Jr, J. Arblaster, V.B. Wayland, R. James and Y. Zhang, 2000. Parallel climate model (PCM) control and transient simulations, *Clim. Dyn.*, **16**, 755–774.

Wijffels, S. E., J. Willis, C. M. Domingues, P. Barker, N. J. White, A. Gronell, K. Ridgway and J. A. Church, 2008. Changing Expendable Bathythermograph Fall Rates and Their Impact on Estimates of Thermosteric Sea Level Rise, *J. Clim.*, **21**, 5657–5672.

Willis, J. K., D. P. Chambers and R. S. Nerem, 2008. Assessing the Globally Averaged Sea Level Budget on Seasonal to Interannual Time Scales, *J. Geophys. Res.*, **113**(C06015).

Wonnacott, T. H. and R. J. Wonnacott, 1990. Introductory Statistics, Wiley & Sons, fifth edition ed.

Woodward, R. S., 1886. On the Form and Position of the Sea-level as Dependent on Superficial Masses Symmetrically Disposed with Respect to a Radius of the Earth's Surface, *Ann. Mathem.*, **2**(6), 121–131.

Woodward, R. S., 1887. On the Form and Position of the Sea-level as Dependent on Superficial Masses Symmetrically Disposed with Respect to a Radius of the Earth's Surface, *Ann. Mathem.*, **3**(1), 11–26.

Woodworth, P. L., 1999. High waters at Liverpool since 1768: the UK's longest sea level record, *Geophys. Res. Lett.*, **26**(11), 1589–1592.

Woodworth, P. L. and R. Player, 2003. The Permanent Service for Mean Sea Level: an update to the 21st century, *J. Coast. Res.*, **19**(2), 287–295.

Wöppelmann, G., B. Martin Miguez, M.-N. Bouin and Z. Altamimi, 2007. Geocentric sea-level trend estimates from GPS analyses at relevant tide gauges world-wide, *Glob. Planet. Change*, **57**, 396–406.

Wunsch, C. and D. Stammer, 1997. Atmospheric loading and the oceanic "inverted barometer" effect, *Rev. Geophys.*, **35**(1), 79–107.

Yin, J., S. M. Griffies and R. J. Stouffer, 2010. Spatial Variability of Sea-Level Rise in 21st Century Projections, *J. Clim.*, **23**, 4585–4607.

Yukimoto, S. and A. Noda, 2002. Improvements of the Meteorological Research Institute Global Ocean-atmosphere Coupled GCM (MRI-CGCM2) and its climate sensitivity, *Tech. rep. 10*, NIES, Japan.

Zuo, Z. and J. Oerlemans, 1997. Contribution of glacier melt to sea-level rise since AD 1865: a regionally differentiated calculation, *Clim. Dyn.*, **13**, 835–845.

Bedankt! / Thanks!

In mijn eentje was het nooit gelukt om dit proefschrift te voltooien, en daarom wil ik op deze plek iedereen bedanken die mij de afgelopen vier jaar op de een of andere manier heeft geholpen, op het werk of juist daarbuiten.

Als eerste wil ik Roderik van de Wal bedanken voor de dagelijkse begeleiding. Je deur staat altijd open voor een discussie, en nadat ik mijn aanvankelijke verlegenheid kwijt was heb ik daar dan ook gretig gebruik van gemaakt. Jouw manier van begeleiden was een goede mix waarbij je mij zelf dingen liet uitzoeken en toch de vinger aan de pols hield. Ik heb onze samenwerking als zeer prettig ervaren, bedankt!

Wat verder weg, maar toch erg belangrijk voor de richting van dit onderzoek was Bert Vermeersen, mijn tweede begeleider aan de TU Delft. Bedankt voor je altijd snelle en duidelijke antwoorden als ik er weer eens niet helemaal uitkwam met het zelfgravitatie-effect. Je enthousiasme bij het uitleggen van zelfgravitatie werkt aanstekelijk!

Mijn promotor, Hans Oerlemans, overzag mijn project als stille kracht op de achtergrond. Met hier en daar een tip, vraag of suggestie hielp je me om na te denken over wat ik nou precies opschreef, waarvoor dank.

Vanuit het KNMI kreeg ik gedurende het onderzoek een onofficiële derde begeleider, Caroline Katsman. Bedankt voor de goede samenwerking en je geweldige hulp met de belangrijkste papers in deze thesis.

Grazie mille to Riccardo Riva from the TU Delft, for letting me use your sea-level model. Your help and explanations were priceless. *Grazie* also to Paolo Stocchi from TU Delft (and later IMAU), for helping me a great deal with all things GIA.

For my last paper I've been working with Mark, Armin and Detlef from the University of Hamburg. I really enjoyed working with you guys, and I think we've learned a lot from each other. *Vielen Dank*!

Een belangrijke factor bij het succesvol voltooien van deze PhD is de prettige werksfeer die er heerst op het IMAU. Fijne kamergenootjes, een gezellige ijs-en-klimaat groep, gezamelijke koffie- en lunchpauzes, en daarnaast de vele 'buitenschoolse' activiteiten (beachvolley, klaverjassen, jeu-de-boules, borrels) hebben allemaal bijgedragen aan het verhogen van de feestvreugde, waarvoor dank! Het voordeel van een groot instituut is dat er gedurende de afgelopen vier jaar vele 'lotgenoten' waren om mee te kunnen lachen en klagen, waaronder Erik, Selma, Leela, Peter, Rianne, Marianne, Paul, Bas, Jan, Jan, Ward, Stefan en Malou. Allemaal bedankt voor de gezellige tijd! Daarnaast dank aan Marcel voor het gezond houden van mijn Mac, en aan Yvonne, Sandra en Wanda voor jullie goede zorgen.

One of the perks of being a PhD-student is that you get the chance to visit summer schools and conferences, and to go on exciting fieldwork. I've met many great people in Karthaus, Gaëvle and the NEEM-camp on Greenland, and I'm grateful for these opportunities and the friendships that grew from them. In het bijzonder wil ik Carina bedanken voor de goede tijd in het NEEM-kamp.

Veel dank aan mijn vrienden buiten het werk, voor jullie vriendschap en gezelligheid. In het bijzonder de Berend-groep (quizavondjes, Wampexen, CBC's en zelfs een kwart triatlon), de BWA-girls (van grondboren tot samen eten), mijn oudste vriendinnen Annelieke en Sanne (voor de lange telefoongesprekken) en mijn volleyteamgenootjes bij VCV (lekker kleppen en meppen).

Ik wil alle familie en schoonfamilie hartelijk bedanken voor jullie interesse in mijn onderzoek en jullie steun. Lieve mam en pap, ik weet dat jullie zo trots zijn als pauwen! Jullie hebben me altijd vrij gelaten om mijn eigen keuzes te maken, waarvoor ik erg dankbaar ben. Guido, mijn kleine grote broertje, altijd als ik in Delft was voor een vergadering of vak kon ik bij jou terecht om even bij te kletsen, bedankt voor die gezellige middagjes. Mijn schoonfamilie in Lippenhuizen, bedankt dat jullie me een extra thuis hebben gegeven in het hoge noorden.

Wietse, mijn lief. Als geen ander begrijp je de ups en downs van het aio-schap. Alleen met jou aan mijn zijde kon ik dit volbrengen, en ik hoop dat ik hetzelfde voor jou kan betekenen. Bedankt dat je er altijd voor me bent!

Publications

Slangen, A.B.A. and R.S.W. van de Wal, An assessment of uncertainties in using volume-area modelling for computing the twenty-first century glacier contribution to sea-level change, *The Cryosphere*, 5, 673–686, 2011, doi: 10.5194/tc-5-673-2011.

Slangen, A.B.A., C.A. Katsman, R.S.W. van de Wal, L.L.A. Vermeersen and R.E.M. Riva, Towards regional projections of twenty-first century sea-level change based on IPCC SRES scenarios, *Climate Dynamics*, 38 (5-6), 1191–1209, 2012, doi: 10.1007/s00382-011-1057-6.

Slangen, A.B.A., M. Carson, C.A. Katsman, R.S.W. van de Wal, A. Köhl, L.L.A. Vermeersen and D. Stammer, Projecting twenty-first century regional sea-level changes, *In preparation.*

Slangen, A.B.A., R.S.W. van de Wal, L.L.A. Vermeersen and Y. Wada, Regional sea-level variations in the recent past (1961–2003), *In preparation.*

Siddall, M., J. Bamber, S. Sparks, R. Hindmarsh, R. van de Wal, A. Carlson, R. Gladstone, A. Payne, A. Slangen and F. Nick, Sea level hazard from accelerated ice sheet discharge, *In preparation.*

Curriculum Vitae

Aimée Slangen was born in Rotterdam (The Netherlands) on the 26$^{\text{th}}$ of November, 1984. When she was two years old the family moved to the south of the Netherlands, where she grew up in Eijsden, a small town near Maastricht. In July 2003 she obtained her high school diploma at the Jeanne d'Arc College in Maastricht, after which she decided to move to Wageningen to study Bodem, Water en Atmosfeer. After completing her Bachelor of Science in 2006, she stayed in Wageningen to pursue a Master of Science in Meteorology. During the first 6 months of 2007 she took additional Mastercourses at the ETH in Zürich, Switzerland, where she was introduced to meteorology in connection to snow and ice. After writing her Master thesis at the Royal Netherlands Meteorological Institute (KNMI) in De Bilt, she did an internship with MeteoConsult in Wageningen. In August 2008 she graduated from Wageningen University and applied for a PhD position at IMAU in Utrecht. The research focused on modelling regional variations in sea-level change, and the results are written in this thesis.